Université d'Ottawa · University of Ottawa

Université d'Ottawa · University of Ottawa

FACULTÉ DES ÉTUDES SUPÉRIEURES ET POSTDOCTORALES

FACULTY OF GRADUATE AND POSTDOCTORAL STUDIES

Khawaja Shahid KHURSHID

AUTEUR DE LA THÈSE - AUTHOR OF THESIS

M. Sc. (Geography)

GRADE - DEGREE

Department of Geography

FACULTÉ, ÉCOLE, DÉPARTEMENT - FACULTY, SCHOOL, DEPARTMENT

TITRE DE LA THÈSE - TITLE OF THE THESIS

Estimation and Mapping of Wheat Crop Chlorophyll Content Using Hyperion Hyperspectral Data

A. Bannari

DIRECTEUR DE LA THÈSE - THESIS SUPERVISOR

CO-DIRECTEUR DE LA THÈSE - THESIS CO-SUPERVISOR

EXAMINATEURS DE LA THÈSE - THESIS EXAMINERS

M. Sawada

K. Staurt

J.-M. De Koninck, Ph.D.

LE DOYEN DE LA FACULTÉ DES ÉTUDES SUPÉRIEURES ET POSTDOCTORALES

DEAN OF THE FACULTY OF GRADUATE AND POSTDOCTORAL STUDIES

Estimation and Mapping of Wheat Crop Chlorophyll Content Using Hyperion Hyperspectral Data

Presented by

Khawaja Shahid Khurshid

A thesis submitted to the Faculty of Graduate and Post Graduate Studies
in partial fulfillment of the requirements
for the Master of Science in Geography

Remote Sensing And Geomatic Environment Laboratory
Department of Geography
University of Ottawa,
Ottawa, Ontario
Canada

Your file Votre référence
ISBN: 0-494-01511-X
Our file Notre référence
ISBN: 0-494-01511-X

ABSTRACT

The estimation of chlorophyll content is an essential biochemical parameter to track the main developmental stages and yield of cereals relevant for precision agriculture. Traditional techniques for chlorophyll content measurements are time consuming, expensive and laborious. Measurements at field level have proven to be a good alternative, but their use is limited due to extensive sampling designs and techniques. Several spectral chlorophyll indices have been developed to estimate chlorophyll content both at the leaf and canopy level using remote sensing data. A methodology of using spectral chlorophyll indices to estimate chlorophyll content from laboratory and satellite hyperspectral data was carried out in this study for wheat crops. The application of this technique under agricultural field conditions has been very limited and not rigorously validated for wheat crops. The main objective of this study is to validate the chlorophyll content estimation using spectral chlorophyll indices, and to examine the potential for chlorophyll content estimation using hyperspectral remote sensing data in the context of precision agriculture.

Image data were acquired over two agricultural fields, near Indian Head, Saskatchewan, with the Hyperion sensor. Ground data were measured from sampling sites. Ground measurements included the GER-3700 spectroradiometric data, leaf chlorophyll content measurements using the SPAD-502 meter, and leaf chemical analysis for chlorophyll content estimation. The SPAD-502 readings were correlated with laboratory extracted leaf chlorophyll content to establish calibration equations for the computation of chlorophyll-ab and chlorophyll-a content. These estimates were used to establish relationships against spectral chlorophyll indices calculated from the laboratory

GER-3700 data. The leaf level established equations were then used to estimate chlorophyll content from the Hyperion hyperspectral data and validated against those derived from the SPAD-502 measurements.

Two calibration equations for converting SPAD-502 meter readings into chlorophyll content were established for chlorophyll-ab and chlorophyll-a contents with a coefficient of determination (R^2) of 0.72 and 0.69 and a root mean square error (RMSE) of 3.53 and 1.94 μg /cm^2, respectively. Five spectral chlorophyll indices, such as NDPI, SIPI, NPCI, PRI and SRPI were found sensitive to the variation of leaf chlorophyll content with a R^2 of 0.56, 0.62, 0.84, 0.54 and 0.57, and a RMSE 11.06, 10.27, 0.11, 11.32 and 10.96, respectively. The NDPI index showed the best results for chlorophyll content estimation using the Hyperion data against those derived from the SPAD-502 measurements with an index of agreement (D) of 0.66 and a RMSE of 2.89 μg /cm^2. The performance of the NDPI both at leaf and canopy level makes it suitable tool to calibrate biophysical process models used in precision agriculture. It is possible to estimate chlorophyll content by using the NDPI index from the Hyperion data.

Acknowledgements

I would like to thank and express my sincere gratitude to Prof. Abderrazak Bannari and Prof. Karl Staenz for providing me with the opportunity to work on this project, for their guidance, support, constructive criticisms and immense patience in preparing this research. A particular thanks to Prof. Karl Staenz, who gave me the opportunity to work at the Canada Center for Remote Sensing (CCRS), and therefore benefited from the facilities and valuable resources provided by the institution. There was an enormous amount of data in this project, and I would not have been able to accomplish this thesis without the competent and generous assistance provided by the research team at the CCRS, especially Lixin Sun for his assistance, valuable discussions, immediate implementation of new ideas into ISDAS. Special thanks to Dr. Robert Neville, Dr. Peter White, Catherine Champagne, Dr. Heather McNairn, Robert Hitchcook, Anna Pacheco, Jean-Calude Deguise and Jiali Shang for their comments and guidance. I would like to express my gratitude for financial support provided by the University of Ottawa Faculty of Graduate and Postdoctoral Studies and the National Science and Engineering Research Council for its assistance for academic fees. Last but not least, I would like to thank my family and friends for their kind support for the completion of this thesis; above all my mother and father.

Table of Contents

Appendices

List of Tables

List of Figures

Abbreviations and Acronyms

ASL	Above Sea Level
ASCII	American Standard Code for Information Interchange
AVIS	Airborne Visible Infrared Imaging Spectrometer
b	Band
BOREAS	Boreal Ecosystem-Atmosphere Study
c	Current Processed Band
C_c	Charge Conversion Factor
CAI	Chlorophyll Absorption Integral
CARI	Chlorophyll Absorption in Reflectance Index
CCRS	Canada Center for Remote Sensing
CH_4	Methane
Chl_{SPAD}	SPAD-502 Chlorophyll Arbitrary values
Chl-a	Chlorophyll-a
Chl-ab	Chlorophyll-ab
cm	Centimeter
CO_2	Carbon Dioxide
D	Index of Agreement
DM	Dry Mass
DN	Digital Number
e	End of a Pixel Block
em	endmember
EO	Earth Observation
f	Fractional Abundance
F	Frame
$\bar{F}$	Average Curve
FOV	Field Of View
g^D	DN-to-Radiance Gain
g^O	Original Gain
G	Gain Coefficient Frame

GCP	Ground Control Point
GER	Geophysical And Environment Research
GIS	Geographic Information Systems
GNDVI	Green Normalized Difference Vegetation Index
GMT	Greenwich Mean Time
GPS	Global Positioning Systems
GSD	Ground Sample Distance
H	Similar Spectra
H_2O	Water
hNDVI	Hyperspectral Normalized Difference Vegetation Index
i	Line
I	Independent
ID	Identical
IHARF	Indian Head Agricultural Research Foundation
ISDAS	Imaging Spectrometer Data Analysis Systems
j	Column
k	Spectral Band
km	Kilometer
kg	Kiogram
l	Neighboring Band
L	Spectral Band Dimension
LA	Leaf Area
LAI	Leaf Area Index
LR	Linear Regression
LUT	Look Up Table
m	Meter
M	Along-track Dimension
MCARI	Modified Chlorophyll Absorption in Reflectance Index
MD	Mean Difference
MODIS	Moderate-Resolution Imaging Spectroradiometer
n	Sample size

$n_{i,j,k}$	Noise
N	Across-track Dimension
N_f	Noise Floor
N_o	Normally Distributed
NASA	National Aeronautics and Space Administration
NDPI	Normalized Difference Pigment Index
NDVI	Normalized Difference Vegetation Index
nm	nanometer
NPCI	Normalized Pigment Chlorophyll Index
N-P-K	Nitrogen-Phosphorous-Potassium
o^D	DN-to-Radiance Offset
o^O	Original Offset
O_2	Oxygen
O_3	Ozone
OSAVI	Optimized Soil Adjusted Vegetation Index
P	Pixel Block Number
PAR	Photosynthetically Active Radiation
PC	Principal Component
PCA	Principal Component Analysis
ppm	Part Per Million
PRI	Photochemical reflectance Index
PSND	Pigment Specific Normalized Difference
PSSR	Pigment Specific Simple Ratio
PS-I	Photosystem I
PS-II	Photosystem II
r	Reflectance
re	Reference Reflectance
r_{EQ}	Envelope Quotient
r_{ref}	Reflectance at a Reference Wavelength
r_{sc}	Reflectance of the Vegetation Spectrum at a Band c
r_{ec}	Reflectance of the Envelope at a Band c

R^2	Coefficient of Determination
RARS	Ratio Analysis of Reflectance Spectra
RMSE	Root Mean Square Error
ROI	Region of Interest
RT	Radiative Transfer
s	Start of a Pixel Block
S	Spectrum
$\bar{S}$	Average Spectrum
SAIL	Scattering by Arbitrary Inclined Leaves
SAVI	Soil Adjusted Vegetation Index
SIPI	Structure Insensitive Pigment Index
SMA	Spectral Mixture analysis
SNR	Signal to Noise Ratio
SLA	Specific Leaf Area
SLR	Simple Linear Regression
SRPI	Simple Ratio Pigment Index
SRVI	Simple Ratio Vegetation Index
STD	Standard Deviation
SWIR	Short-wave infrared
TCARI	Transformed Chlorophyll Absorption in Reflectance Index
USGS	United States Geological Survey
V	Radiance Cube
$\bar{V}$	Average Radiance
VNIR	Visible Near-infrared
X	Independent Variable
$\bar{X}$	Mean Value of X
X'	Difference between X and Observed Value
X_E	Average of Estimated Value
X_M	Average of Measured Value
Y	Dependent Variable

$\bar{Y}$	Mean Value of Y
Y'	Difference between Y and Observed Value
$\hat{Y}$	Predicted Value
λ	Wavelength
λ_{re}	Red-edge Inflection point
λ_0	Wavelength at Minimum
δ	Shape Parameter
μg	Microgram
α	Intercept
$\hat{\alpha}$	Estimator of α
β	Slope
$\hat{\beta}$	Estimator of β
ε	Error
σ^2	Variance
σ_E	Standard Deviation of Estimated Value
σ_M	Standard Deviation of Measured Value

Chapter 1
Introduction

1.1. Introduction

Photosynthetic pigments are integrally related to the physiological functions of the plant leaf. Chlorophyll is one of the key photosynthetic pigments that controls the reflectance properties of the leaf. The main function of chlorophyll is to absorb light and transfers it to the photosynthetic process. When plants are under stress or during leaf senescence, chlorophyll tends to decline more rapidly than the other pigments. This variation in chlorophyll content results in changes of leaf optical properties. Thus, it may provide valuable information about the physiological performance of leaves (Gitelson and Merzlyak, 1994). The estimation of plant chlorophyll content, along with other biochemical and biophysical indicators related to plant growth and development, plays a major role in agricultural production.

The modernization of agricultural production has undergone changes both in philosophy and technology. These changes have brought increases in crop productivity and profitability for farmers. Increased production has come largely due to application of agricultural inputs such as chemical fertilizers, pesticides / herbicides, improved agricultural practices, new crop varieties, and proper irrigation systems in order to increase the overall fertility of soil. Besides the increased agricultural production, farm managers / producers have observed variations in crop yield and productivity within agricultural fields. These variations are often related to differences in soil fertility and crop stress conditions. Farm managers / producers generally make decisions regarding these variations based on average conditions within those agricultural fields.

Accordingly, the fields are often treated as one homogeneous unit with uniform agricultural inputs.

Precision agriculture also known as site-specific crop management can be viewed as a cyclic process of within-field data collection, data analysis, optimum decision-making, variable rate application, and estimation of crop yield (Moran *et al.,* 1997). The main objectives of precision agriculture are to increase the productivity, optimize the yield, and protect the environment. The estimation of crop chlorophyll content has a potential for use in early detection of crop stress, health condition, nitrogen content, early yield prediction, and as an input into crop growth models. Traditional methods of the estimation of plant chlorophyll content, through extraction or spectrophotometric measurements, require the destruction of the measured leaves, which is expensive, time consuming and thus makes crop stress or health assessment impractical. In contrast, remote sensing techniques to estimate chlorophyll content are nondestructive, rapid, and can be applied across large areas (Gamon and Qiu, 1999). Predictions of crop chlorophyll content or other biochemical and biophysical parameter from field, airborne or satellite canopy reflectance can be carried out through different methodologies, such as:

(1) Statistical relationships between ground measured biochemical data (using handheld chlorophyll meter or laboratory measured chlorophyll content) and canopy measured reflectance (Johnson *et al.,* 1994).

(2) Applying leaf-level relationships derived between spectral indices and the chlorophyll content directly to canopy measured reflectance (Peterson *et al.,* 1988).

(3) Approaches to estimate leaf and canopy-level chlorophyll content using physical models.

Developments of new sensors have opened up the possibility to study in detail the interaction of solar radiation with surface features. Based on field, laboratory and aircraft measurements, it has been long recognized that high spectral resolution (i.e., hyperspectal) remote sensing data have the potential to provide more accurate estimates of crop bioindicators than broadband data (Goetz, 1984). Broadband sensors collect data in a few bands, each covering a large portion of the electromagnetic spectrum. For example, the Landsat 7 has seven bands with bandwidths larger than 60 nanometer (nm). The significant advantages of hyperspectral sensors over the multispectral sensors are narrow contiguous bands (i.e., 10 –15 nm wide). Much more detailed spectra from hyperspectal data make it possible to detect differences in shape and resolve absorption features, which allow to distinguish different target materials and to extract quantitative information for crop management. For example, hyperspectral remote sensing techniques have opened up new possibilities of quantifying individual photosynthetic pigments within plants. Since the changes in optical properties of plant leaves are based on cellular level processes, the estimation of these can only be done using narrow band sensors. This information helps to assess crop stress, estimate crop productivity, and discriminate crop species (e.g., weed infestation). More importantly, many techniques were developed to extract quantitative information on crop productivity and crop stress using hyperspectral data. Therefore, a growing need to manage agricultural operations more efficiently and profitably required a sensor with higher spectral and spatial resolution. The 220-band

Hyperion sensor on the EO-1 platform, launched in November 2000, was the start of civilian hyperspectral data acquisition from space (Staenz *et al.,* 2002).

Nowadays, there is an increased interest in site-specific crop management and the development of advanced systems for sustainable agriculture. Information is valuable when it leads to management decisions for seasonally stable and variable crop conditions and the cause of within-field variability with respect to the achievement of more sustainable and efficient agricultural practices. In this context, hyperspectral remote sensing techniques can play a very important role to provide quantitative information on biophysical and biochemical characteristics of a plant canopy. These techniques are increasingly identified as relatively inexpensive for site-specific crop management (Moran *et al.,* 1997; Daughtry *et al.,* 2000). Hyperspectral remote sensing techniques are found to be an alternative to conventional sampling methods. Many studies and experiments demonstrated the usefulness and feasibility of remote sensing to address various agricultural issues, such as crop classification and mapping, crop yield predictions, crop status and condition, land use/land cover, soil properties, soil inventory, and nutrient deficiency (Goetz, 1984; Moran *et al.,* 1997; Daughtry *et al.,* 2000).

Very little work has been done for the wheat (*Triticum aestivum*) crop canopy chlorophyll content estimation using hyperspectral remote sensing techniques. Therefore, the estimation of chlorophyll content at the leaf and canopy scale using hyperspectral remote sensing data is the main objective of this study.

1.2. Objectives

The main goal of this thesis is to examine the potential for chlorophyll content estimation for the wheat crop-canopy using hyperspectral remote sensing data in the context of precision agriculture. The objectives are stated as follow:

i. To investigate the correlation between leaf chlorophyll content derived from SPAD-502 measurements and laboratory-extracted chlorophyll content.

ii. To examine the relationship between estimated chlorophyll content derived via spectral chlorophyll indices from GER-3700 spectroradiometer data and measured chlorophyll content in the laboratory.

iii. To examine the relationship between estimated chlorophyll content derived via spectral chlorophyll indices from Hyperion hyperspectral data and ground measured chlorophyll content.

iv. To find the best chlorophyll index for both GER-3700 and Hyperion hyperspectral data.

1.3. Hypotheses

The following are the main hypothesis of this study.

i. SPAD-502 measured arbitrary chlorophyll content should be correlated with laboratory extracted chlorophyll content. The relationship should be strong for wheat to establish a calibration equation for converting SPAD-502 readings into chlorophyll content estimates.

ii. Leaf chlorophyll content derived from GER-3700 data using spectral chlorophyll indices should be correlated with ground leaf chlorophyll content.

iii. Crop canopy chlorophyll content estimated from Hyperion data using spectral chlorophyll indices should be correlated with measured leaf chlorophyll content.

iv. The Hyperion hyperspectral data should be suitable for chlorophyll estimation in the context of precision agriculture.

1.4. Thesis structure

Chapter 1 presented the introduction and problematic of the thesis. Objectives and hypotheses were also defined in the previous sections. The thesis will then follow with review of how Chlorophyll content can be used and integrated into crop management, the current status of chlorophyll content estimation using direct and remote sensing techniques and how hyperspectral remote sensing can contribute to chlorophyll content estimation (Chapter 2). The third chapter describes the experimental methods and materials used for the investigation of the chlorophyll content. The experimental results are discussed in chapter 4. Finally, the conclusions and recommendations for further research are described in chapter 5.

Chapter 2
Measurements of Crop Chlorophyll Content for Precision Agriculture

2.1. Introduction

This chapter will provide a brief overview of the literature on the characterization of plant chlorophyll content and plant stress condition. The first part will confine the role of remote sensing to retrieve crop chlorophyll content. The second and third part will focus on main plant photosynthetic pigments and optical properties of plants, respectively. The fourth part will then discuss the measurements and characterization of plant chlorophyll content using optical remote sensing.

2.2. Precision Agriculture and Remote Sensing of Crop Chlorophyll Content

Remote sensing data along with geographic information systems (GIS) and global positioning systems (GPS) can provide an integrated approach to assist farm managers / producers to manage their farms more efficiently. This integrated approach results in valuable spatial and temporal information, which can play a very important role in measuring and assessing the soil and crop status at specific critical times. These can be divided in to two main crop growth stages (Haboudane *et al.*, 2002):

- Firstly, the early growth stages in which supply of adequate fertilizer quantities is important to obtain normal growth, and
- Secondly, the advanced development stage for health monitoring is critical for crop yield prediction.

Remote sensing can play a valuable role to provide time-specific and time-critical information due to its capability in measuring biophysical and biochemical indicators and detecting their spatial variability. Most importantly in precision agriculture, remote sensing techniques have been used to assess whether crops are healthy or stressed. Assessment of sources of plant stress is an integral part of precision agriculture. This assessment could assist in planning and management, particularly if results are available in advance to take measures for conservation of crop health and productivity. Remote sensing is an important tool for the study of many field variables such as crop condition, soil physical characteristics, nutrient availability, extent of fungal, insect or weed infestation, and crop pheonlogy. These variables have an impact on the spectral signature of crop canopies.

Stress in plants can be caused by several factors that can be divided into the two main classes, natural and human induced causes. The basic idea behind crop health or stress detection is to determine the plant's physiological state. This state is reflected by its biophysical and biochemical characteristics, which results in spectral changes (i.e., absorption, reflectance and transmittance) as observed by a remote sensing device (Blackmer *et al.,* 1994). Photosynthetic pigments (Appendix I) are integrally related to the physiological functions of the leaves. Leaf chlorophyll is one of the key photosynthetic pigments that controls the reflectance properties of the leaves and is found to be one of the most important indicators of whether vegetation is stressed or healthy. Changes in the content of leaf chlorophyll as detected by a remote sensor, might be used to predict / forecast stress in plants, and could allow predictions of crop productivity.

These predictions of within-field stress can play an important role in mapping of within-season physiological stress and its integration into crop growth models.

Integration of remote sensing data into crop growth models have shown improved results in comparison to agronomy models without using remote sensing information (Moulin, 1998). The crop growth models, used to compute the potential growth of crop from emergence to maturity, describe the relationship between plant physiological processes and environmental factors such as solar irradiation, atmospheric carbon dioxide, precipitation, temperature, and nutrient availability. Crop growth models often appear to fail in operational applications for land management decision-making.

Two main limitations of these models are expensive and destructive collection of input parameters for soil and crop characteristics and lack of taking into account the spatial variability of these parameters within-fields. In this context, remote sensing data can be used to provide input parameters into these crop growth models in order to more accurately predict crop yield and to provide an improved understanding of the factors that determine crop yield. In addition, remote sensing data have the potential to enable crop growth models to take into account the within-field spatial variability (Delecolle *et al.*, 1992).

2.3. Measurements of Chlorophyll Content Using Optical Remote Sensing

Precision agriculture requires a means of determination of chlorophyll content that bears the potential for detection of physiological states and stresses in plants. Traditional techniques of measurements of plant chlorophyll content require destructive

point sampling that is costly, laborious, time consuming and provides limited spatial coverage. Remote estimation of chlorophyll content has the potential of overcoming the problems of ground-based measurements.

Many satellites launched in the last few decades provided multispectral images available for different applications used for crop management (Moran *et al.,* 1997). In the beginning, the data acquired by these sensors were used for regional crop identification, acerage estimation, crop condition assessment, and the establishment of relationships between reflectance and biophysical properties. Later on, many studies related multispectral reflectance data of crop canopies to basic physiological processes, such as photosynthesis, leaf area index (LAI), and chlorophyll content. Many vegetation indices were developed to indirectly estimate vegetation density, biomass, LAI and chlorophyll content (Bannari *et al.,* 1995). These estimated parameters, retrieved from remote sensing data, were used in precision agriculture as input to crop growth and yield models in combination with soil, crop and climate data.

The use of optical remote sensing to quantify plant photosynthetic pigment concentration works in principle similar to those used in the field of spectroscopy in analytical chemistry. Fortunately, plant pigments have distinct spectral absorption characteristics, which means potential discrimination between them is possible. It is for this reason that broadband sensor data are inadequate for resolving the finer spectral changes between different photosynthetic pigments. Blackburn (1998a and b) identified optimal wavelengths at 680 nm for chlorophyll-a, 635 nm for chlorophyll-b, and 470 nm for the carotenoids. There is little agreement found in the literature on the optimal wavelength position for photosynthetic pigments absorption features (Chapelle *et al.*,

1992; Blackburn 1998a and b). Jacquemoud and Baret (1990) indicated that wavelengths with high absorption coefficients should be more sensitive to low concentration of plant photosynthetic pigments, whereas spectral regions with low absorption coefficients are less sensitive to plant photosynthetic pigments. At leaf-level, changes in plant photosynthetic pigments concentration impact the optical properties of the leaves in two ways. First changes in concentration of these pigments affect the reflectance spectra directly, causing changes in the depth of absorption features of these pigments. Second the changes in concentration also affect the photosynthetic process by changing the light absorption, energy transfer, and electron transfer functions between the two photoreaction centers, i.e. Photosystem I & II (Zarco-Tejada, 2000). (In the chloroplast two functional units called Photosystems I & II absorb light energy. Photosystems use to power the transfer of electrons through series of compounds connecting Photosystem I with Photosystem II. Photosystem I (PS-I) is also called P700, because the center of the maximum absorption is at 700 nm, and Photosystem II (PS-II) is also called P680 with a maximum absorption at 680 nm.)

2.3.1. Methodologies for Estimation of Plant Pigment Content

The extraction of quantitative pigment concentration from airborne or satellite remote sensing data is based on three basic approaches; empirical and semi-empirical techniques, statistical approaches, and modeling or analytical approaches.

2.3.1.1. Empirical and Semi-Empirical Approaches

Empirical approaches are based on correlations between canopy-measured reflectance by a field, airborne or satellite sensor with a ground-measured variable of interest. Semi-empirical approaches have a physical basis i.e., their mathematical formulation for a variable of interest's state is related empirically to spectral data. Empirical studies at both leaf and canopy scales have three main types of spectral approaches. The first type uses the reflectance in various individual bands (Filella *et al.*, 1995; Lichtenthaler *et al.*, 1996; Blackburn 1998a and b). The second type uses spectral pigment indices both at the leaf and canopy-levels. These indices have been developed to take into account several vegetation and environmental factors, such as overlapping absorption spectra of different pigments, effects of the leaf structure, canopy structure, canopy shadow, leaf area index, and background soil reflectance (Chappelle *et al.*, 1992; Blackburn, 1999; Daughtry *et al.*, 2000; Zarco-Tejada *et al.*, 2001; Haboudane *et al.*, 2002). The third type relates the characteristics of the derivative of reflectance spectra to pigment concentrations. The first and second derivatives of reflectance spectra are more useful than the original reflectance spectra due to their ability to reduce variability caused by changes in background reflectance and illumination (Curran *et al.*, 1991). Many studies illustrated the relationship between the derivative of the red-edge reflectance and the total chlorophyll content (Horler *et al.*, 1983; Curran *et al.*, 1990; Penuelas *et al.*, 1994).

2.3.1.2. Statistical Approaches

These approaches use statistical methods to characterize parameters. For example, the stepwise multiple regression technique was used to establish relationships at leaf-level, which were applied to canopy reflectance for pigment estimation (Peterson *et al.*, 1988). This method allows the determination of relationships based on spectral indices using wavelengths where important changes in leaf reflectance correspond to specific biophysical processes, which are targeted for measurement at the canopy scale (Zarco-Tejada *et al.*, 2001).

2.3.1.3. Modeling or Analytical Approaches

The modeling or analytical approaches are based on physical models. At leaf-level, the relationship between leaf reflectance and plant biochemical constituents is not only a function of the concentration of the constituents. Leaf reflectance also depends on the leaf structure, which changes over the different stages of the plant growth. At canopy-level, the quantification of plant pigments by sensor-measured-canopy reflectance needs a link between leaf and canopy-levels, which includes the effect of canopy structure, viewing geometry, leaf structure, leaf size, leaf inclination, LAI, background soil reflectance and shadow. For this purpose, many models have been developed to estimate plant biochemical properties both at leaf and canopy-level. These models are based on the radiative transfer equation and are also known as leaf and canopy radiative transfer models. It is also found that physically based models can be truly validated, because these models can be inverted (Verstraete, 1994). An example of a leaf radiative transfer model and a canopy radiative transfer model is PROSPECT (Jacquemoud and Baret, 1990;

Jacquemoud *et al.,* 1996) and SAIL (Scattering by Arbitrary Inclined Leaves; Verhoef, 1984).

2.3.1.4. Method used for this study

The chlorophyll molecule is an important plant photosynthetic pigment and its concentration in plant leaves is one of the most important indicators of vegetation stress. Therefore, this plant photosynthetic pigment will be used in this study to predict crop stress. This work is focused on the quantitative estimation of chlorophyll from wheat crop canopy reflectance using hyperspectral remote sensing data. Many spectral chlorophyll indices have been developed using field, laboratory, and airborne hyperspectral remote sensing data to estimate chlorophyll content for different plant species. It is found that these indices, besides sensitive to chlorophyll content, are also affected by several vegetation and environmental factors, such as LAI and underlying soil reflectance (Kim *et al.,* 1994). The main objective of the index techniques is to use different combinations of spectral bands to minimize variations due to unwanted factors and maximize sensitivity with respect to chlorophyll content. Many studies and experiments have demonstrated the usefulness of these indices for chlorophyll content extraction based on the relationship existing between chlorophyll content and some specific narrow bands. In this context, hyperspectral sensors offer a better potential to analyze and to extract more specific information of target materials than the broadband sensors (Curran, 1994). Accordingly, the hyperspectral airborne and spaceborne sensors are more suitable for quantifying chlorophyll concentration or content than previous remote sensing instruments.

2.3.2. Spectral Indices related to Plant Chlorophyll Content

Over the recent years, many studies and experiments have been carried out to understand the relationship between vegetation optical properties and photosynthetic pigment concentration within tissues. These pigments have different spectral behavior with specific absorption features at different wavelengths, which allow remote sensing techniques to assess their respective effects on vegetation (Chappelle *et al.,* 1992; Blackburn, 1998a). The concentrations of these photosynthetic pigments relate strongly to the photosynthetic potential of a plant and, therefore, give an indication of its overall physiological status (Young and Britton, 1990; Blackburn and Steele, 1999). Amongst these pigments, chlorophyll-a and chlorophyll-b absorb the largest proportion of photosynthetically active radiation (PAR), which provides energy for the reaction of photosynthesis. The carotenoids protect the reaction centers from excess light and help intercept PAR as auxiliary pigments of chlorophyll-a (Blackburn, 1998b). Therefore, photosynthetic pigments are strongly related to the physiological condition of the plant and its productivity.

The spectral indices have been and are still used to extract information on vegetation biochemical and biophysical properties. These indices provide an alternative to the spectroscopic analysis of the vegetation spectrum. The development and use of these indices are often performed with empirical techniques. These indices are developed as empirical models relating directly the biochemical constituent of interest with spectral properties (Jacquemoud and Ustin, 2001).

When a plant is under stress condition, the changes in the chlorophyll concentration may be small in the initial stages. Moreover, as the stress level increases,

the chlorophyll content in the plant decreases more quickly than in the other pigments. These changes in chlorophyll content are the indicative of stress condition of a plant. Based on this idea, many chlorophyll indices have been developed to estimate the chlorophyll content from remote sensing data in different environments for different types of vegetation. A description of several spectral chlorophyll indices and related appropriate optimal wavelengths is given below.

2.3.2.1. Red-Edge Position

Thomas and Gausman (1977) demonstrated the inverse relations of the red region of the solar spectrum to the leaf chlorophyll content. The main chlorophyll-a absorption region near 675 nm has been shown to become saturated at medium to high chlorophyll contents. Horler *et al.* (1980 and 1983) discussed changes in the slope and position of the red-edge to leaf chlorophyll concentrations for a variety of species, including wheat. The wavelength position of the inflection point of the red-edge, λ_{re}, is defined as the wavelength of maximum slope. Horler *et al.* (1980 and 1983) found that for a pile of leaves, the inflection point of the red-edge was unaffected by its background. However, the effect of leaf stacking caused spectral shifts of λ_{re} towards longer wavelengths. This is known as the red shift as observed for increased chlorophyll contents of single leaves. In addition, the position and the slope of the red-edge also change with the loss of chlorophyll content towards the shorter wavelengths, this shift in the position of the red-edge is known as the blue shift (Horler *et al.*, 1980 and 1983).

Vogelmann *et al.* (1993) also found promising results from correlation of red-edge spectral parameters and chlorophyll content in sugar maple leaves affected by

intensive insect damage. The indices used in this study were λ_{re}, the ratio of the reflectance at wavelengths 740 and 720 nm (r_{740} / r_{720}), and the ratio of the first derivative values at 715 and 705 nm (d_{715} / d_{705}). The three parameters were found highly correlated with chlorophyll-a, chlorophyll-b and total chlorophyll content.

Horler *et al.* (1983) and Curran *et al.* (1990) reported that the position and slope of the red-edge is sensitive to total canopy chlorophyll content. Moreover, Demetriades and Steven (1988) found no correlation at all between the canopy red edge and chlorophyll content of crop leaves. Filella and Penuelas (1994) showed that it was difficult to separate the chlorophyll content and canopy scattering properties effects in order to find a good estimate for each parameter in case of low correlations between LAI and chlorophyll content. Penuelas *et al.* (1993) .also found, that besides chlorophyll, water stress is another factor that affects the shape of the near-infrared plateau of the reflectance curve

In the *Boreal Ecosystem-Atmosphere Study* (BOREAS) project Zarco-Tejada and Miller (1999) reported that land cover mapping, based solely on red-edge spectral parameters, appeared feasible, and for some cover classes outperformed other current classification methods. Three red-edge spectral parameters: the red-edge inflection point (λ_{re}), the wavelength at the minimum (λ_0), and a shape parameter (∂) as defined by the inverted-Gaussian red-edge curve fit model (Hare *et al.,* 1984; Miller *et al.,* 1990) were used with a land cover mapping approach based on unsupervised classification.

2.3.2.2. Photochemical Reflectance Index (PRI)

PRI was proposed by Gamon *et al.* (1992) and was developed to estimate the photosynthetic activity of canopies. This index is defined as follows:

$$PRI = (r_{Ref} - r_{531}) / (r_{Ref} + r_{531}), \quad (2.1)$$

where "r_{Ref}" is a reflectance at a wavelength to minimize complications associated with diurnal sun angle changes, and r_{531} is the reflectance at 531 nm. In many studies and experiments, the wavelength of r_{Ref} has been set to 550 nm (Gamon *et al.*, 1992) or 570 nm (Filella *et al.*, 1996). The wavelength of R_{531} has been shifted to 530 nm (Penuelas *et al.*, 1994) and then to 539 nm (Filella *et al.*, 1996). This index is a physiological reflectance index, which correlates with the epoxidation state of the xanthophylls cycle pigments (i.e., particular group of carotenoids, violaxanthin, antheraxanthin, and zeaxanthin) and with the efficiency of plant canopy's photosynthesis. The epoxidation state is the concentration of xanthophylls cycle pigments. This xanthophylls cycle may be associated with a diurnal reduction in photosynthetic efficiency (Gamon *et al.*, 1992). Therefore, the epoxidation state of the xanthophylls cycle pigments may be a useful indicator of short-term changes in photosynthetic activity. In several studies, this index showed its usefulness in the assessment of radiation use efficiency at canopy-level. Filella *et al.* (1996) showed that PRI is significantly correlated with epoxidation, zaxanthin, and photosynthetic radiation use efficiency for a cereal canopy. Penuelas *et al.* (1997) found significant results to assess photosynthetic radiation use efficiency at leaf-level in Mediterranean trees, *Quercus ilux* and *Phillyrea latifolia.* However, this relationship between radiation use efficiency and PRI at the canopy-level has not always

been confirmed in the literature (Guyot, 1990). The PRI applications at larger scales would cause problems due to various landscape compositions, atmospheric interference and instrument calibration errors.

2.3.2.3. Ratio Analysis of Reflectance Spectra (RARS)

RARS was proposed by Chappelle *et al.* (1992) for individual photosynthetic pigments, such as chlorophyll-a ($RARS_a$), chlorophyll-b ($RARS_b$), and carotenoids ($RARS_c$) concentrations in a study of individual soybean leaves. These indices for individual pigments are defined as follows:

$$RARS_a = (r_{675} / r_{700}) / (re_{675} / re_{700}), \quad (2.2)$$

$$RARS_b = (r_{675} / r_{650} * r_{700}) * (re_{650} * re_{700} / re_{675}) \quad (2.3)$$

and

$$RARS_c = (r_{760} / r_{500}) / (re_{760} / re_{500}), \quad (2.4)$$

where r is the reflectance value for any soybean leaf and re is the reference reflectance. The selection of the wavelengths for these indices represents the absorption maxima of chlorophyll-a (675 nm), chlorophyll-b (650 nm), and carotenoids (500 nm). Furthermore, they indicate that 700 nm represents the minimum of chlorophyll-a absorption and 760 nm represents where is no further absorption of PAR and the slope towards increased reflectance is at a maximum (i.e., the red edge). They found strong linear relationships between the RARS indices and chlorophyll-a, chlorophyll-b and carotenoids for

individual soybean leaves. Blackburn (1998a and b) reported that chlorophyll-a and chlorophyll-b were most highly correlated with pigment concentrations of individual leaves and bracken canopies by modifying the wavebands used in the index, for example, by substituting r_{680} for r_{635} and r_{800} for r_{700}. $RARS_c$ failed to predict the carotenoid concentrations. Blackburn & Steele (1999) also failed to improve the relationships between the RARS indices and pigment concentrations per unit ground area for matorral vegetation using such waveband modifications.

2.3.2.4. Simple Ratio Pigment Index (SRPI)

SRPI which is based on carotenoid / chlorophyll-a content was proposed by Penuelas *et al.* (1993). This index is defined as follows:

$$SRPI = r_{430} / r_{680.} \qquad (2.5)$$

Penuelas *et al.* (1995) defined SRPI as the ratio between blue (r_{430}) and red (r_{680}) reflectance for estimation of carotenoid and chlorophyll-a concentration. It was shown that carotenoid concentration provides complimentary information on canopy physiological status. However, it was often observed that there is an increase in the relative concentration of carotenoids when plants are subjected to stress (Young and Britton, 1990). Penuelas *et al.* (1993 and 1994) also found that SRPI correlates well with different levels of mite attacks in apple trees. In addition, carotenoid / chlorophyll-a ratio increases with increasing level of mite attack, whereas many reflectance indices such as the Normalized Difference Vegetation Index (NDVI) (Rouse *et al.*, 1974) or the red-edge

position were unable to distinguish among the herbicide treatments for mites. This index was found slightly sensitive at lower chlorophyll concentrations. Penuelas *et al.* (1995) also suggested that this index is empirically derived and, therefore, it might suffer from confounding effects introduced by the leaf structure.

2.3.2.5. Normalized Difference Pigment Index (NDPI)

Penuelas *et al.* (1993 and 1994) proposed NDPI in the same way as SRPI to evaluate the ratio of total pigments to chlorophyll-a. NDPI is defined as follows:

$$NDPI = (r_{\lambda 1} - r_{\lambda 2}) / (r_{\lambda 1} + r_{\lambda 2}), \qquad (2.6)$$

where λ_1 and λ_2 are the set of wavelength location tested for NDPI. The best results were obtained for $r_{\lambda 1}$ located in the wavelength range from 400-530 nm, and $r_{\lambda 2}$ in the one from 600-700 nm. This index is functionally related to SRPI as follows:

$$NDPI = (1 - SRPI) / (1 + SRPI). \qquad (2.7)$$

It was found that carotenoids and chlorophyll pigments absorb radiations in the 300 to 500-nm spectral region (Margalef, 1974). However, it is difficult to retrieve carotenoid concentrations independently from chlorophyll concentrations using reflectance measured at one given wavelength. Unlike chlorophyll, carotenoids do not absorb strongly in the red. Penuelaus *et al.* (1993 and 1994) found in sunflower and aquatic plants that the NDPI was highly correlated with the ratio between total cartenoids

and chlorophyll-a at the leaf and plant levels. Penuelaus *et al.* (1995) reported that similar to SRPI, NDPI is also empirically derived and, therefore, it might suffer from confounding effects introduced by the leaf surface and structure.

2.3.2.6. Chlorophyll Absorption in Reflectance Index (CARI)

CARI was developed by Kim *et al.* (1994) and was designed to reduce the variability of photosynthetically active radiation due to the presence of diverse non-photosynthetic materials. CARI is calculated as follows:

$$CARI=[(r_{700} - r_{670}) - 0.2 * (r_{700} - r_{550})]. \quad (2.8)$$

It uses bands corresponding to the minimum absorption of the photosynthetic pigments, centered at 550 nm and 700 nm, in conjunction with the chlorophyll-a maximum absorption around 670 nm. The choice of the 700 nm wavelength position is due to its location at the boundary between the region where vegetation reflectance is dominated by pigments absorption and the beginning of the red-edge where vegetation structural characteristics have more influence on the reflectance (Kim *et al.*, 1994). The CARI is often very sensitive to background reflectance properties and is difficult to interpret for low LAI values (Rondeaux *et al.*, 1996). Due to the sensitivity of CARI for background reflectance, Daughtry *et al.* (2000) presented the Modified Chlorophyll Absorption in Reflectance Index (MCARI) as follows:

$$MCARI = [(r_{700} - r_{670}) - 0.2 * (r_{700} - r_{550})] * (r_{700} / r_{670}). \quad (2.9)$$

The main change from CARI is the introduction of the ratio (r_{700} / r_{670}) to minimize the combined effect of the underlying soil reflectance and the canopy non-photosynthetic materials. This ratio is the slope of the spectrum when the canopy contains no green biomass (Daughtry *et al.,* 2000). Even though this index was developed to be both responsive to chlorophyll variations and resistant to non-photosynthetic materials effects, Daughtry *et al.* (2000) reported that MCARI is still influenced by various parameters, such as LAI, chlorophyll, LAI-chlorophyll interaction and the background reflectance. Haboudane *et al.* (2002) also found that MCARI showed sensitivity limitation at low pigment concentrations in a study of chlorophyll estimation of corn.

As leaf reflectance plays a vital role in assessing the individual plant's condition, canopy reflectance is required for assessing the spatial variability of crop conditions in fields. Many factors complicate the transition from leaf to canopy reflectance. Therefore, the shape of the canopy reflectance results from a complex interaction between pigment concentrations, canopy structural development and in some respects the underlying soil contribution. In order to overcome this problem for accurate assessment of crop chlorophyll content from remote sensing data, Daughtry *et al.* (2000) suggested that the intrinsic index MCARI be combined with a soil line vegetation index like OSAVI (*Optimized Soil-Adjusted Vegetation Index*; Rondeaux *et al.,* 1996). In the same study of corn leaf chlorophyll estimation, both at the leaf and canopy scale, Daughtry *et al.* (2000) presented the MCARI / OSAVI Ratio Index. The OSAVI is a variation of SAVI (*Soil Adjusted Vegetation Index*; Huete, 1988). The OSAVI attempts to minimize brightness-related soil effects by considering first-order soil vegetation interaction by means of a

soil-adjustment parameter, which usually depends on the vegetation amount and has to be empirically determined. OSAVI is defined as follows:

$$OSAVI = [(1 + 0.16) * (r_{800} - r_{670})] / (r_{800} + r_{670} + 0.16). \quad (2.10)$$

Combining these spectral indices will further reduce background reflectance contributions and enhance the sensitivity to leaf chlorophyll content variability at the same time. Daughtry *et al.* (2000) found that the MCARI / OSAVI ratio index was linearly related to leaf chlorophyll concentrations over a wide range of foliage cover of corn (*Zea mays L.*) and background reflectance. The combined use of spectral indices MCARI and OSAVI was successful in producing accurate assessment of crop chlorophyll concentrations from remote sensing data (Daughtry *et al.*, 2000). However, this combination was not implemented for predictive purposes, nor have further developments dealt with LAI effects on pigment content estimation from canopy reflectance measurements.

Haboudane *et al.* (2002) presented another variation of CARI, the *Transformed Chlorophyll Absorption in Reflectance Index* (TCARI). This index is defined as follows:

$$TCARI = 3 * [(r_{700} - r_{670}) - 0.2 * (r_{700} - r_{550})] * (r_{700} / r_{670}). \quad (2.11)$$

The main reason to develop TCARI was to improve its sensitivity at low chlorophyll values of corn crop. However, this index is sensitive to the underlying soil reflectance properties, particularly for low LAI.

In the same study of integrated narrow-band indices for corn crop chlorophyll prediction, Haboudane *et al.* (2002) proposed the TCARI / OSAVI ratio index. The use of this ratio enables accurate predictions of corn chlorophyll content from hyperspectral remote sensing imagery. Haboudane *et al.* (2002) scaling-up relationship was established to make chlorophyll estimations as a function of TCARI / OSAVI derived from above canopy reflectance data. The ratio was found to be relatively insensitive to canopy cover variations, even for very low LAI values. The best fits were obtained for logarithmic and polynomial functions with a coefficient of determination exceeding 0.98.

However, Kneubuhler (2002) found that the use of the TCARI / OSAVI ratio was not successful to track leaf chlorophyll content for spring wheat and winter barley. He reported that this index involved spectral data of the transitional region between the visible and near infrared part of the electromagnetic spectrum, where multiple scattering within the canopy becomes an important factor affecting the reflectance.

2.3.2.7. Structure Insensitive Pigment Index (SIPI)

SIPI was proposed by Penuelas *et al.* (1995) with the aim of assessing the pigment ratio for a wide range of leaves from several species (maize, wheat, tomato, soybean and sunflower) and conditions with high spectral resolution spectroradiometers. They established an empirical estimation of the carotenoid / chlorophyll-a ratio. This index is defined as follows:

$$SIPI = (r_{800} - r_{445}) / (r_{800} - r_{680}). \qquad (2.12)$$

They found that SIPI provided the best estimate for a range of individual leaves of different species and conditions. A near infrared band (r_{800}) was incorporated into the index to minimize the confounding effects of leaf structure. The r_{680}-nm and r_{445}-nm bands correspond to the absorption maxima of chlorophyll-a and carotenoids, respectively. These wavelengths were selected empirically. Blackburn (1998a) confirmed that SIPI has a curvilinear relationship with the carotenoids-chlorophyll-a ratio, which is best described using a logarithmic model (i.e., this model gives the highest coefficient of determination). SIPI lacks sensitivity for low values of the carotenoids-chlorophyll-a ratio, and becomes more sensitive for higher values.

2.3.2.8. Normalized Pigment Chlorophyll Ratio Index (NPCI)

NPCI was proposed by Penuelas *et al.* (1994) in a study related to nitrogen and water in sunflower leaves, which are related to the plant physiological changes. This index is defined as follows:

$$NPCI = (r_{680} - r_{430}) / (r_{680} + r_{430}). \qquad (2.13)$$

NPCI varies with total pigment / chlorophyll concentration and is associated with plant physiological status. Carotenoid pigments have absorption maxima in the 300-500 nm regions and, therefore, contribute together with chlorophyll to the observed absorption in the visible wavelengths shorter than the green. However, unlike chlorophyll, carotenoids do not absorb strongly in the red region. Therefore, NPCI is sensitive to the proportion of total photosynthetic pigments to chlorophyll, particularly

applicable to nitrogen stress (Penuleas *et al.,* 1994). Plants under nitrogen limitation develop greater concentrations of carotenoids relative to chlorophyll. This may be related to the protective effects of carotenoids under condition of excess radiation or to the greater persistence of carotenoids relative to chlorophyll in senescing leaves (Penuelas *et al.,* 1994).

2.3.2.9. Green Normalized Difference Vegetation Index (GNDVI)

GNDVI was developed by Gitelson *et al.* (1996) using a green band in a study related to the remote sensing of global vegetation using EOS-MODIS data (*Earth Observing Systems-Moderate Resolution Imaging Spectroradiometer*). This index is defined as follows:

$$GNDVI = (r_{801} - r_{550}) / (r_{801} + r_{550}). \qquad (2.14)$$

The development of this index was based on the idea that an index for chlorophyll estimation should be invariant with respect to pigments other than chlorophyll and should not be influenced by other factors. Therefore, the GNDVI uses those spectral bands where only one dominant factor is present. Gitelson *et al.* (1996) reported that the reflectance near 670 nm was almost pigment concentration independent for chlorophyll-a. The lowest variation of reflectance took place both in the near infrared above 750 nm and in the blue below 500 nm. There are no bands near 700 nm among the spectral bands of the MODIS sensor, but a spectral band centered at 550 nm does exist. Accordingly, they used the spectral band at 550 nm for their study. This index was found to be much

more sensitive to the chlorophyll concentration in a wide range of chlorophyll variations than the original NDVI.

Blackburn (1999) reported that there is a curvilinear relationship between GNDVI and total chlorophyll concentration. He used GNDVI in a laboratory experiment using stacks of leaves, obtained from four species of deciduous trees at various stages of senescence. However, he observed that over the wide range of chlorophyll concentrations, which can be experienced at the canopy scale, GNDVI was found only sensitive to low concentrations. The use of a narrow green band, r_{550}, rather than r_{Green} (reflectance in the range of 540-570 nm) in the formulation of this index did not improve the relationship with chlorophyll total concentration. However, no relationship was found between matorral vegetation canopy chlorophyll concentrations per unit ground area and GNDVI (Blackburn, 1999).

2.3.2.10. Pigment Specific Simple Ratio (PSSR)

PSSR was developed by Blackburn (1998a) for individual pigments chlorophyll-a ($PSSR_a$), chlorophyll-b ($PSSR_b$), and carotenoids ($PSSR_c$) concentrations at the leaf scale, using samples from deciduous trees at various stages of senescence. These indices are defined as follows:

$$PSSR\ (a) = r_{800} / r_{680}, \qquad (2.15)$$

$$PSSR\ (b) = r_{800} / r_{635}, \qquad (2.16)$$

and

$$PSSR\ (c) = r_{800} / r_{470}. \qquad (2.17)$$

The basis of this approach was also to develop a simple spectral index for each pigment of interest, using a similar structure to that of the *Simple Ratio Vegetation Index* (SRVI) (Pearson and Miller, 1972). PSSR itself is a measure of the overall depth of the chlorophyll absorption feature. Each index uses a near-infrared band centered at 800 nm, which was used to minimize the effects of radiation interactions at the leaf surface and in the internal structures in the mesophyll as suggested by Penuelas *et al.,* (1995). (Mesophyll is a plant cell found in leaves, whose primary function is to house the machinery of photosynthesis. These cells are located between the upper and lower leaf epidermal layer.) The wavelengths 680 nm, 635 nm, and 470 nm are used for absorption maxima of chlorophyll-a, chlorophyll-b, and carotenoids content, respectively (Blackburn, 1998b). In his initial study, the first two indices were found to have a strong relationship with chlorophyll-a and chlorophyll-b, respectively. However, the third index failed to predict carotenoid concentrations in individual leaves of four deciduous tree species at various stages of senescence. In another experiment of matorral vegetation canopy Blackburn (1999) reported that $PSSR_a$ has a reasonably strong linear relationship with chlorophyll-a concentration per unit ground area. However, this relationship is much weaker for low concentrations. Weaker linear relationships were also found between $PSSR_b$ and chlorophyll-b concentration per unit ground area and $PSSR_c$ and carotenoid concentration per unit ground area. McNairn *et al.* (2001) reported the same conclusions for chlorophyll-a estimates for corn and beans using two optimal wavelengths located at 810.4 and 676.0 nm.

Kneubuhler (2002) found that both $PSSR_a$ and $PSSR_b$ involve spectral data of the transitional region between the visible and the near-infrared part of the electromagnetic spectrum, where multiple scattering within the canopy becomes an important factor affecting the reflectance. The wavelength used for the absorption maximum of chlorophyll-a was 675 nm. Kneubuhler (2002) also showed that the main chlorophyll-a absorption feature, located around 675 nm, represents a reflectance minimum, above which the strong increase in reflectance, known as the red edge, occurs.

2.3.2.11. Pigment Specific Normalized Difference (PSND)

PSND was also proposed by Blackburn (1998a) in the same study as mentioned in section 2.5.2.10. Indices are defined for individual pigment chlorophyll-a ($PSND_a$), chlorophyll-b ($PSND_b$), and carotenoids ($PSND_c$) concentrations as follows:

$$PSND_a = (r_{800} - r_{680}) / (r_{800} + r_{680}), \quad (2.18)$$

$$PSND_b = (r_{800} - r_{635}) / (r_{800} + r_{635}), \quad (2.19)$$

and

$$PSND_c = (r_{800} - r_{470}) / (r_{800} + r_{470}). \quad (2.20)$$

This set of indices possesses a structure similar to that of NDVI. It incorporates a near infrared band that uses the pigment absorption maxima suggested by Chappelle *et al.* (1992). In this way, the indices provide a measure of the depth of the pigment absorption features in leaf spectra relative to the highly reflective near-infrared plateau. Like the

PSSR indices, the $PSND_a$ and PSNDb were found to have a strong exponential relationship with chlorophyll-a and chlorophyll-b, respectively. However, $PSND_c$ failed to predict carotenoids concentrations in individual leaves of four deciduous tree species at various stages of senescence (Blackburn, 1998b). Blackburn (1999) found that these indices are less correlated with matorral vegetation canopy pigment concentrations per unit ground area than in his previous studies (Blackburn, 1998 a and b). The author suggested that this is due to variable background conditions and structural/spectral complexity of the study sites.

2.3.2.12. Hyperspectral Normalized Difference Vegetation Index (hNDVI)

NDVI is the most commonly used index for multispectral remote sensing applications. NDVI was proposed by Rouse *et al.* (1974) and was used in various regional and global applications for studying the state of vegetation (Tucker, 1979; Deblonde and Cihlar, 1993).

Oppelt and Mauser (2004) used hNDVI in a study of monitoring physiological parameters of wheat, which is defined as follow:

$$hNDVI = (r_{827} - r_{668}) / (r_{827} + r_{668}). \qquad (2.21)$$

They found hNDVI and OSAVI become insensitive at chlorophyll content below 0.3 gm/m^2 as well as above 1.5 gm/m^2.

2.3.2.13. Chlorophyll Absorption Integral (CAI)

CAI was proposed by Oppelt and Mauser (2001) for chlorophyll content of maize (*Zea mays*) derived from *Airborne Visible Near-infrared Imaging Spectrometer* (AVIS) data. CAI estimates chlorophyll content by measuring the area between a straight line connecting two points of the red edge and the curve of the red edge itself as shown in Figure 2.1.

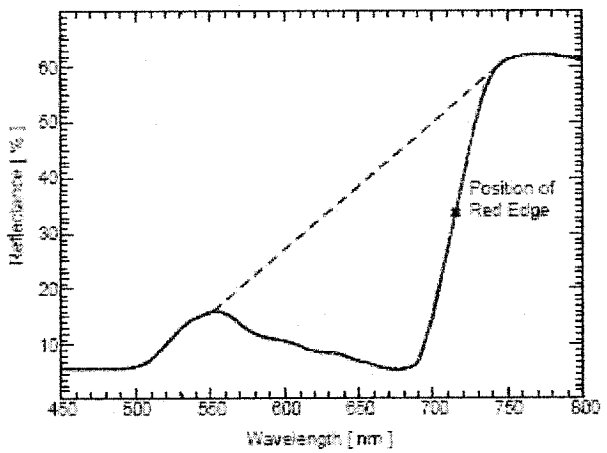

Figure 2.1: Principle of CAI measurement proposed by Oppelt and Mauser (2001).

The two points can be selected interactively and CAI is defined as follows:

$$CAI = \int_{r_{600}}^{r_{735}} r_{EQ}, \tag{2.22}$$

where r_{735} and r_{600} are the reflectance at 735 nm and 600 nm, respectively. r_{EQ} is the envelope quotient, which is calculated as:

$$r_{EQ} = r_{Sc} / r_{ec}, \tag{2.23}$$

where r_{Sc} is the reflectance of the vegetation spectrum at band c and r_{ec} is the reflectance of the envelope at band c. The vegetation spectrum for CAI calculation was retrieved from the unmixing technique.

Oppelt and Mauser (2001) found CAI to be a good predictor for the wheat canopy chlorophyll content, but they suggested that different chlorophyll levels of the wheat crop varieties has to be taken into consideration.

2.3.3. Selected Spectral Indices for Chlorophyll Estimation

Considerable studies and experiments have been undertaken in the search for spectral indices for accurate chlorophyll estimation from hyperspectral remote sensing data. Blackburn and Steele (1999) reported that empirical studies at both leaf and canopy scales have indicated that three broad types of spectral approaches may have some use for predicting plant pigment concentrations and all rely upon the reflectance in narrow spectral bands. The first approach uses the reflectance in various individual narrow bands. The second approach, using ratios of reflectance in narrow bands, has been proposed as a method to solve the problems with respect to the overlapping absorption spectra of different pigments and the effects of leaf structure, leaf surface interactions, and canopy structure. The third approach utilizes the relationship between characteristics of the first and second derivatives of reflectance spectra and pigment concentrations.

More specifically, one could conclude from the review of the spectral chlorophyll indices that not a single approach is likely to have a strong relationship with chlorophyll content under all conditions. Consequently, there is a need to evaluate the potential of

different approaches for different vegetation types and conditions. The majority of spectral chlorophyll indices discussed in previous sections were developed for crops other than wheat. Some indices were originally constructed mainly for estimating chlorophyll content at the leaf-level, while others were established at the canopy-level only. The reason to include leaf-level indices in this study is to evaluate their performance at the canopy-level.

Accordingly, the main objective of this study is to investigate the relationship between a wide range of spectral approaches and chlorophyll concentrations at the wheat canopy-level while minimizing the effects of factors, such as variations in LAI and underlying soil. A list of the selected indices based on the performance as reviewed in the previous sections is presented in Table 2.1.

Table2.1: Summary of spectral indices for chlorophyll estimation to be used for this study.

Spectral Chlorophyll Indices	Authors
$PRI = (r_{550}-r_{531}) / (r_{550}+r_{531})$	Gamon *et al.* (1992)
$SRPI = r_{430} / r_{680}$	Penuelas (1993)
$NDPI = (r_{\lambda 1} - r_{\lambda 2}) / (r_{\lambda 1} + r_{\lambda 2})$	Penuelas *et al.* (1993 and 1994)
$CARI=[(r_{700} - r_{670}) - 0.2 * (r_{700} - r_{550})]$	Kim *et al.* (1994)
$NPCI = (r_{680} - r_{430}) / (r_{680} + r_{430})$	Penuelas *et al.* (1994)
$SIPI = (r_{800} - r_{445}) / (r_{800} - r_{680})$	Penuelas *et al.* (1995)
$GNDVI = (r_{801} - r_{550}) / (r_{801} + r_{550})$	Gitelson *et al.* (1996)
$OSAVI = [(1 + 0.16) * (r_{800} - r_{670})] / (r_{800} + r_{670} + 0.16)$	Rondeaux *et al.* (1996)
$PSND_a = (r_{800} - r_{680}) / (r_{800} + r_{680})$	Blackburn (1998)
$PSSR\ (a) = r_{800} / r_{680}$	Blackburn (1998)
$MCARI / OSAVI = \frac{[(r_{700} - r_{670}) - 0.2 * (r_{700} - r_{550}) * (r_{700} / r_{670})}{[(1+0.16) * (r_{800} - r_{670})] / (r_{800} + r_{670} + 0.16)}$	Daughtry *et al.* (2000)
$hNDVI = (R_{827} - R_{668}) / (R_{827} + R_{668})$.	
$CAI = \int_{r_{600}}^{r_{735}} r_{EQ}$, where $r_{EQ} = r_{Sc} / r_{ec}$.	Oppelt and Mauser (2001)
$TCARI / OSAVI = \frac{3 * [(r_{700} - r_{670}) - \{0.2 * (r_{700} - r_{550}) * (r_{700}/r_{670})\}]}{[(1+0.16) * (r_{800} - r_{670})] / (r_{800} + r_{670} + 0.16)}$	Haboudane *et al.* (2002)

2.4. Conclusions

Plant chlorophyll content or concentration can be estimated by many methods, depending on the characteristic of the canopy under study. It is of great importance to investigate the potential of accurate models relating canopy reflectance to plant biochemical and biophysical parameters for operational use in precision agriculture. Hyperspectral remote sensing has opened up the possibility of using narrow-band reflectance indices for the estimation of plant chlorophyll content. Many indices have shown promising results in different environments and under different measurement conditions for different species other than the wheat. The objective of this study is to investigate several existing spectral indices for the quantification of chlorophyll content of the wheat crop canopy using spaceborne Hyperion data in order to determine their potential and limitations for use in precision agriculture.

Chapter 3
Methodology

3.1. Introduction

Details about the methodology of this study are presented in this chapter. It can be divided into several sections: description of the study site, data collection, preprocessing of the Hyperion data, calculation of spectral chlorophyll indices and statistical analysis. A flowchart shown in Figure 3.1 summarizes all processing steps.

3.2. Study Site

Data for this study were collected in an agricultural region near Indian Head, Saskatchewan (50°N, 104°W), east of Regina (Figure 3.2). The selected site is an intensively cultivated agricultural area. The two test fields are located on a precision agricultural farm near the *Indian Head Agricultural Research Foundation* (IHARF). Principal economic activities of this area are based on agricultural practices. Major crops grown are wheat, pea, canola, and corn. The main cereal investigated in this study is wheat, which belongs to the tribe *Tritiace* of the family *Poaceae*.

The climate of Indian Head can be regarded as typical northern continental. The summer months are characterized by hot temperatures and occasional dry periods. The winter months are cold and snowy with temperature remaining below freezing until early March. The Indian Head area is dominated by Black Chernozemic soils, which developed on neutral to slightly alkaline and uniform clayey lacustrine deposits.

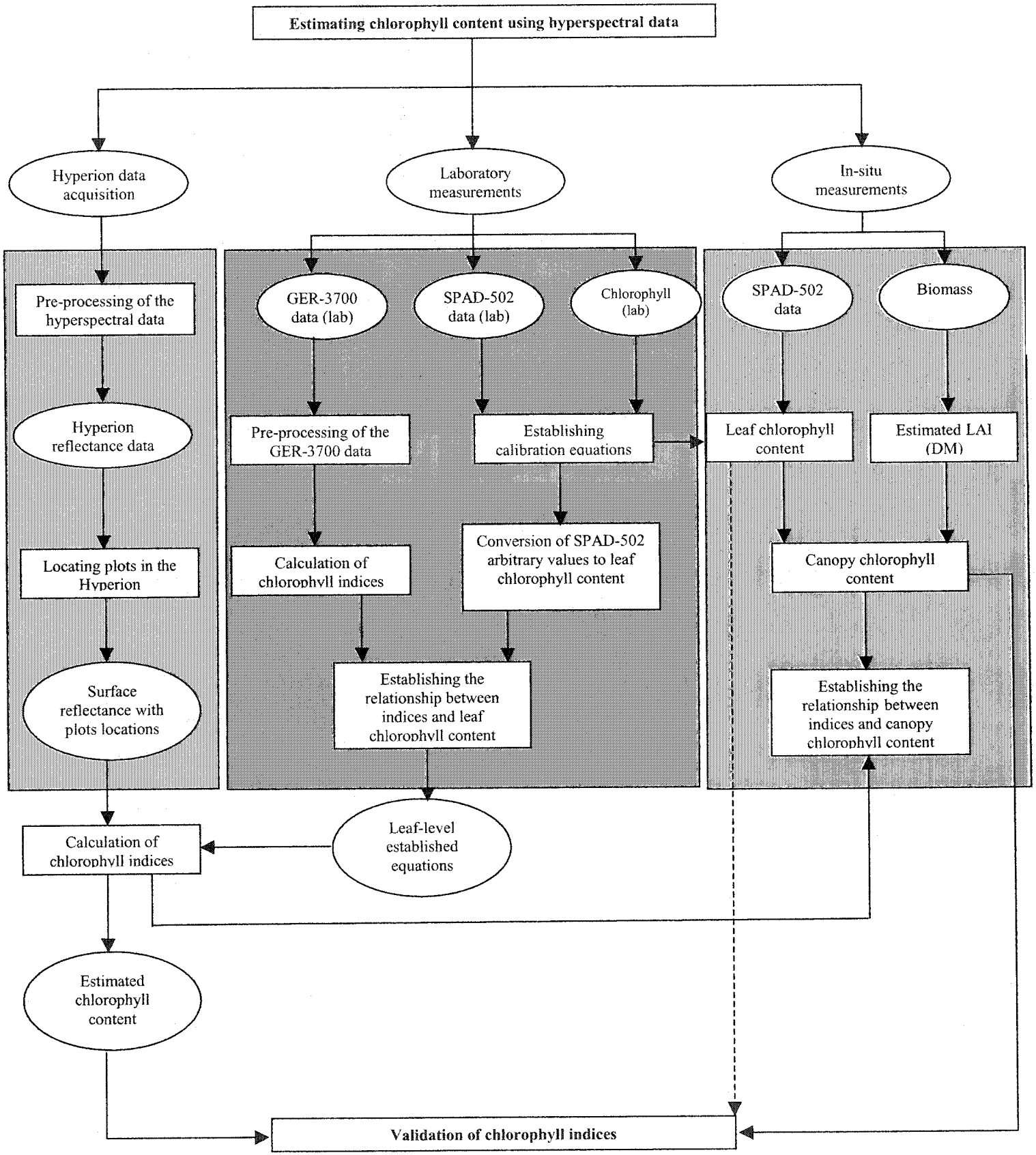

Figure 3.1: Processing sequence for the estimation of chlorophyll content from the GER-3700 and Hyperion hyperspectral data

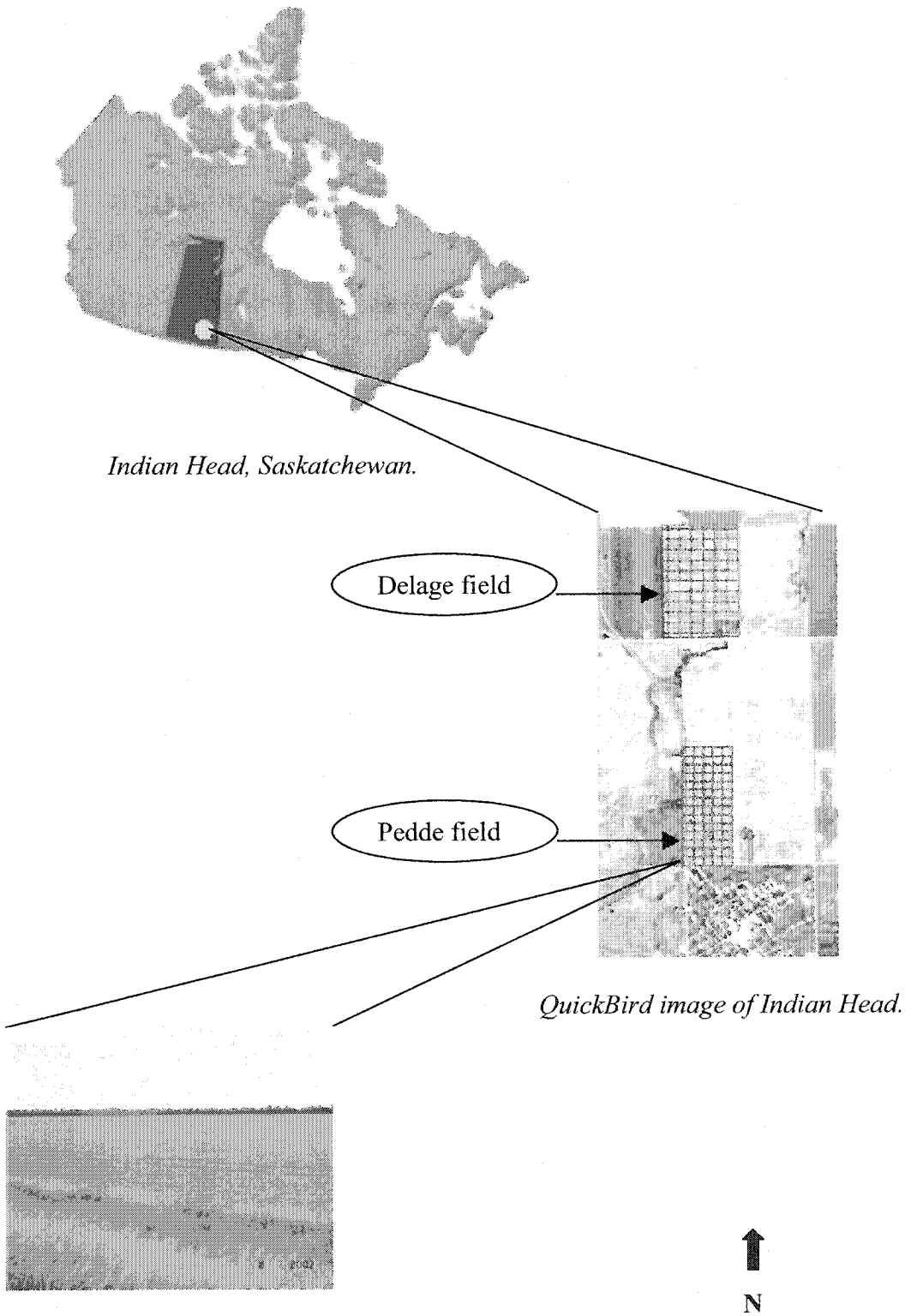

Figure 3.2: Location of the Indian Head study site.

3.3. Data Description

A standardized methodology for acquisition of data using different techniques and instruments play a very important role for a successful data collection. Two main types of available data are discussed in this section, i.e. field data and hyperspectral image data.

3.3.1. Field Data

The collection of ground data consists of various activities performed in the field during a four-week period in support of the Hyperion data acquisition. A standardized approach for laboratory analysis was carried out for the determination of various parameters, such as chlorophyll content, nitrogen content and soil moisture.

3.3.1.1. Spatial Sampling

A total of 35 plots were selected in the two test fields of wheat crop, including 16 plots from the Pedde field and 19 plots from the Delage field (Figure 3.3). The Pedde field is based on a 120-meter grid and the Delage field is based on a 150-meter grid. Each grid cell represents a plot. These plots in each field were given four types of fertilizer application. Both fields received a starter fertilization of 28-0-0 gallons/acre (Nitrogen-Phosphorous-Potassium or N-P-K). A detailed description of the fertilizer application is given in Appendix II. The plot selection from the two fields was mainly based on the idea to include at least three representatives for each distribution of fertilizer application.

Given their sizes, each of these plots was characterized by at least five measurements (samples). An X pattern strategy for the collection of these samples was carried out within about a 30-m^2 area, i.e., center, north-east, north-west, south-east, and

south-west of each plot as shown in Figure 3.4. These measurements consist of leaf chlorophyll content, crop cover, crop height, and spectral reflectance. For each sample, a characteristic area (of the sample site) was selected and overlaid with a standard sampling quadrat of 0.5 m by 0.5 m. All of the above-ground crop biomass was harvested within this area. These samples were weighed immediately after collection to obtain fresh weight.

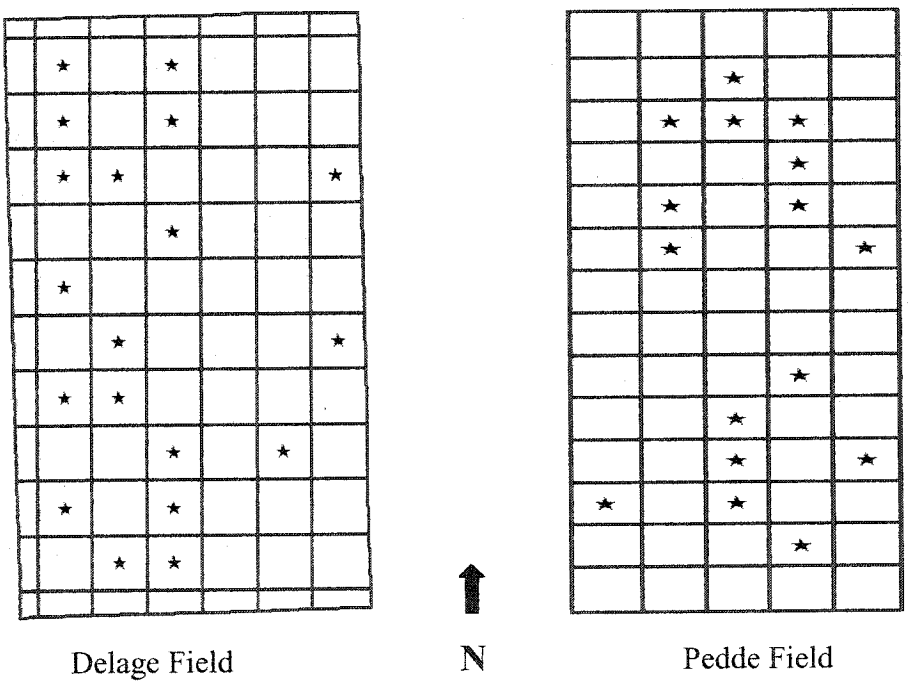

Figure 3.3: Plots layout in the Delage and Pedde fields. Each red color cell or block represents a plot and black color stars indicate the selected plots in each study field.

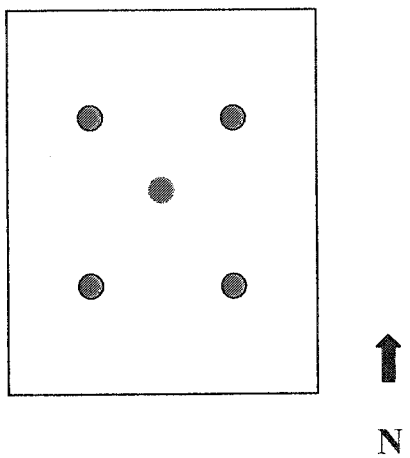

Figure 3.4: Sampling design for each plot of the Indian Head fields. The blue circle represents the sampling sites in each plot.

3.3.1.2. Chlorophyll Content Measurements

Methods have been developed to measure in-situ chlorophyll content of plant leaves, which are practical and fast, such as measuring leaf chlorophyll content with the handheld Minolta chlorophyll meter SPAD-502 (Spectrum Technologies Inc., 2001) (Figure 3.5). Leaf chlorophyll content was measured using this instrument for this study. The amount of chlorophyll per unit leaf area is a good indicator of the overall condition of plants. The meter has two diodes active at 650 nm and 940 nm, which emit red and infrared light onto the upper surface of a leaf. The light, which passes through the sample leaf, strikes the receptor. It converts this transmitted light to an analog electrical signal. This signal after amplification is converted into a digital signal by the A/D converter. A microprocessor uses this digital signal to calculate the SPAD value. This value is in arbitrary units of chlorophyll content, and is calculated as a ratio of leaf transmittance at 650 nm, which is affected by leaf chlorophyll content, and transmittance of light at 940 nm that is not sensitive to chlorophyll content and, therefore, serves as a reference. The claimed accuracy of the SPAD-502 measurements is ± 1.0 SPAD units. For this study

SPAD-502 chlorophyll measurements, which were taken from the plants outside the quadrat for logistical reasons, were collected from June 28 to July 11, 2002. About three to four healthy leaves per plant were selected for measurements. The reading from each leaf was taken 2/3 down from the leaf tip. This procedure was repeated in the same manner for other plants until at least 30 SPAD-502 measurements were acquired at each sample site.

In order to convert the SPAD arbitrary ratio (index) value to the chlorophyll (i.e., chlorophyll-a, and chlorophyll-ab) content, calibration equations were required. For this purpose, plant extracted chlorophyll content was determined in the laboratory according to the procedure described by Arnon (1949). Plant leaves were collected from the two fields and were immediately stored in bags in a cooler box for transportation of the samples from the field to the laboratory. For the chlorophyll analysis, a small piece (1cm x 1cm) from the middle of the leaf was used.

Figure 3.5: SPAD-502 instrument in-situ measurements.

3.3.1.3. Spectroradiometric Measurements

Reflectance measurements of the wheat crop canopy were performed using the GER-3700 spectroradiometer (Geophysical & Environmental Research Corp., 2002) (Figure 3.6). This instrument covers a spectral range from 350 to 2500 nm. It measures the reflectance spectra by comparing the radiance of the target with the radiance of a standard of known spectral characteristics (i.e., a Spectralon panel). The GER-3700 is a fixed grating array-based spectroradiometer. When the target's spectral radiation enters the GER-3700 instrument, it splits the beam onto three spectrometers. They cover the wavelength ranges from 350-1050 nm, 1050-1900 nm, and 1900-2500 nm.

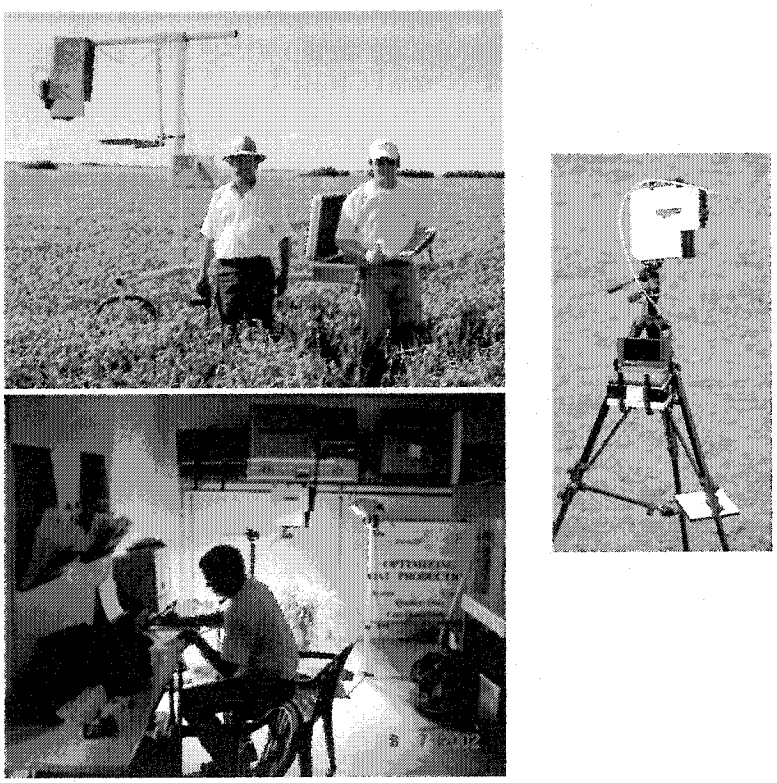

Figure 3.6: GER-3700 spectroradiometer showing laboratory and in-situ measurements.

The GER-3700 measurements were acquired at selected sampling sites simultaneously to the image data acquisition of the study site. These in-situ spectral measurements were collected only for conditions when solar illumination was appropriate (bright sunny condition). In addition, they were also carried out in the laboratory using 2 x 500 Watts Halogen floodlights.

In case of the in-situ spectral measurements, a 10^{o} foreoptic lens from a height of 1.5 m, resulting in circular field-of-view (FOV) on the ground with a diameter of 0.26 m, was used to measure spectra of the crop canopy by averaging a minimum of seven spectral measurements.

For laboratory spectral measurements, a 3^{o} FOV lens was used to measure spectra of vegetation stacks by averaging nine spectral measurements. This instrument setup provided a circular FOV on the ground with a diameter of 0.079 m from a height of 1.5 m.

3.3.2. Hyperion Data Acquisition and Sensor Parameters

3.3.2.1. Data Acquisition

Image data were acquired using the Hyperion hyperspectral sensor on NASA's Earth Observer-1 (EO-1) platform during the 2002 growing season. The acquired data sets are shown in Appendix III and details are given in Table 3.1. Data acquired on June 30, 2002 were used for this study. The data acquired on May 20 and June 21 could not be used because of the field conditions mentioned in Table 3.1. Whereas, the data acquired on July 16 and 30 could also not be utilized due to the severe cloud coverage and associated cloud shadow over the study area.

Table 3.1: Description of the hyperspectral data sets.

Data set	Date of image acquisition	Field condition	Cloud coverage
Image 1	May 20	Bare	None
Image 2	June 21	Early stage of wheat crop	None
Image 3	June 30	Heading stage of crop	5 % cloud
Image 4	July 16	Flowering stage of crop	70 % cloud
Image 5	July 23	Ripe and mature crop	40 % cloud

3.3.2.2. Hyperion Sensor Characteristics

Hyperion is a push broom imaging spectrometer that collects data in along-track direction flying. This sensor collects the upwelling radiance in 220 spectral bands, each 10-nm wide with an average of a 10-nm sampling interval. Hyperion has a single telescope and consists of two spectrographs, one covering the visible near-infrared (VNIR) wavelength range from 357 to 1055 nm, the other, the short-wave infrared (SWIR) from 851 to 2576 nm. Since Hyperion is a push broom sensor, the entire swath is obtained in a single frame. Its telescope images the Earth onto a slit with a FOV of 0.624^0, resulting in a swath width of 7.65 km from a 705 km altitude. Each data set acquired by this sensor covers a nominal along-track length of 40 km. The Hyperion sensor parameters are summarized in Table 3.2.

Table 3.2: Hyperion sensor parameters.

Launch date	November 21, 2000
Altitude	705 km
Orbit	Sun-synchronous
Repeat time	16 days
Satellite launch mass	529 kg
Atitude control	0.03 degree
Data downlink	X-band @ 150 Mb/s
Onboard data storage	40 Gbyte
Nominal area coverage	7.65 km x 40 km
Spectral range	357-2576 nm
Number of spectral bands	220
Spectral Resolution	10 nm
SNR (signal-to-noise ratio)*	
550 nm	192:1
650 nm	140:1
700 nm	140:1
1025 nm	65:1
1225 nm	96:1
1575 nm	64:1
2125 nm	38:1
GSD (ground sampling distance)	30 m
FOV	0.624^0
Roll Angle	+ / - 22 degree
Pitch	None

* SNR results were calculated from test data for seven wavelengths for a zenith angle of 60 degree and an albedo of 30 % (EO-1 / Hyperion Science Data User's Guide, 2001).

3.4. Preprocessing of the Hyperspectral Data

The hyperspectral data of the Hyperion sensor were preprocessed with an aim to correct for sensor artifacts, atmospheric and geometric effects. For extraction of accurate information and interpretation, the data needed to be corrected for these errors, which cause significant distortions in the data. Data preprocessing is an important step in correcting various types of errors in the remote sensing data. The *Imaging Spectrometer Data Analysis Systems* (ISDAS; Staenz *et al.,* 1998), a software package, developed at the *Canada Center for Remote Sensing* (CCRS), was used to perform the processing and analysis of the Hyperion data. This section is designed to go into details of the Hyperion data preprocessing. The topics to be included are the spatial and spectral alignment, destriping, noise reduction, gain/offset correction, and atmospheric correction. Figure 3.7 provides a step-by-step flow diagram of the preprocessing of Hyperion at-sensor radiance to at-surface reflectances.

Hyperion data of the Indian Head sites were already Level 1 processed by the data provider, the *United States Geological Survey* (USGS). The Level 1 process means that data was converted from digital number (DN) to radiance applying the radiometric calibration coefficients and several data correction procedures as outlined in the EO-1 / Hyperion Science Data User's Guide, 2001. The Hyperion data was first thoroughly inspected in ISDAS for various types of errors, such as stripes, pixel / column dropouts, and noise. After inspection, the data was cropped for noisy bands and the final data set spans the spectral range from 426.82 to 2355.20 nm with a total of 192 bands (excluding the overlap bands between the VNIR and SWIR spectrographs).

In a first step, the SWIR data was corrected for a single pixel offset from 129 to 256 pixels across-track (i.e., spatial shift of the left of the image). Furthermore, the first and last columns of the data set were also removed, providing an across-track swath of 254 pixels. The stripes and pixel / column dropouts were then removed from the whole cube. The noise was then reduced in the Hyperion data set. In a next step, the keystone and spectral smile / frown distortions were detected. After atmospheric correction the data was corrected for smile effects. The keystone distortion was not significant (i.e., 0.3 pixels for VNIR and 0.1 pixels for SWIR) for this image data. Most importantly, due to unavailability of distinct features and sharp edges (i.e., building corners) in this within field study work; therefore, the data was not corrected for keystone effects. The post-processing concluded the corrections by removing artifacts that still remained after the correction of sensor artifacts and atmospheric effects.

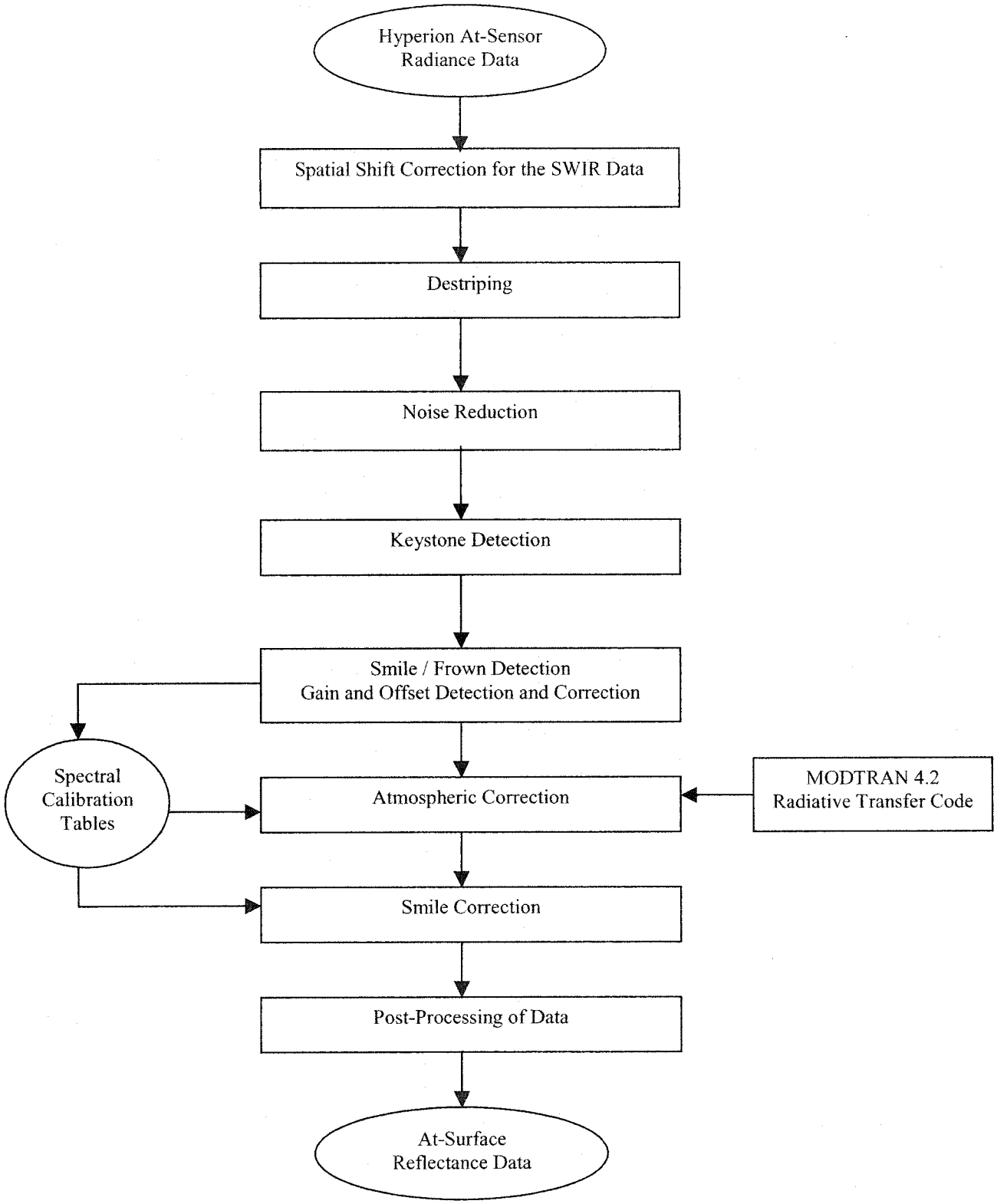

Figure 3.7: Hyperspectral data (Hyperion) preprocessing steps for retrieval of surface reflectance.

3.4.1. Spatial Shift Correction for the SWIR Data Set

A one-pixel shift (shift occurs between pixels 128 or 129) of the right half versus the left half image of the SWIR data as shown in Figure 3.8. This vertical offset is due to the different readout process for the VNIR and SWIR spectrometers and has been corrected to be able to look spectrally at the same pixel on the ground in the VNIR and SWIR.

The offset was corrected from the Hyperion at-sensor radiance data using the "Spatial Shift" tool in ISDAS. This tool simply shifts the right half of the image up by one pixel as shown in Figure 3.8.

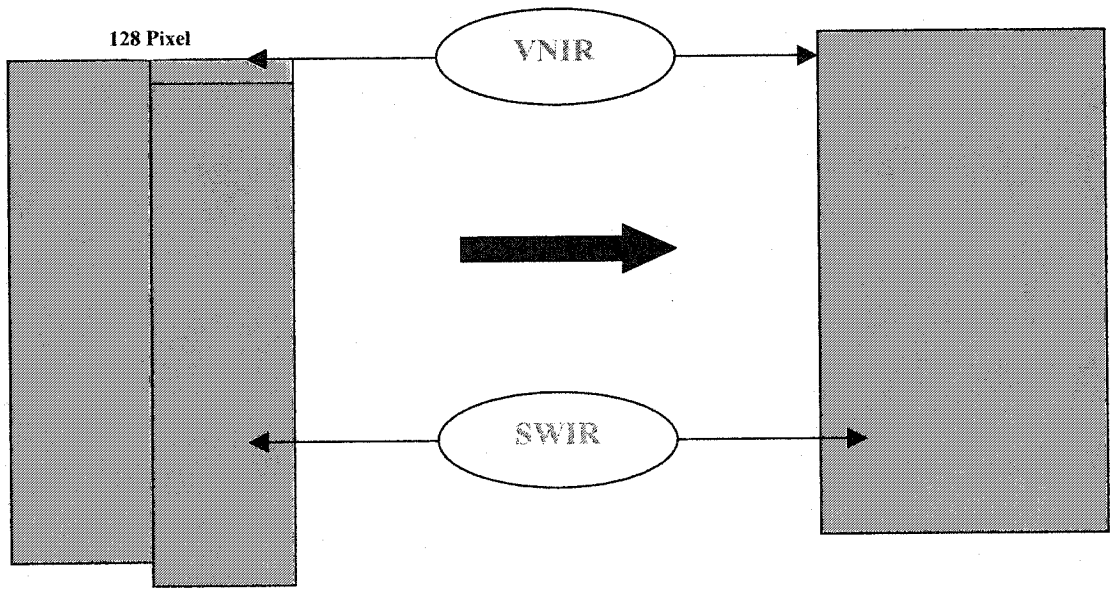

Figure 3.8: Spatial shift correction for the SWIR data.

The results of the successful spatial shift correction of the SWIR data set was verified visually by using the 'Flicker" module in ISDAS (Figure 3.9).

(a) *Before correction*

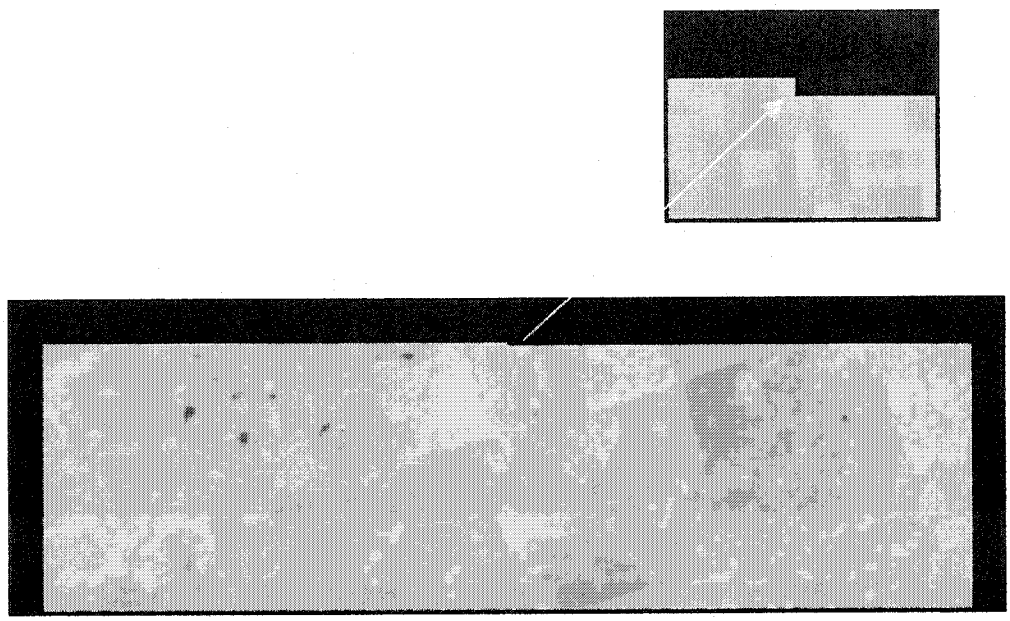

(b) After correction

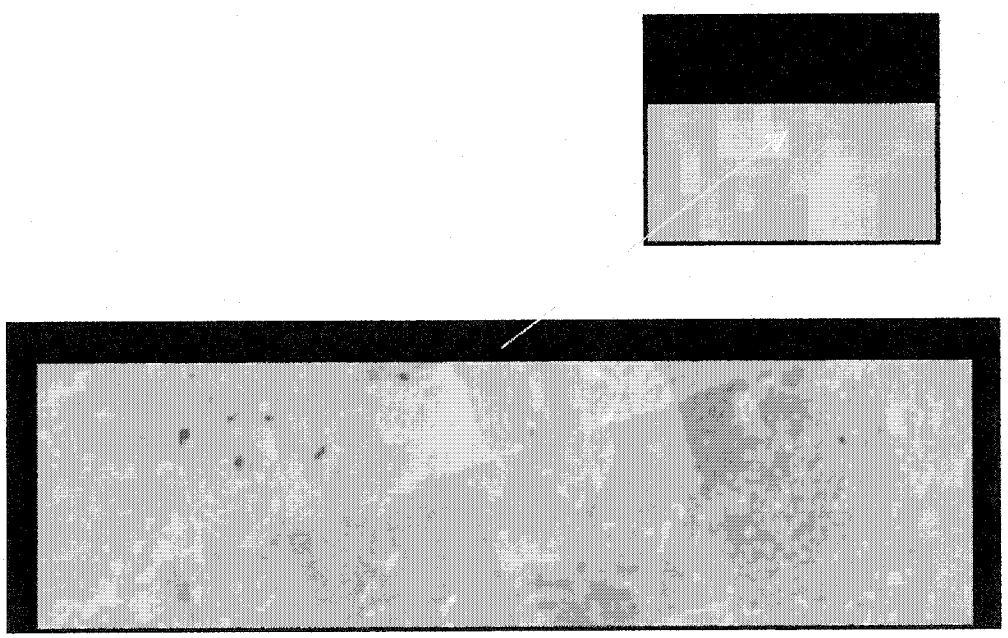

Figure 3.9: Results of the spatial shift correction of the SWIR data presented in (a) before and (b) after correction.

3.4.2. Destriping or Removal of Stripes

The stripes in the Hyperion data set are due to the systematic noise caused by factors such as detector non-linearity, movement of the slit with respect to the focal plane and temperature effects (Kruse *et al.*, 2003). When viewing single bands, stripes in the vertical direction may be noticed in Hyperion data. It was found that the VNIR data contains fewer stripes than those of the SWIR data. The column dropout or dead pixel is a functional failure of a single detector element during acquisition. These errors were also found in the Hyperion data for some bands.

The stripes and column dropouts from the Hyperion data were corrected using the "Auto-Destriping" tool in ISDAS. It uses the information from both the spatial and spectral domains to correct a specific stripe in a specific band from the radiance cube. Let V_{MxNxL} to represent a given radiance cube that will be destriped, then it can be mathematically described as follows (Sun, 2004):

$$V_{M\times N\times L} = \{v_{i,j,k} : 1 \le i \le M,\ 1 \le j \le N,\ 1 \le k \le L\}, \qquad (3.1)$$

where M is the along-track dimension, N is the across-track dimension, L is the spectral band dimension and $v_{i,j,k}$ represents the radiance of a pixel in line i of column j for a spectral band k. By averaging each pixel's column along-track, a two-dimensional frame F_{NxL} can be produced and written as follows (Sun, 2004):

$$F_{N\times L} = \{f_{j,k} : f_{j,k} = \frac{1}{M}\sum_{i=1}^{M} v_{i,j,k},\ 1 \le j \le N,\ 1 \le k \le L\}, \qquad (3.2)$$

where $f_{j,k}$ represent the average radiance of column j for a band k. If each row of $F_{N\times L}$ is represented by a vector $F_N^k = \{f_{1,k}, f_{2,k}, \cdots, f_{N,k}\}$, $F_{N\times L}$ can then be rewritten as $\{F_N^1, F_N^2, \cdots, F_N^L\}^T$. This frame $F_{N\times L}$ is the main basis for the removal of stripes from a currently processed band c with respect to several neighboring bands. If $D_{j,c} = f_{j,c} - f_{j-1,c}$ is the difference between two adjacent pixels (i.e., $j-1$ and j) in the swath of band c, the mean difference ($MD_{j,c}$) and standard deviation $STD_{j,c}$ of the two pixels over a certain number of neighboring bands (i.e., $2l$) can be calculated using the following two equations (Sun, 2004):

$$MD_{j,c} = \frac{1}{2l+1}\sum_{k=c-l}^{k=c+l} D_{j,k} \qquad (3.3)$$

and

$$STD_{j,c} = \sqrt{\sum_{k=c-l}^{k=c+l} (D_{j,k} - MD_{j,c})/2l}\,, \qquad (3.4)$$

where k is the neighboring band of the band c and l is the equal number of bands before and after the c. Similarly, the mean differences and standard deviations for all the pixels in the swath are calculated. These pixels are then grouped into a number *(P)* of pixel blocks $\mathrm{B}_c = \{Block_{p,c} : 1 \le p \le P\}$ (where p is a pixel block number) by comparing the $D_{j,c}$ to $MD_{j,c}$ and with user defined number of $STD_{j,c}$. A reference curve $\overline{F}_N^c$ is used to classify the $Block_{p,c}$ into three categories. $\overline{F}_N^c$ is the average of the column j for bands before and after band c and is given as follows (Sun, 2004):

$$\overline{F}_N^c = \{\overline{f}_{j,c} : \overline{f}_{j,c} = \frac{1}{2l+1}\sum_{k=c-l}^{k=c+l} f_{j,k},\ 1 \le j \le N\}. \qquad (3.5)$$

The three categories for the $Block_{p,c}$ are given as follows:

- A $Block_{p,c}$ belongs to without stripe pixel blocks if there is at least one intersection between $Block_{p,c}$ and $\overline{F}_N^c$.
- A $Block_{p,c}$ belongs to bright stripe pixel blocks if all swath pixels values are bigger than the corresponding values in $\overline{F}_N^c$.
- A $Block_{p,c}$ belongs to dark stripe pixel blocks if all swath pixels values are smaller than the corresponding values in $\overline{F}_N^c$.

Finally the bright and dark stripe pixel blocks are corrected by the following equation (Sun, 2004):

$$\frac{1}{2}[(MD_{s,c} - D_{s,c}) + (MD_{e,c} - D_{e,c})], \qquad (3.6)$$

where s and e are the start and end pixel of a block. The dropped-out pixels or columns are also assigned brightness values by using linear interpolation between the means of the two valid neighboring unaffected columns or pixels.

The successful correction of stripes and dropout pixels or columns from the Hyperion data is shown in Figures 3.10 and 3.11, respectively.

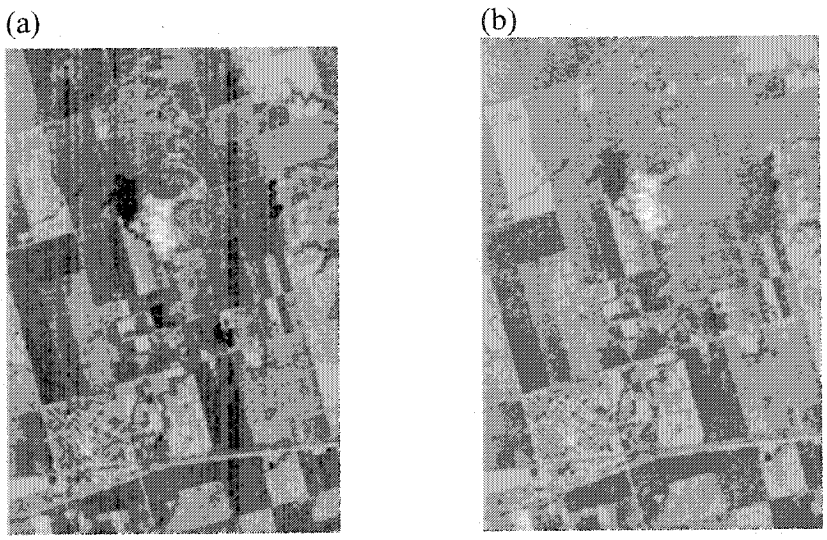

Figure 3.10: Results of the removal of along-track stripes shown for band 187 before (a) and after correction (b).

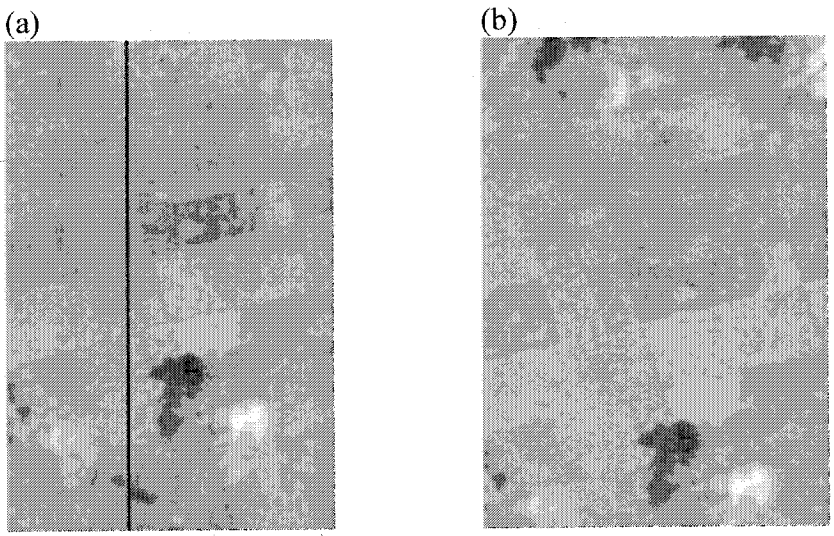

Figure 3.11: Results of the removal of dropout columns (black stripes) are shown for band 99 before (a) and after correction (b).

3.4.3. Noise Reduction

The noise reduction is an important step for improving the quality of the remote sensing data. This quality is directly related to the noise level of the sensor relative to the signal level. This is generally expressed as the SNR. Noise in a system or sensor is

caused by many factors, such as detector performance / sensitivity and noise characteristics of the electronics in the sensor. During acquisition of remote sensing data, the signal levels are affected by many factors such as atmospheric effects, solar zenith angle and surface reflectance. As an example, the SNR for the Hyperion sensor for seven wavelengths are reported in EO-1 / Hyperion Science Data User's Guide, 2001 and is given in Table 3.3. The SNR results affect the ability to extract information.

The tool "Average-Smooth" was used in ISDAS to reduce noise for the Hyperion data. The approach uses the DN-to-radiance gain coefficient frame (G_{NxL}) provided with the Hyperion data set to generate a noise model on a per pixel basis. G_{NxL} is given as follows (Sun and Neville, 2004):

$$G_{N\times L} = \{g_{j,k} : 1 \le j \le N,\ 1 \le k \le L\}, \tag{3.7}$$

where $g_{j,k}$ is the gain coefficient for a pixel in column j of band k. The formula to calculate the noise $n_{i,j,k}$ for a single pixel for a given at-sensor radiance cube is given as follows (Sun and Neville, 2004):

$$n_{i,j,k} = \sqrt{(N_f \cdot g_{j,k})^2 + \frac{v_{i,j,k} \cdot g_{j,k}}{C_c}}, \tag{3.8}$$

where N_f is the noise floor and C_c is the charge conversion factor. Subsequently, the noise cube N_{MxNxL} is generated and can be written mathematically as follows (Sun and Neville, 2004):

$$N_{M\times N\times L} = \{n_{i,j,k} : 1 \le i \le M,\ 1 \le j \le N,\ 1 \le k \le L\}. \qquad (3.9)$$

From N_{MxNxL}, a user defined number of similar spectra are selected for each pixel by moving a window (or kernel) along-track direction with the assumptions that all the pixels within the window were acquired under similar atmospheric conditions and viewing angles. For example, $S_1 = \{v_{1,k} : 1 \le k \le L\}$ and $S_2 = \{v_{2,k} : 1 \le k \le L\}$ are the two spectra, and $N_1 = \{n_{1,k} : 1 \le k \le L\}$ and $N_2 = \{n_{2,k} : 1 \le k \le L\}$ are their corresponding noise boundaries. The S_1 and S_2 are similar if

- $| v_{1,k} - v_{2,k} | \le \min(n_{1,k}, n_{2,k})$; and
- S_1 and S_2 are similar in all bands.

A user-defined number of similar spectra ($H = \{S_1, S_2, \cdots, S_H\}$) are selected from the moving window. The average spectra for these H similar spectra ($\bar{S} = \{\bar{v}_k : 1 \le k \le L\}$) were then calculated using the following formula (Sun and Neville, 2004):

$$\bar{v}_k = \frac{1}{H}\sum_{i=1}^{H} v_{i,k}, \qquad (3.10)$$

where $\bar{v}_k$ is the average spectrum for band k. Finally the original spectrum is replaced by the above-calculated average spectrum. In a first step, the noise reduction was performed using 100 similar spectra for the whole wavelength range. Secondly, noise was reduced using 200 of similar spectra for the 912-974 nm wavelength range.

The successful noise reduction was determined in two ways. Firstly, a randomly picked region of interest (ROI) and a single pixel spectra of vegetation were compared with and without noise reduction. The results are shown in Figure 3.12 for the combined reflectance cube.

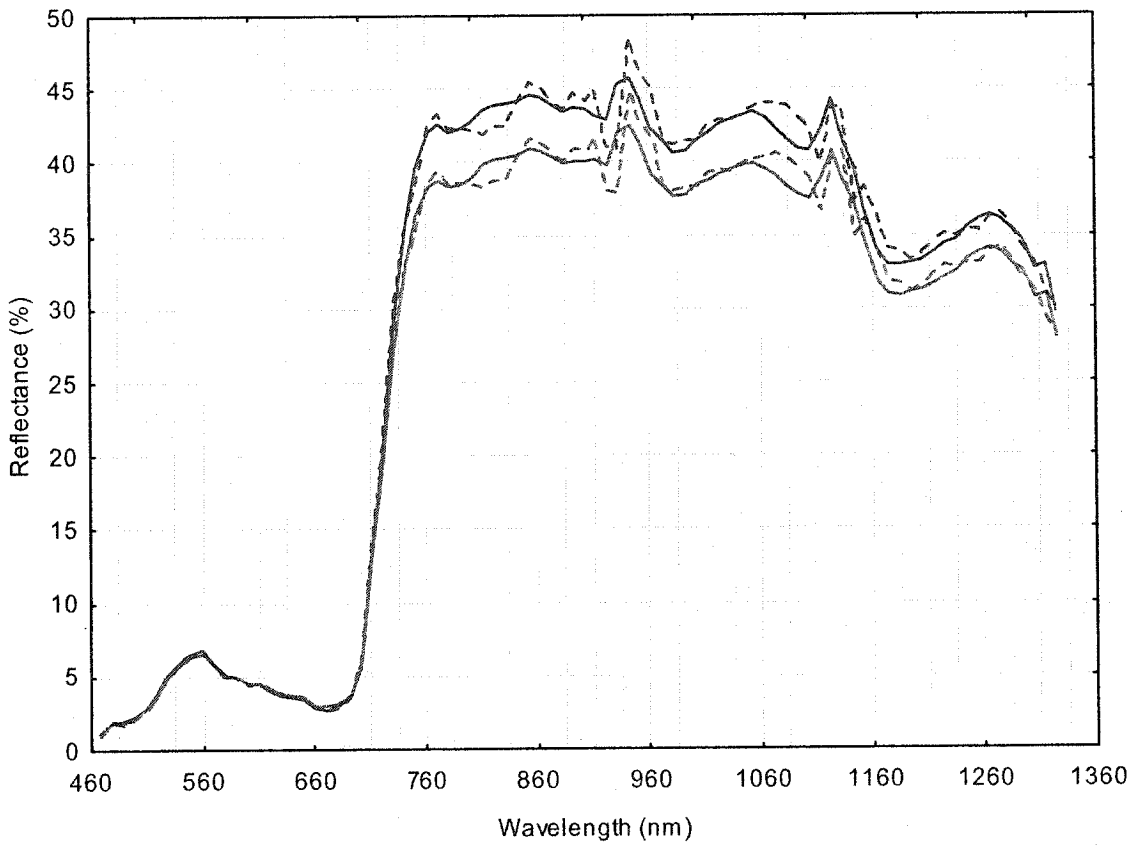

Figure 3.12: Comparison of reflectance spectra retrieved from a region of interest (ROI) in red and a single pixel in blue without (dashed-line) and with (solid-line) noise reduction.

Furthermore, the results are compared before and after noise reduction applying the principal component analysis (PCA) to the Hyperion data set to verify visually the success of the noise reduction. The PCA produces principal component (PC) images, which are sorted by decreasing variance. Generally, noise increases with higher PC number. The noise appears stronger within the first six PCs derived from the original

image compared to those derived from the noise corrected image. The successful results are shown in Appendix IV.

3.4.4. Keystone Detection

Keystone is a term used in the hyperspectral remote sensing community to refer to the inter-band spatial mis-registration in imaging spectrometers (Neville *et al.,* 2004). These distortions may be caused by geometric distortions or by chromatic aberration, or a combination of both. Due to these distortions, a particular spatial pixel, corresponding to a specific detector element in the across-track dimension, in one specific band will not be registered on the ground with the corresponding pixel in the other spectral bands. Neville *et al.* (2004) reported in a study of keystone detection in imaging spectrometer data that the Hyperion sensor has minor keystone distortions, ranging from –0.05 to 0.49 pixels for the VNIR spectrometer and –0.06 to 0.07 pixels for the SWIR spectrometer.

Keystone distortion effects were detected for the Hyperion data set using the "Keystone Detection" tool in ISDAS. The VNIR and SWIR data were processed separately. The technique used is based upon the inter-band correlation of spatial features (Neville *et al.,* 2004). The Hyperion data with prominent spatial features such as roads, field boundaries are suited to detect the keystone. The tool applies a 3x3 Sobel filter to detect the edges of the prominent features in the across-track direction for each spectral band. This is followed by a thresholding to extract the most prominent edges. The spatial locations of these prominent edges are determined for each spectral band to a reference band by correlating the edge patterns in each band relative to those in the reference band. This is done by calculating the Pearson correlation coefficient over a user defined sliding

window (i.e., 5x7 pixels). The sub-pixel shifts are then calculated by interpolating the correlation values. For each across-track pixel, the shifts so determined are averaged together; these are assembled to generate a two-dimensional matrix of shifts, one for each across-track pixel and each spectral band. Finally, a quadratic polynomial is fitted to the measured shift values, both for the across-track and each spectral dimension for both spectrographs. The results of the keystone detection are shown in Figure 3.13. All pixels across-track were selected for exhibiting the impact of keystone on the VNIR and SWIR data sets.

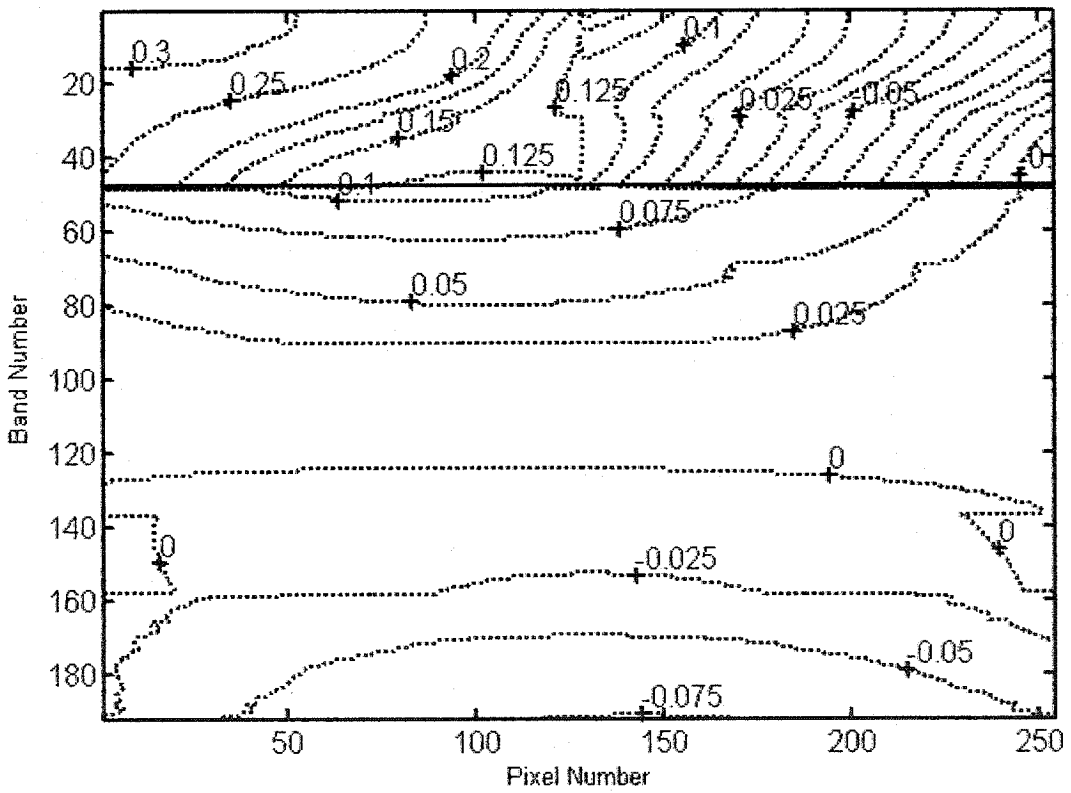

Figure 3.13: The impact of keystone exhibited in the contour plot in the VNIR (1-48 bands) and SWIR (49-192 bands) spectrometer data.

Bands 1 to 48 of the VNIR spectrometer has shifts ranging from –0.075 to 0.3 pixels. The SWIR spectrometer containing bands 49 to 192 exhibits smaller shifts,

ranging from – 0.075 to 0.1 pixels. For the instrument as a whole, the shift ranges from a minimum of – 0.075 pixels to a maximum of 0.3 pixels, giving a total span of 0.375 pixels. These results are found in agreement with those reported by Neville *et al.* (2004).

3.4.5. Smile / Frown Detection

The spectral smile/frown, also known as spectral line curvature, is a wavelength shift in the spectral domain, which is a function of the across-track pixel (column) in the swath (Richter, 2004). In an ideal case, all pixels in across-track dimension correspond to the same wavelength. Neville *et al.* (2003) reported that spectral smile is caused by many sources, such as spatial distortions caused by the dispersion element, prism or grating, or by aberrations in the collimator and imaging optics. In the case of a grating spectrograph as used for the Hyperion sensor, the smile effect derives from the grating equation and can be shown to vary as the product of the wavelength, the angular dispersion and the square of the off-axis field angle. The Hyperion instrument is susceptible to the smile effect because it has two-dimensional detector arrays where the spectrum is dispersed along the columns and the spatial dimension is oriented along the rows. Ideally, the output should be in 2-dimensional spectral-spatial data frames such that each column represents a single band center wavelength and bandwidth. However, the presence of a frown prevents this as shown in Figure 3.14.

The band center wavelengths were provided for the Hyperion data on a across-track pixel basis, which provides information on the sensor frown. The band center wavelengths are plotted for the 823-nm, 942-nm and 1134-nm water absorption

features to assess the magnitude of the wavelength shift within the image data. The frown effect is stronger in the 823-nm band compared to the 942-nm and 1134-nm bands.

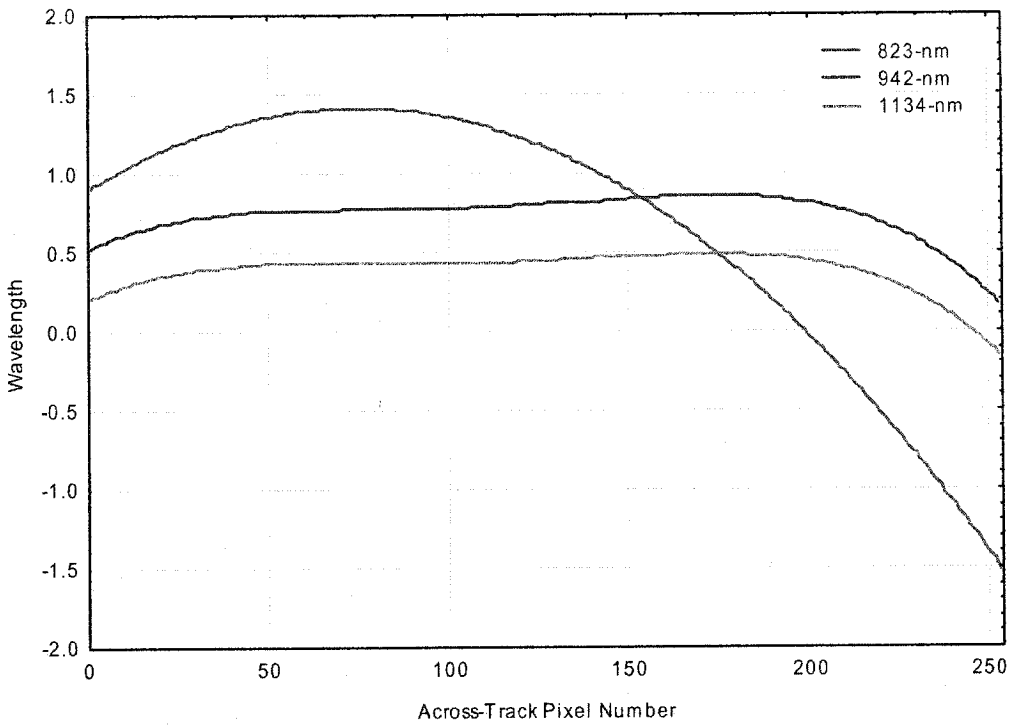

Figure 3.14: Spectral frown of the Hyperion 823, 942 and 1134-nm bands.

A technique developed at CCRS (Neville *et al.*, 2003), which uses atmospheric absorption features (Table 3.3) present in the at-sensor radiance spectra to detect and, subsequently, adjust the band center wavelengths and bandwidths. These atmospheric absorption features are common to all pixels in the scene. The correct band center wavelengths and bandwidths are determined by correlating the at-sensor Hyperion radiance with a modeled at-sensor radiance calculated with the radiative transfer (RT) code MODTRAN 4.2 (Berk *et al.*, 1989). The latter one is computed from spectrally correct reflectance with an iterative procedure. The method of smile / frown detection is summarized in Figure 3.15.

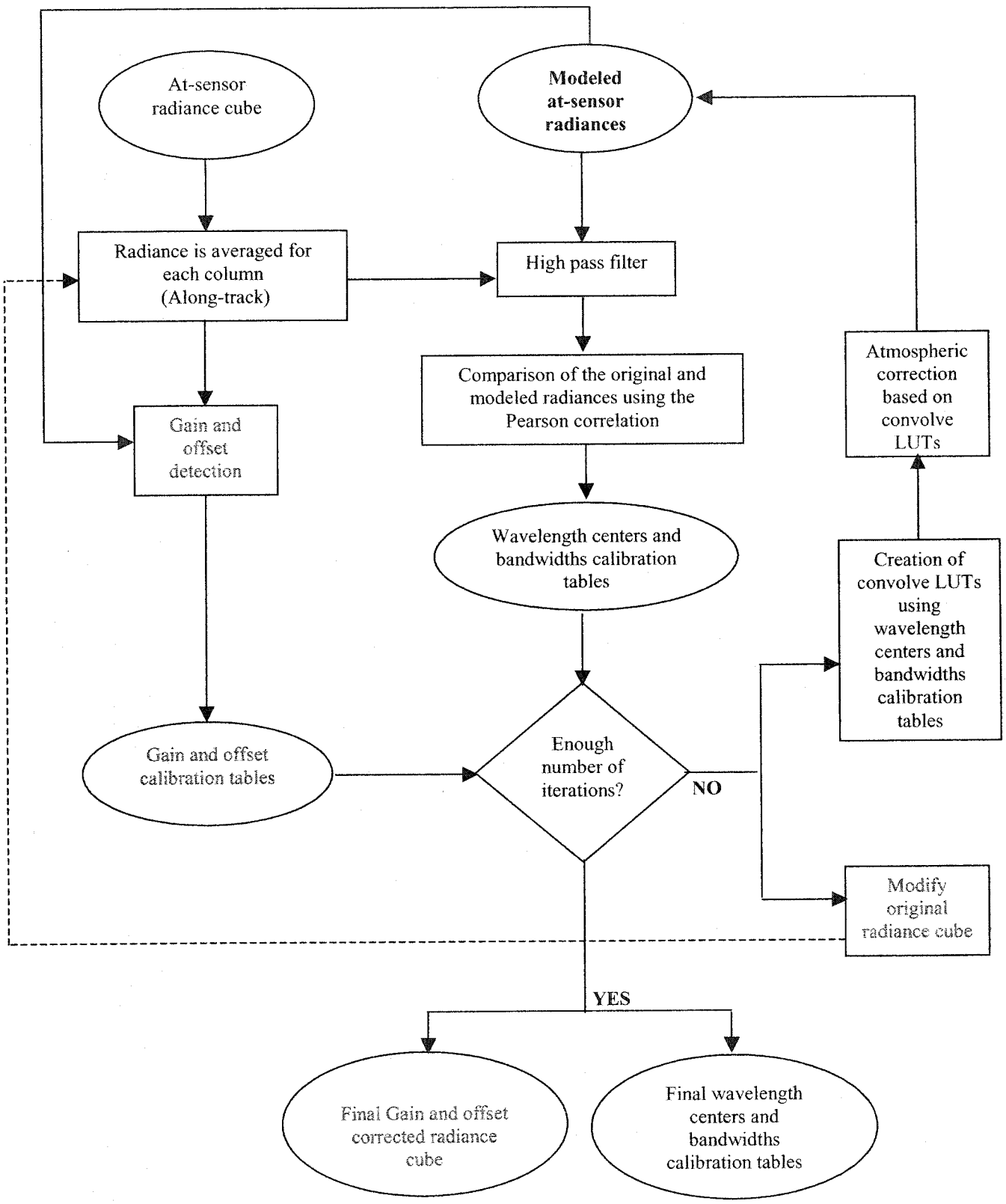

Figure 3.15: Summarized steps for smile / frown detection (black) and gain / offset correction (blue) procedure.

Table 3.3: Atmospheric absorption features selected for smile/frown detection. Absorption minimum for each feature is adapted from Schlapfer (1998). The wavelength range and absorption minima in the blue color are used for gain and offset detection.

Spectrometer	Atmospheric Constituent	Wavelength range (nm)	Absorption Minimum (nm)
VNIR	Ozone (O_3)	457 538	574
	Oxygen (O_2)	732 782	687
	Water (H_2O)	782 854	823
SWIR	Water (H_2O)	912 1003	942
	Water (H_2O)	1013 1235	1134
	Oxygen (O_2)	1235 1295	1268
	Carbon dioxide (CO_2)	1548 1638	1601
	Carbon dioxide (CO_2)	2022 2113	2055
	Methane (CH_4)	2244 2355	2276, 2317

Initially, the surface reflectance was retrieved for the averaged columns (i.e., along-track) of the at-sensor radiance using the original (incorrect) band center wavelengths and bandwidths, which cause spikes in the atmospheric absorption regions. These spikes were corrected for selected atmospheric absorption features by spectral filtering using a low-pass filter (Table 3.3). The smoothed reflectance was then used to calculate modeled at-sensor radiances (Figure 3.16) using a look-up-table (LUT) approach, which will be explained in Chapter 3.4.8 (Staenz and Williams, 1997). LUTs were generated for a set of sensor-specific spectral band response profiles. These profiles cover a user selected wavelength and bandwidth range, within the spectral smile / frown is expected to vary. These LUTs were first generated for the range of bandwidths and then each of these LUTs were sampled for the range of wavelengths. This way, a LUT for every band center wavelength / bandwidth combination was created. This set of LUTs was then convolved and used to calculate a set of modeled at-sensor radiances from the

smoothed reflectance. In a first step, both measured and modeled radiances were then filtered with a high-pass filter in order to reduce the influence of the background scene reflectance.

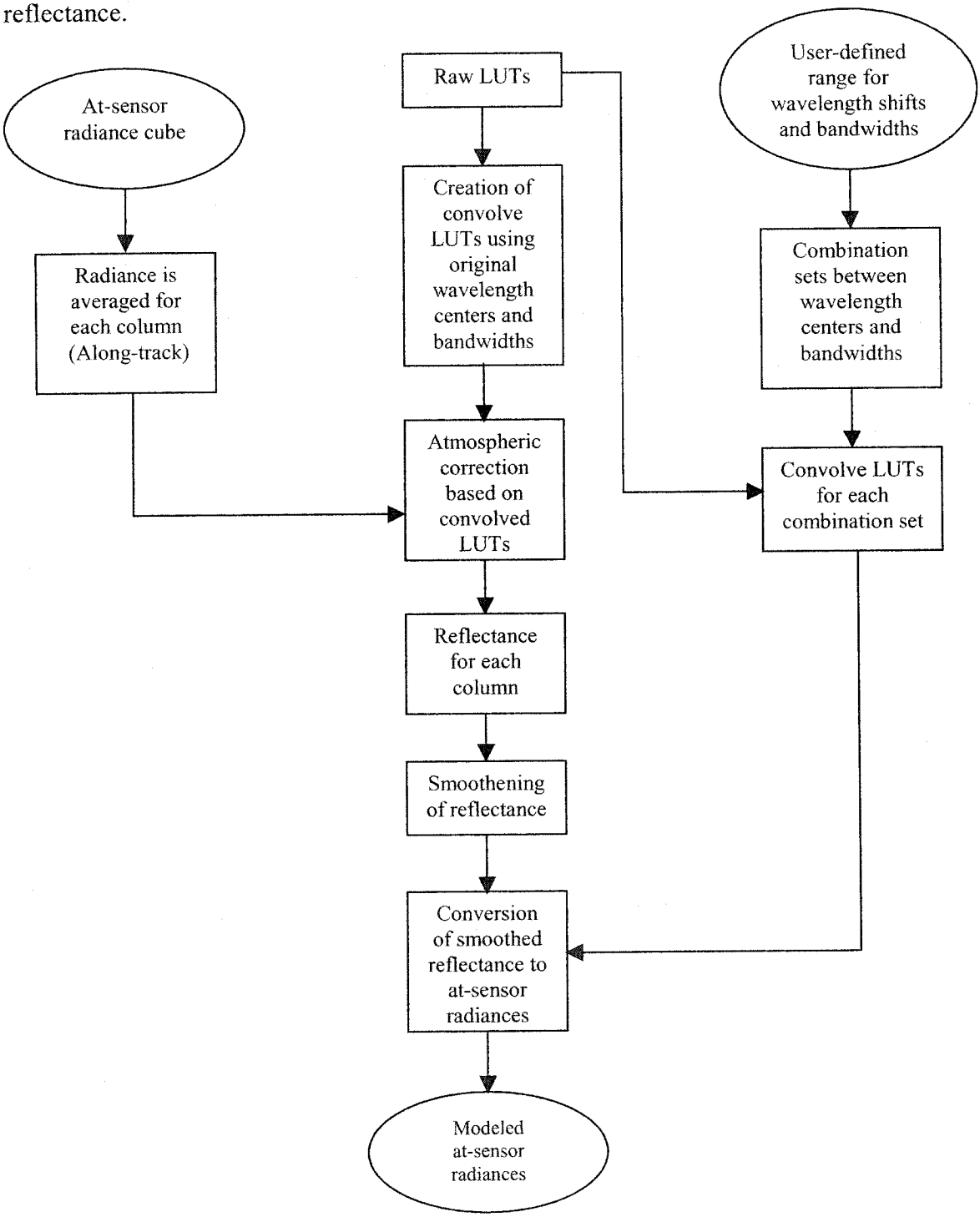

Figure 3.16: Modeled at-sensor radiance retrieval steps for smile / frown detection procedure.

The comparison between the modeled and measured at-sensor radiances is performed using the Pearson correlation coefficient for each selected atmospheric absorption feature. The band center wavelength / bandwidth combination that gives the highest correlation is selected as the correct value. This is performed for each selected atmospheric absorption feature and for each across-track pixel. The band center wavelength and bandwidth values for the bands located between the selected atmospheric absorption features wavelengths are interpolated using a piecewise fit, whereas the bands beyond the wavelength range of the selected atmospheric absorption features are extrapolated. This process was repeated and updated using an iterative procedure (three to five iterations were found adequate for smile / frown detection procedure), until stable results were obtained. The procedure outputs two two-dimensional calibration tables, one each for the band center wavelength and bandwidth for each across-track pixel for each band. These tables were used to retrieve new surface reflectance.

Figures 3.17 and 3.18 display the results achieved for the 823-nm and 942-nm bands, respectively. Included in these Figures are the laboratory calibration curves for the 823 and 942-nm bands. The results show significant differences between the measured and laboratory values.

The mean shift values for the above-mentioned two bands, which are listed in Table 3.4, were obtained by calculating the means over the across-track pixels for both the measured and laboratory calibration values. The total spectral shift along with the differences between measured and laboratory shift are also listed in this Table. The frown mean difference is positive in the 823-nm feature, which means that the measured wavelength has shifted towards the longer wavelength for a specific sensor band. In the

942-nm feature, the mean difference is negative, i.e., the measured wavelength for a specific sensor band has shifted towards the shorter wavelength. In addition, the frown retrieved from the Hyperion data is offset by approximately 1.5 nm for the 942-nm feature. These results are in agreement with the results from Neville *et al.* (2003).

Table 3.4: Statistics for the spectral frown measurements made from the Hyperion data set for the 823 and 942-nm bands.

Absorption Feature & Wavelength (nm)	Water vapor 823 nm	Water vapor 942 nm
Mean Shift (Measured – Lab) (nm)	-0.04	1.30
Shift as Measured (nm)	3.54	0.64
Shift as per Lab Calibration (nm)	2.96	0.72
Shift Difference (Measured – Lab) (nm)	0.58	-0.08

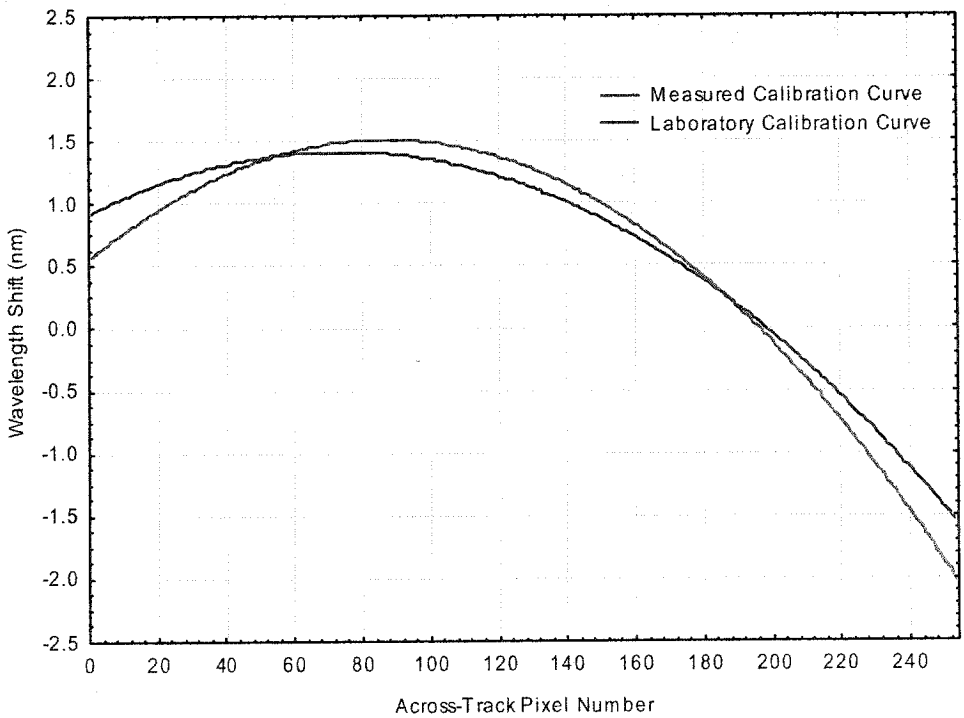

Figure 3.17: Comparison of measured and laboratory frown in the 823-nm band of the Hyperion data set.

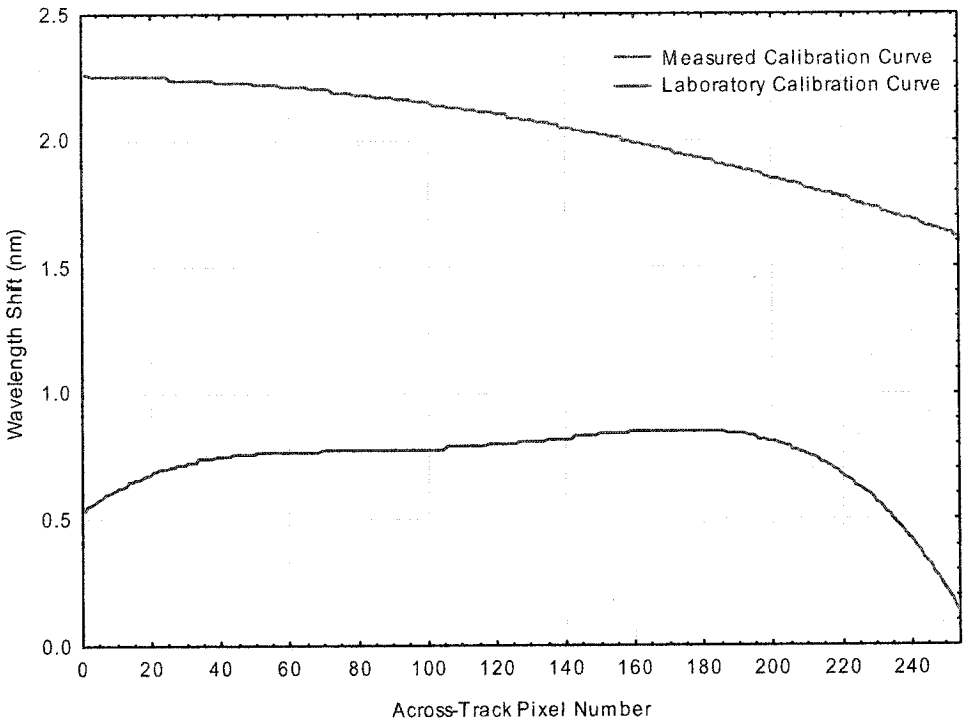

Figure 3.18: Comparison of measured and laboratory frown in the 942-nm band of the Hyperion data set.

3.4.6. Gain and Offset Detection and Correction

In order to transform DN to radiance data for a given pixel in a spectral band, the calibration coefficients, i.e. gain and offset of the sensor, must be known. A gain coefficients file was provided with zero offset for the Hyperion radiance data. An approach was developed and implemented to re-calibrate gain and offset values for the retrieval of more accurate Hyperion at-sensor radiance. This technique is incorporated in the smile detection procedure of ISDAS as shown in Figure 3.15.

The approach produces new gains and offsets for the bands within the selected atmospheric absorption features as shown in Table 3.3. Suppose the relationship between DN ($d_{i,j,k}$) and radiance ($v_{i,j,k}$) of a pixel in line i of column j for a spectral band k in a given radiance cube can be mathematically written as follows (Sun and Neville, 2004):

$$v_{i,j,k} = (d_{i,j,k} + o^D_{j,k}) \times g^D_{j,k}, \qquad (3.11)$$

where $o^D_{j,k}$ is the DN-to-radiance offset and $g^D_{j,k}$ is the DN-to-radiance gain. By substituting $o^D_{j,k}$ and $g^D_{j,k}$ with the original values $o^O_{j,k}$, $g^O_{j,k}$ and their corresponding errors by $\Delta o^D_{j,k}$ and $\Delta g^D_{j,k}$, the equation 3.11 can then be written as follows:

$$\begin{aligned} v_{i,j,k} &= (d_{i,j,k} + o^O_{j,k} + \Delta o^D_{j,k}) \times g^O_{j,k} \times \Delta g^D_{j,k} \\ &= (d_{i,j,k} + o^O_{j,k}) \times g^O_{j,k} \times \Delta g^D_{j,k} + \Delta o^D_{j,k} \times g^O_{j,k} \times \Delta g^D_{j,k}. \end{aligned} \qquad (3.12)$$

Since $(d_{i,j,k} + o^O_{j,k}) \times g^O_{j,k}$ is the original radiance value $v^O_{i,j,k}$, the equation 3.12 can be rewritten as follows (Sun and Neville, 2004):

$$v_{i,j,k} = v^O_{i,j,k} \times \Delta g^D_{j,k} + \Delta o^D_{j,k} \times g^O_{j,k} \times \Delta g^D_{j,k}. \qquad (3.13)$$

If a dark ($v_{d,j,k}$) and bright ($v_{b,j,k}$) pixel can be found for a column j of band k, then $\Delta o^D_{j,k}$ and $\Delta g^D_{j,k}$ can be calculated by solving the following equations (Sun and Neville, 2004):

$$\begin{cases} v_{d,j,k} = v^O_{d,j,k} \times \Delta g^D_{j,k} + \Delta o^D_{j,k} \times g^O_{j,k} \times \Delta g^D_{j,k} \\ v_{b,j,k} = v^O_{b,j,k} \times \Delta g^D_{j,k} + \Delta o^D_{j,k} \times g^O_{j,k} \times \Delta g^D_{j,k} \end{cases} \qquad (3.14)$$

or

$$\begin{cases} \Delta g^D_{j,k} = (v_{b,j,k} - v_{d,j,k}) / (v^O_{b,j,k} - v^O_{d,j,k}) \\ \Delta o^D_{j,k} = \dfrac{(v_{d,j,k} \times v^O_{b,j,k} - v_{b,j,k} \times v^O_{d,j,k})}{g^O_{j,k} \times (v_{b,j,k} - v_{d,j,k})} \end{cases}, \qquad (3.15)$$

where $v^{O}_{d,j,k}$ and $v^{O}_{b,j,k}$ are the original radiance values for the $v_{d,j,k}$ and $v_{b,j,k}$ pixels, respectively. The average values for $v_{d,j,k}$ and $v_{b,j,k}$ are calculated in a first step to solve the equations 3.14 and 3.15. If $C_{j,k} = \{v_{i,j,k} | 1 \le i \le M\}$ is a vector for column j of band k, the mean value of the vector ($Mean^{C}_{j,k}$) can then be calculated as follows (Sun and Neville, 2004):

$$Mean^{C}_{j,k} = \frac{1}{M}\sum_{i=1}^{M} v_{i,j,k} \,. \tag{3.16}$$

The calculated mean value $Mean^{C}_{j,k}$ can then be used as a threshold to calculate the bright $C^{B}_{j,k}$ and dark $C^{D}_{j,k}$ sub-vectors in the following way (Sun and Neville, 2004):

$$\begin{cases} v_{i,j,k} \in C^{B}_{j,k}, & if \quad v_{i,j,k} \ge Mean^{C}_{j,k} \\ v_{i,j,k} \in C^{D}_{j,k}, & if \quad v_{i,j,k} < Mean^{C}_{j,k}. \end{cases} \tag{3.17}$$

Subsequently, the averaged bright $\bar{v}_{b,j,k}$ and dark $\bar{v}_{d,j,k}$ pixels can be calculated for a column j of band k as follows (Sun and Neville, 2004):

$$\begin{cases} \bar{v}_{b,j,k} = \dfrac{1}{|C^{B}_{j,k}|}\displaystyle\sum_{i=1}^{|C^{B}_{j,k}|} v_{i,j,k}, & v_{i,j,k} \in C^{B}_{j,k} \\ \bar{v}_{d,j,k} = \dfrac{1}{|C^{D}_{j,k}|}\displaystyle\sum_{i=1}^{|C^{D}_{j,k}|} v_{i,j,k}, & v_{i,j,k} \in C^{D}_{j,k}, \end{cases} \tag{3.18}$$

where $|C^B_{j,k}|$ and $|C^D_{j,k}|$ are the dimensions of $C^B_{j,k}$ and $C^D_{j,k}$ sub-vectors, respectively. Finally, the new gains and offsets are calculated by solving the equation 3.15. This procedure was implemented using an iterative process.

To apply the measured gain and offset, the original radiance cube is converted to DN using the provided gains and offsets delivered with the Hyperion radiance data. These DNs were then converted into corrected radiance data using the new gain and offset coefficients.

Figure 3.19 displays the results of the corrected reflectance (new gain and offset coefficients) against the reflectance retrieved from the uncorrected data for randomly selected vegetation and soil pixel spectra.

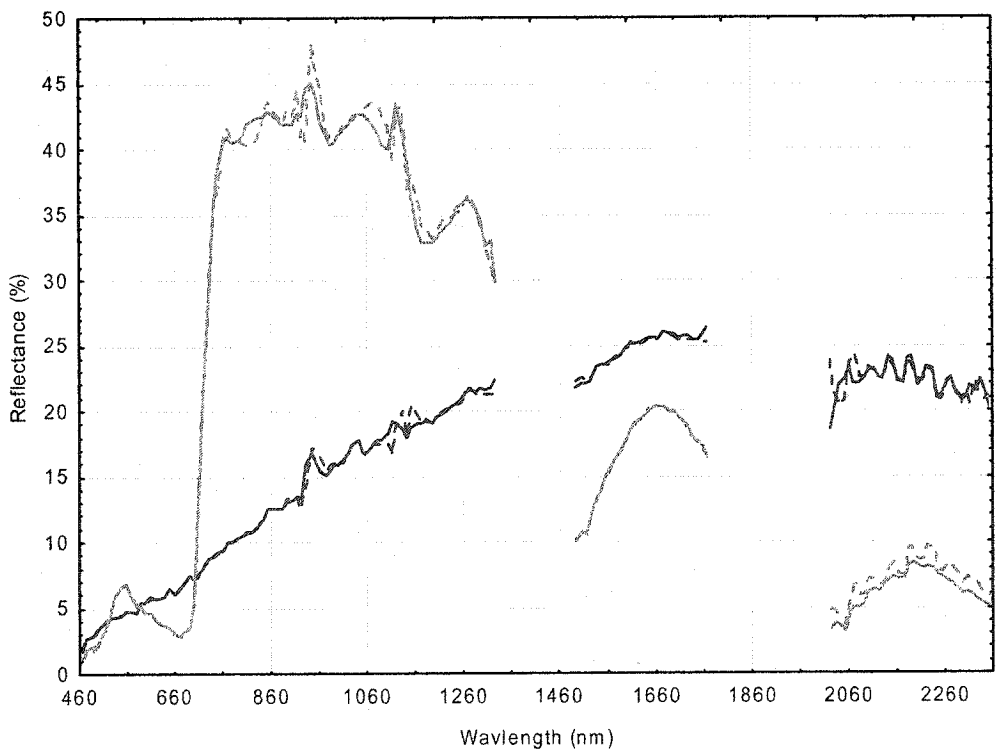

Figure 3.19: Comparison of single pixel reflectance spectra retrieved from vegetation (green) and soil (red) with (solid-line) and without (dashed-line) gain and offset correction.

3.4.7. Atmospheric Correction

For the retrieval of the surface reflectance from the at-sensor radiance, the influence of the atmosphere has to be eliminated. Many techniques exist for the retrieval of surface reflectance from at-sensor hyperspectral radiance data. The Hyperion corrected at-sensor radiance data was converted to surface reflectance using the "Atmospheric Correction" tool in ISDAS. The technique is based on a LUT approach using an atmospheric RT code (Staenz and Williams, 1997). To provide additive and multiplicative coefficients for the removal of atmospheric gaseous and scattering effects, two five-dimensional raw radiance LUTs with tunable breakpoints were generated with the MODTRAN 4.2 RT code for a 5% and a 60% flat reflectance spectrum. The LUTs dimensions were wavelength range, pixel position, range of atmospheric water vapor content, aerosol optical depth and terrain elevation. The input parameters for the RT code are listed in Table 3.5.

The raw LUTs were then convolved with the Hyperion sensor characteristics. The convolved (sensor-specific) LUTs were then used in combination with a curve-fitting technique in the 1134-nm water vapor absorption region to estimate the atmospheric water vapor content on a pixel-by-pixel basis from the data themselves (Green *et al.*, 1991; Gao and Goetz, 1990). The technique assumes that the reflectance spectrum is linear over the 1134-nm water vapor absorption feature with the exception for the absorption due to leaf liquid water at about 1180-nm (Curran, 1989). The 942-nm water vapor absorption region was not used for the Hyperion data due to the fact that this feature lies in the overlapping region between the VNIR and SWIR. Finally, the estimated atmospheric water vapor content was used on a per pixel basis for the

interpolation of the sensor specific LUTs to retrieve the surface reflectance for each spectral band.

Table 3.5: Input parameters for the MODTRAN 4.2 raditive transfer code.

Atmospheric Model	Mid-latitude Summer
Aerosol Model	Rural (Continental)
Date of overflight	June 30, 2002
Time of overflight (GMT)	17:36
Solar Zenith angle	31.72^0
Solar Azimuth angle	142.17^0
Terrain elevation (ASL)	0.579 km
Horizontal Visibility	23 km
Water Vapor	1.5-2.5 gm/cm^2
CO_2 mixing ratio	365.00 ppm (as per model)

GMT= Greenwich Mean Time; ASL= Above Sea Level; ppm=parts per million

Figure 3.20 shows the results of the retrieved reflectance spectra. This process revealed errors (spikes) mainly in the 940 and 1130-nm regions as a result of uncertainties in atmospheric modeling and remaining sensor artifacts. These errors were finally removed in the post-processing process.

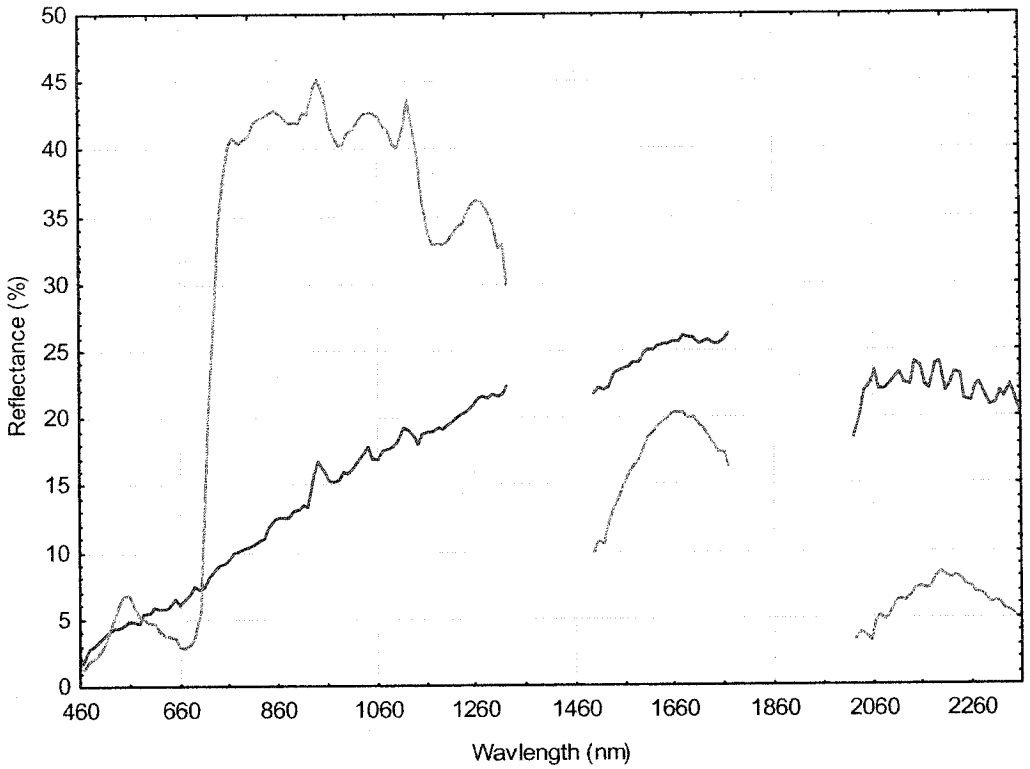

Figure 3.20: Retrieved reflectance spectra for single vegetation (green) and soil (red) pixels.

3.4.8. Smile Correction

The spectral smile / frown correction was applied to the reflectance data. This process was done using the "Smile Corrector" tool in ISDAS. This technique is based on the combined resampling (deconvolution / convolution methods) for the band center wavelengths and bandwidths. This process results in a common band center wavelength and bandwidth for the entire data cube.

The results of the smile / frown correction process are shown in Figures 3.21 and 3.22. The measured bandwidth is compared against the laboratory (incorrect) bandwidth in Figure 3.21. It decreased considerably for bands 1-27, 39-48, 55-76, and 164-192. An increase in bandwidth is found for bands 28-34 and 77-159. There is no change in

bandwidth for bands 49-54 and 160-163. The differences of measured and laboratory (incorrect) band center wavelengths are plotted against the band number in Figure 3.22. The wavelength shift ranges from 0.191-1.382 nm for bands 1-116 and from 0.829-3.28 nm for bands 117-192.

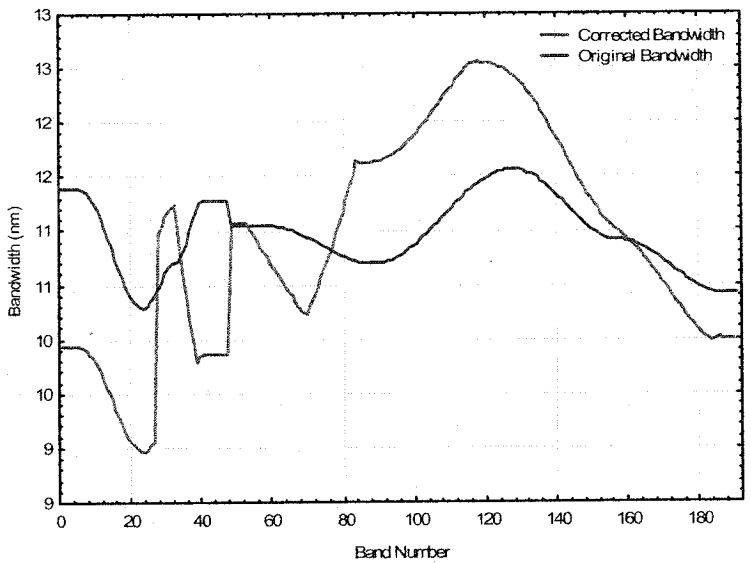

Figure 3.21: Comparison of measured and laboratory bandwidths for all bands.

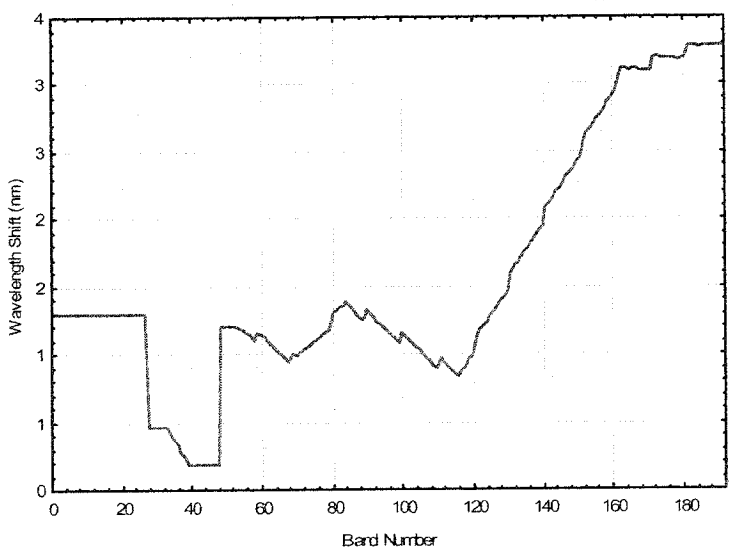

Figure 3.22: Wavelength shift between measured and laboratory band center wavelengths for all bands.

3.4.9. Post-Processing of Data

The smile / frown corrected reflectance spectra were analyzed in the vicinity of known atmospheric absorption features for quality purposes. The inspection revealed band-to-band errors mainly in the 760 to 1326 nm region. These errors were removed using the "Post-processing" tool in ISDAS. The tool involves the calculation of correction gains and offsets using a spectrally flat target pixel approach (Staenz *et al.*, 1999). The technique assumes that there are a number of pixels whose reflectance spectra are flat, or nearly flat (feature-less) and their brightness range covers a major portion of the full range for all the pixels in the scene. A second-order polynomial fit to the reflectance spectra using χ-squared as a goodness of fit measure is calculated on a pixel-by-pixel basis. The pixels with the smallest χ-squared values are selected as "spectrally flat target pixels". Finally, linear fits are performed on a band-by-band basis providing slopes and offsets, which are used as gain and offset for the correction of the reflectance data. For the Hyperion data set, 10 spectrally flat target pixels were selected from the cube. The spectra of these pixels were checked for presence of features before processing. They were located right in the town of Indian Head. These pixels were then used to correct spectra in the wavelength region from 760 to 1326 nm.

The results of the post-processing are shown in Figure 3.23. Reflectance spectra of two randomly selected pixels for vegetation and soil are plotted before and after post-processing.

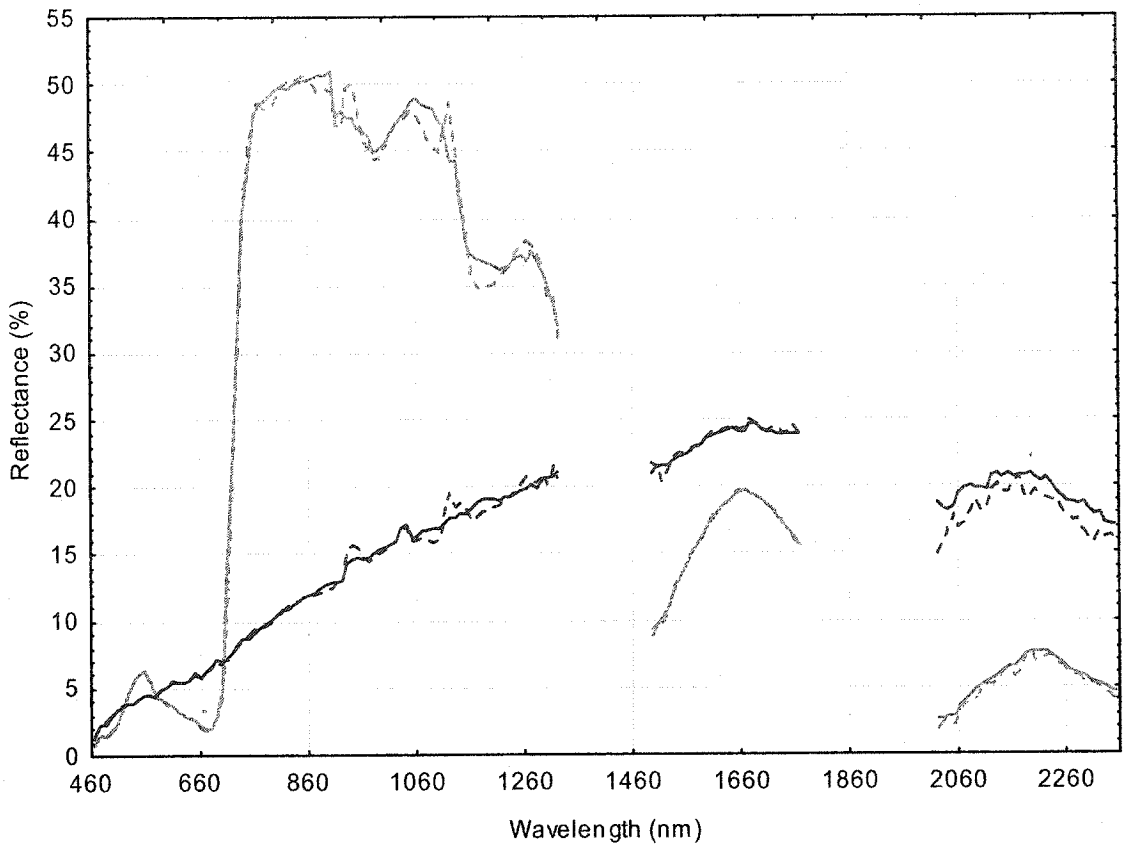

Figure 3.23: Comparison of single-pixel reflectance spectra for vegetation (green) and soil (red) before (dashed-line) and after (solid-line) post-processing.

3.5. Plot Locations in the Hyperion Image

To avoid resampling of the Hyperion image data no geometric correction was carried out in order to preserve the radiometric integrity of each image pixel. Champagne (2002) reported a technique, which locates plot locations in the hyperspectral image (master) by first locating them on a geo-referenced image (slave) and then wraping this image to match the hyperspectral data. For this purpose, a high spatial resolution 0.69-m panchromatic QuickBird image of the study area was used to locate the plot locations. This section describes the processing sequence, which is shown in Figure 3.24.

3.5.1. Plot Locations in the QuickBird Image

All plots locations were measured with a differential global positioning system (GPS) during ground-based data measurements. The locations of the plots were "burned" (encoding vector information into a raster image) into the QuickBird image using the Xpace module of the PCI Software (PCI Geomatics, 2000) so that the locations would still be detectable in the warped image.

3.5.2. Image-to-Image Registration

The QuickBird image was then registered to the Hyperion imagery with a 2^{nd} order polynomial using the GCPWorks module of the PCI software. About 20 GCPs were selected at the corner of each field and intersections of roads from both images. The GCPs were selected evenly over the entire image to get a better image fit and even the distribution of registration errors. In the registration process, a cubic convolution resampling method was used. This approach applies the weighted average of the 16 surrounding pixels (i.e., 4x4 pixel window) to calculate the brightness value. Finally, pixel and line coordinates from the warped image were recorded for each plot position.

The root mean square error (RMSE) is used for the registration accuracy between QuickBird and Hyperion data. The RMSE was 0.33 and 0.61 pixel in x and y directions, respectively. Thirty plots of the study site were covered by the Hyperion flight line with exception of five plots located in the Delage field.

The recorded pixel and line coordinates of each plot were used to extract information, which was carried out using a data extraction network in ISDAS. The

network simply collects data for a certain pixel in a certain line and records it in the American Standard Code for Information Interchange (ASCII) format.

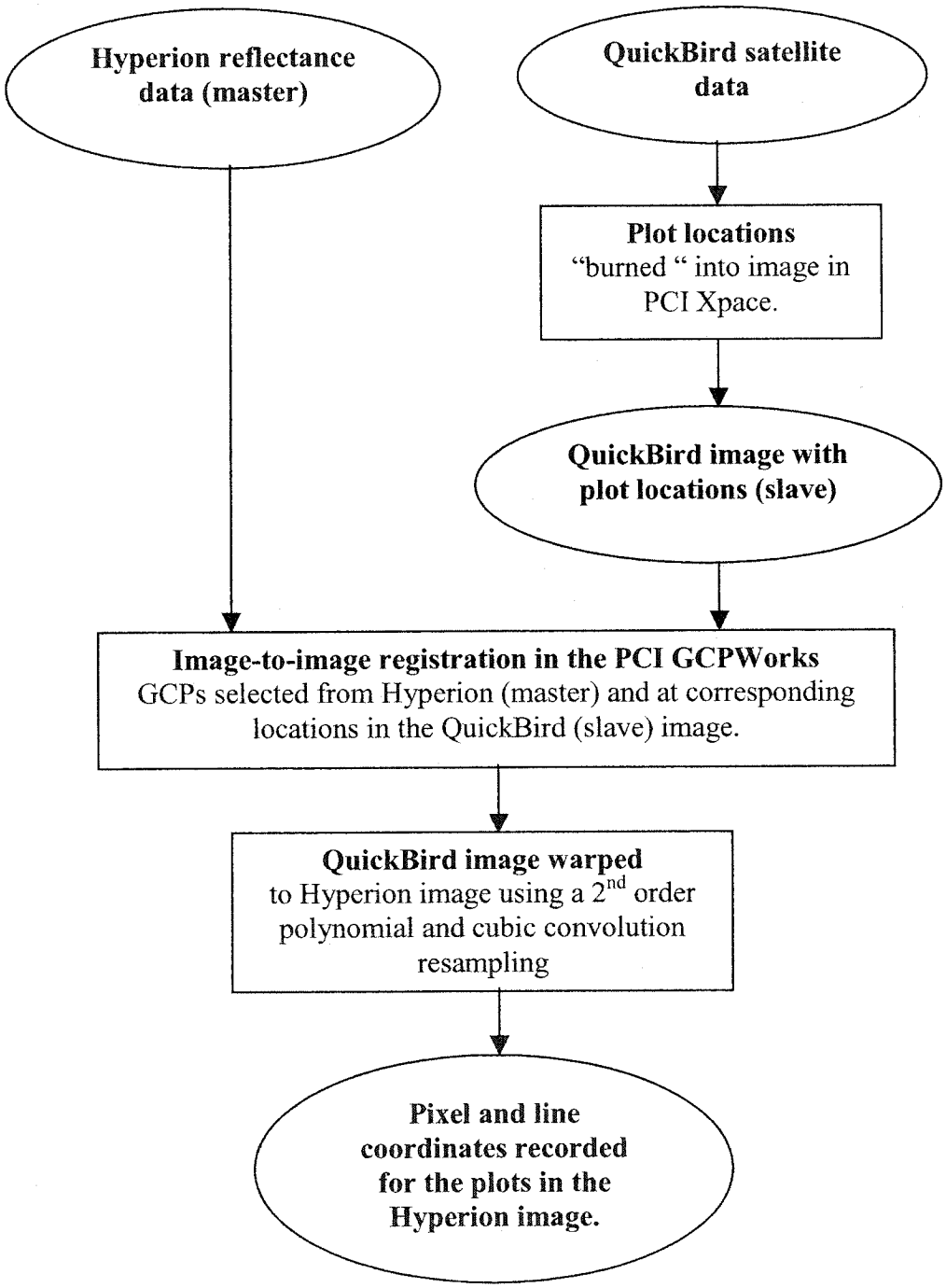

Figure 3.24: Processing sequence for the determination of the plot locations in the Indian Head data (adapted from Champagne (2002)).

3.6. Calculation of Spectral Chlorophyll Indices

In this section the procedures are discussed for calibration of the SPAD-502 chlorophyll meter, calculation of spectral indices and establishment of their relationships to the chlorophyll content using the indoor GER-3700 spectroradiometer data. The established fit equations in the laboratory were evaluated with respect to the Hyperion hyperspectral data. An approach was also tested to scale-up chlorophyll content from the leaf to the canopy-level for validation against the predicted chlorophyll content derived from Hyperion image data.

3.6.1. Calibration of SPAD-502 Leaf Chlorophyll Meter

Since the laboratory chemical analysis of leaf chlorophyll content is time consuming, not instantaneous, expensive and destructive, the chlorophyll meter SPAD-502 was used. This instrument has the potential of non-destructive and fast determination of leaf chlorophyll content. However, the meter measures the chlorophyll in arbitrary values. For this purpose, a relationship between SPAD-502 values and plant-extracted chlorophyll was explored in this study using laboratory data of two days. The results will be presented and discussed in section 4.2 of chapter 4.

3.6.2. Laboratory Spectroradiometeric Data

For this study, GER-3700 measurements, acquired in the laboratory at July 20, 2002, were used to establish the relationship between the selected spectral chlorophyll indices (as shown in Table 2.1) and chlorophyll content derived from the SPAD-502 meter measurements.

The spectral chlorophyll indices were calculated from GER-3700 data using the "Calculator" tool in ISDAS. Only the VNIR wavelength range from 448-1050 nm of the GER-3700 was used to calculate the indices. The wavelengths given in the equations of selected spectral chlorophyll indices match the GER-3700 bands wavelengths. The layout for the calculation of spectral chlorophyll indices is shown in Figure 3.1. The results will be presented and discussed in the section 4.3.1 of chapter 4.

3.6.3. Hyperspectral Data

3.6.3.1. Direct Approach

The indices-chlorophyll content equations established in the laboratory using the GER-3700 data were evaluated using the Hyperion image data. The indices derived from the Hyperion data, were calculated using the "Field Math" and "Calculator" tools in ISDAS. For this purpose, bands were selected, which most closely match the wavelengths given in the equations of the selected spectral chlorophyll indices. The selected wavelength positions for each spectral chlorophyll index are shown in Table 3.6. Due to errors in the data for 430 nm wavelength position, the first available band (i.e., 448.47 nm) was used for the calculation of spectral indices, such as; NDPI, SIPI, NPCI and SRPI. The estimated chlorophyll content from the Hyperion reflectance data was then validated against the measured leaf chlorophyll content derived from the SPAD-502 meter. The results will be presented and discussed in the section 4.3.2 1 of chapter 4.

The CAI was calculated from the wheat crop fraction map derived from the Hyperion image data using the Spectral Mixture Analysis (SMA) technique in ISDAS for this study. A brief description of the SMA procedure is presented in Appendix V. The

pure vegetation spectrum (S) for a single pixel was calculated from the following formula (Neville 2004):

$$S = \frac{\sum_{i=1}^{m} f_{em} e_{em}}{\sum_{i=1}^{m} f_{em}}, \qquad (3.19)$$

where f_{em} is the fractional abundance and e_{em} is the spectrum endmember em, and m is the total number of endmembers used for unmixing.

Table 3.6: Available wavelength positions in Hyperion data for spectral chlorophyll indices calculation.

Spectral Chlorophyll Index	Wavelength Position (required)	Wavelength Position (available in Hyperion)
NDPI	430 and 680 nm	448.47 and 682.50 nm
SIPI	445, 680 and 800 nm	448.47, 682.50 and 803.54 nm
NPCI	430 and 680 nm	448.47 and 682.50 nm
PRI	531 and 550 nm	529.87 and 550.22 nm
SRPI	430 and 680 nm	448.47 and 682.50 nm
GNDVI	550 and 801 nm	550.22 and 803.54 nm
$PSSR_a$	680 and 800 nm	682.50 and 803.54 nm
$PSND_a$	680 and 800 nm	682.54 and 803.54 nm
MCARI / OSAVI	550, 670, 700 and 800 nm	550.22, 672.32, 702.01 and 803.54 nm
TCARI / OSAVI	550, 670, 700 and 800 nm	550.22, 672.32, 702.01 and 803.54 nm
CARI	550, 670 and 700 nm	550.22, 672.32 and 702.01 nm
hNDVI	668 and 827 nm	671.02 and 823.65 nm
CAI	600 and 735 nm	599.79 and 732.07 nm

3.6.3.2. Scaling-up from Leaf to Canopy-level

In order to scale-up the leaf chlorophyll content derived from the SPAD-502 measurements to canopy chlorophyll content, an approach was tested as described by Johnson *et al.* (1994). According to this technique, the crop canopy chlorophyll content is the product of leaf chlorophyll content and LAI. The LAI was calculated for each plot using the technique reported by Champagne (2002). During the extensive field campaign, the above-ground wheat biomass was harvested within a 0.5 m by 0.5 m area at each sample site. These biomass samples were weighted within one hour of harvest to obtain fresh weight. Samples were then oven-dried at 105^0C for 48-72 hours until no change in weight was observed by further drying to measure dry mass (DM). The leaf area (LA), which is defined as the total one-sided area of leaf surface for this study was estimated from plant DM as (Jacquemoud *et al.*, 1996):

$$LA = DM \, x \, SLA, \qquad (3.20)$$

where SLA is the specific leaf area and defined as the area of leaf per unit of leaf dry matter, which is crop specific. For this experiment, indicative values were used from a table established by Keulen (1986). Finally, LAI was then calculated from the LA by normalizing it to the ground area.

For the above-mentioned approach of estimating LAI, the stem water content constitute a significant portion of the total canopy biomass, particularly in the early stages of growth. For this reason, the values of the biomass were corrected for the stem-to-leaf ratio, in order to compensate for stem water content on these measures. For this study,

measured and modeled dry matter partition as a function of crop growth stage was taken from studies on wheat (Schulze, 1982). Results for this approach are presented and discussed in the section 4.3.2.2 of chapter 4 in two ways. Firstly, the validation of calculated canopy chlorophyll content (using the scaling-up approach) against the estimated chlorophyll content was derived from the Hyperion data using the leaf-level established equations. Secondly, relationships were the relationships between the calculated spectral chlorophyll indices using the Hyperion data and measured canopy chlorophyll content.

3.7. Statistical Analysis

Prior to any statistical analysis, descriptive statistics such as the mean and the variance of both variables (i.e., the dependent variable Y and the independent variable X) were calculated. For this study the dependent (predicted) variable is the measured chlorophyll content and the independent variable is the value of the spectral chlorophyll index. The majority of the plots of Y versus X presented a linear trend, suggesting that a straight line might fit the data. The theoretical linear regression (LR) model is given by (Draper and Smith., 1981):

$$Y_i = \alpha + \beta X_i + \varepsilon_i, \qquad (3.21)$$

where

$$\varepsilon_i \overset{I.ID}{\sim} N_o(0,\sigma^2), \qquad i=1,2,3,\ldots n$$

α is the intercept, β is the slope and ε is the error. The errors ε are assumed as independent (*I*), identical (*ID*), normally (N_o) distributed with mean zero and variance (σ^2) and n is the sample size. The fitted linear model was obtained by the "least squares" method using the Statistica software package (StatSoft Inc, 1994). The fitted model is then given by (Draper and Smith., 1981):

$$\hat{Y} = \hat{\alpha} + \hat{\beta} X, \qquad (3.22)$$

where $\hat{\alpha}$ and $\hat{\beta}$ are the least squares estimates of α and β and $\hat{Y}$ is the predicted value of the Y variable. The estimators for α and β are given as follows (Draper and Smith., 1981):

$$\hat{\alpha} = \bar{Y} - \hat{\beta}\,\bar{X} \qquad (3.23)$$

and

$$\hat{\beta} = \frac{\sum_{i=1}^{n}(X_i - \bar{X})(Y_i - \bar{Y})}{\sum_{i=1}^{n}(X_i - \bar{X})^2}, \qquad (3.24)$$

where $\bar{X}$ and $\bar{Y}$ are the mean values of variables X and Y. The unbiased estimate of the variance σ^2 is given by (Draper and Smith., 1981):

$$\sigma^2 = \frac{\sum_{i=1}^{n} (Y_i - \hat{Y}_i)^2}{n-2}. \qquad (3.25)$$

This estimate σ^2 is also called as the mean square error (MSE). Besides the MSE, the coefficient of determination (R^2) was calculated. The R^2 can be written as follows (Wilmott, 1982):

$$R^2 = \frac{\sum_{i=1}^{n} (\hat{Y}_i - \bar{Y})^2}{\sum_{i=1}^{n} (Y_i - \bar{Y})^2}. \qquad (3.26)$$

R^2 measures the proportion of the variance in the variable Y explained by regressing Y on X.

In the cases where the LR model failed, polynomial and exponential regression models were considered as given below (Draper and Smith., 1981):

$$Y = \beta_0 + \beta_1 X + \beta_2 X^2 + \varepsilon \qquad (3.27)$$

and

$$Y = \alpha e^{\beta X} + \varepsilon, \qquad (3.28)$$

where β_0 is the intercept and β_1, β_2 are the coefficients of the independent variable X for polynomial regression model. In case of exponential regression model α is the intercept and β is the slope.

In addition, appropriate transformations of Y and / or X variables such as the square root, logarithm, and power were applied in case the previous mentioned models failed.

Wilmott (1982) recommended the use of the D-Index (Index of Agreement) for model evaluation. According to Wilmott (1982) the D value is a measure for the 1:1 correspondence between measured and predicted values. D can be expressed as:

$$D = 1 - \left[\sum_{i=1}^{n} (Y_i - X_i)^2 \Big/ \sum_{i=1}^{n} (|Y_i'| + |X_i'|)^2 \right], \qquad (3.29)$$

where Y_i is the predicted value and X_i is the observed value at sample i, Y_i' is the difference between Y_i and the average of the observed values, and X_i' is the difference between Xi and the average of the observed values, and n is the number of values.

3.8. Conclusions

This chapter described the study sites, data collection, ground measurement and techniques, and image data prerocessing methods. Ground measurements and the Hyperion hyperspectral data were acquired in June 2002 over two agricultural study sites,

the Pedde and Delage wheat fields located near Indian Head (Saskatchewan). The SPAD-502 chlorophyll meter was used to measure leaf chlorophyll content. Laboratory chlorophyll content analyses from leaf samples were also performed to establish calibration equations for the estimation of chlorophyll-ab and chlorophyll-a contents from the SPAD-502 measurements. The GER-3700 spectroradiometer was used to measure reflectance of crop leaves in the laboratory. The processing of the hyperspectral Hyperion data was performed in ISDAS. This activity is described in detail together with the achieved results. Calculation of selected chlorophyll indices was performed first on GER-3700 laboratory data and then on Hyperion data. Finally, the statistical techniques applied were described. The next chapter (Chapter 4) will present and discuss the results derived from the chlorophyll indices to estimate the chlorophyll content.

Chapter 4

Results and Discussion

4.1. Introduction

This chapter will examine and discuss the results obtained from the calculation of the spectral chlorophyll indices both from the GER-3700 and Hyperion hyperspectral data. In the first section, the calibration results of the SPAD-502 meter were presented to convert SPAD-502 arbitrary measurements (Chl_{SPAD}) into chlorophyll-ab (Chl-ab) and chlorophyll-a (Chl-a) contents. The selected spectral chlorophyll indices in Table 2.1 were first calculated from the laboratory GER-3700 data and then validated against the Chl-ab and Chl-a contents estimated from the SPAD-502 for laboratory measurements. Furthermore, the relationships developed in the laboratory for the selected indices using the GER-3700 were then evaluated for the Hyperion data and validated against the measured in-situ Chl-ab and Chl-a contents derived from the SPAD-502 meter. Finally, a best-performed index will be found. Sources of errors in the estimation of chlorophyll and validation will also be analyzed.

4.2. Calibration of the SPAD-502 Leaf Chlorophyll Meter

The relationship was established for both the Chl-ab and Chl-a contents, extracted in the laboratory against the Chl_{SPAD} measurements, using a 2^{nd} order polynomial as proposed in the literature (Markwell *et al.,* 1995; Kneubuhler. 2002).

To confirm the predictive capability of the calibration equation for Chl-ab, a test was performed between the Kneubuhler (2002) equation to the one established in this study. For this purpose, the polynomial equation for Chl-ab was forced through the origin

to avoid negative Chl-ab content values as shown in Figure 4.1. The results of the two calibration equations are shown in Figure 4.2. The two equations predict similarly for a range of 0 to 65 μg/cm^2 for Chl-ab with marginal difference. The difference between these two equations may be due to the fact that the equation reported by Kneubuhler (2002) was established based on a joined dataset of wheat and barley.

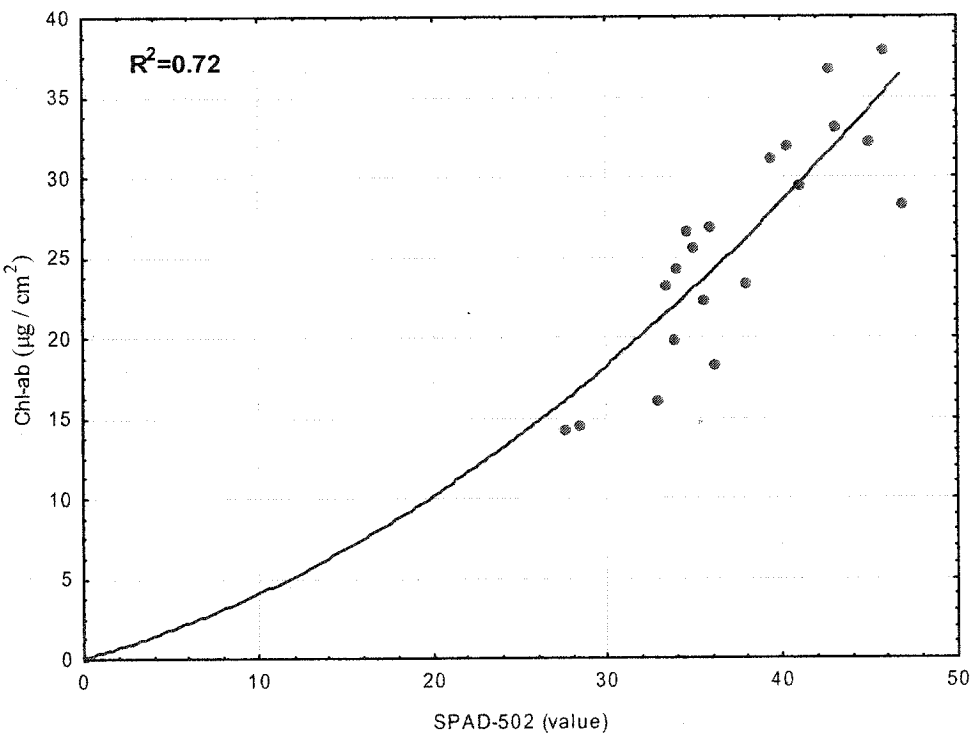

Figure 4.1: Relationship between measured SPAD-502 arbitrary values and laboratory determined Chl-ab content for wheat. The polynomial equation was forced through the origin.

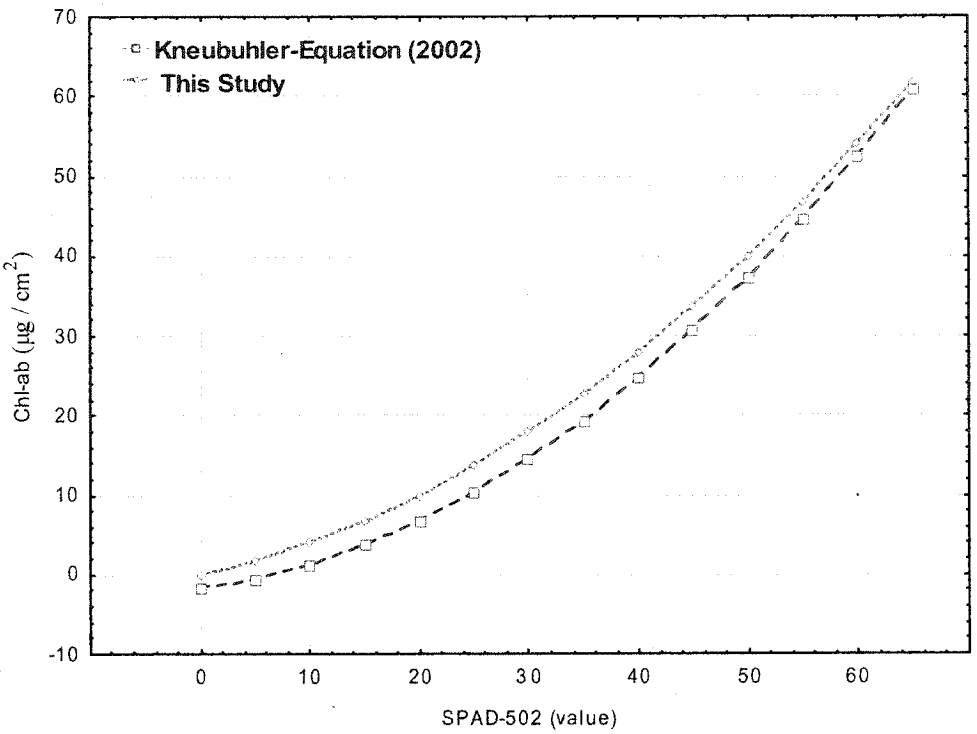

Figure 4.2: Comparison of the calibration equation for Chl-ab established in this study with the one reported by Kneubuhler (2002).

An established fit-equation was not found in the literature for wheat crop to test the predictive capability of the calibration equation for Chl-a content. As for the Chl-ab, the polynomial equation for Chl-a was also forced through the origin to avoid negative values as shown in Figure 4.3. The calibration equations established in this study for Chl-ab and Chl-a are given in Table 4.1 together with the coefficient of determination (R^2) and root mean square error (RMSE). These calibration equations were used to convert Chl_{SPAD} into Chl-ab and Chl-a contents.

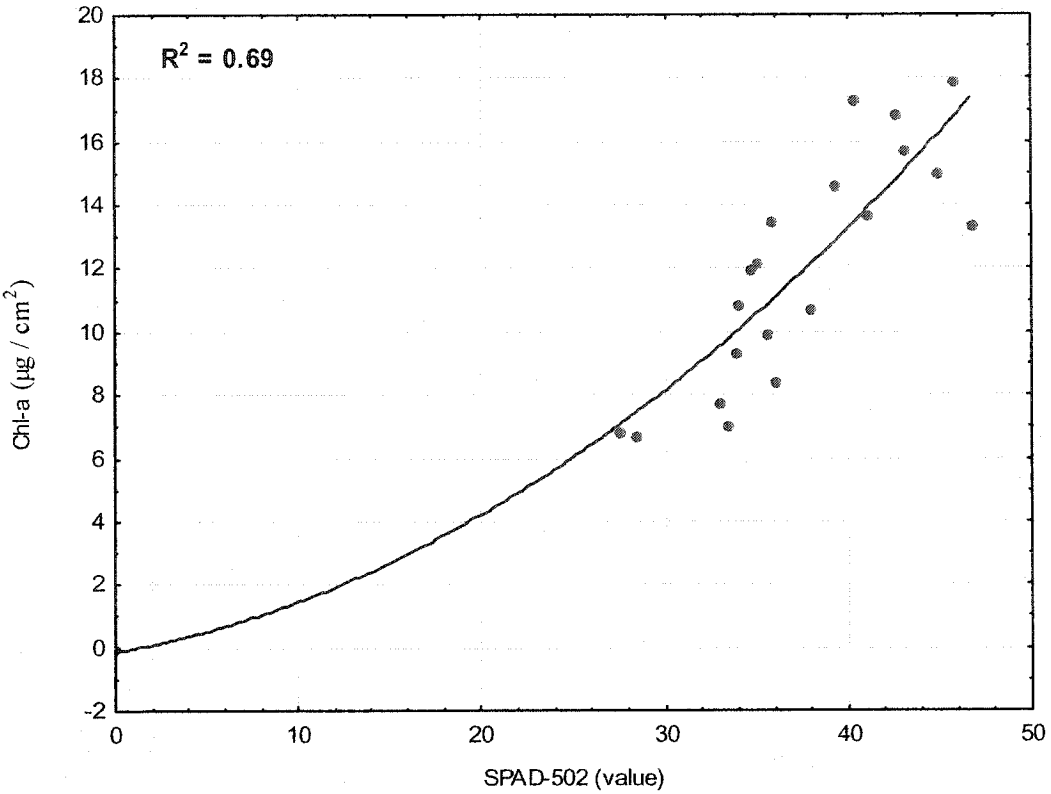

Figure 4.3: Relationship between measured SPAD-502 arbitrary values and laboratory determined Chl-a content for wheat. The polynomial equation was forced through the origin.

Table4.1: Calibration equations for the conversion of the SPAD-502 arbitrary values to chlorophyll content (µg / cm^2).

Pigment	Calibration equation to convert the SPAD value to chlorophyll content	Coefficient of determination (R^2)	Root mean square error (RMSE)
Chl-a	$Y=0.0912*X+0.006*X^2$	0.69	1.94
Chl-ab	$Y=0.3015*X+0.0102*X^2$	0.72	3.53

4.3. Chlorophyll Indices

In this section, the results using the selected chlorophyll indices to estimate chlorophyll content as listed in Table 2.1 of Chapter 2 are presented and discussed both for the GER-3700 spectral data and Hyperion data. The performance of these indices was first tested with the GER-3700 data and then the established relationships for indices were applied to the Hyperion data. The canopy chlorophyll content retrieved from the scaling-up approach (i.e., in-situ chlorophyll content derived from the SPAD-502 measurements were weighted with the LAI) validated against the predicted chlorophyll content estimated from the Hyperion image data using the leaf-level established relationships. In addition, the canopy chlorophyll content was also correlated against the calculated spectral indices from the Hyperion image data. Furthermore, the relationships found in the literature, which were established between indices calculated from hyperspectral data and ground chlorophyll data for wheat crop, were also evaluated for the Hyperion data.

4.3.1. Chlorophyll Content Estimation using GER-3700 Data

All selected spectral chlorophyll indices were calculated from the GER-3700 spectral data. A total of sixteen spectra as shown in Figure 4.4 were acquired indoor together with corresponding SPAD-502 measurements. These measurements were then converted into Chl-a and Chl-ab contents values using the calibration equations as listed in Table 4.1 to establish relationships against spectral chlorophyll indices. The statistics of the Chl-a and Chl-ab contents are summarized in Table 4.2. The variability of Chl-a and Chl-ab content was high with variance values of 64.68 and 258.34, respectively.

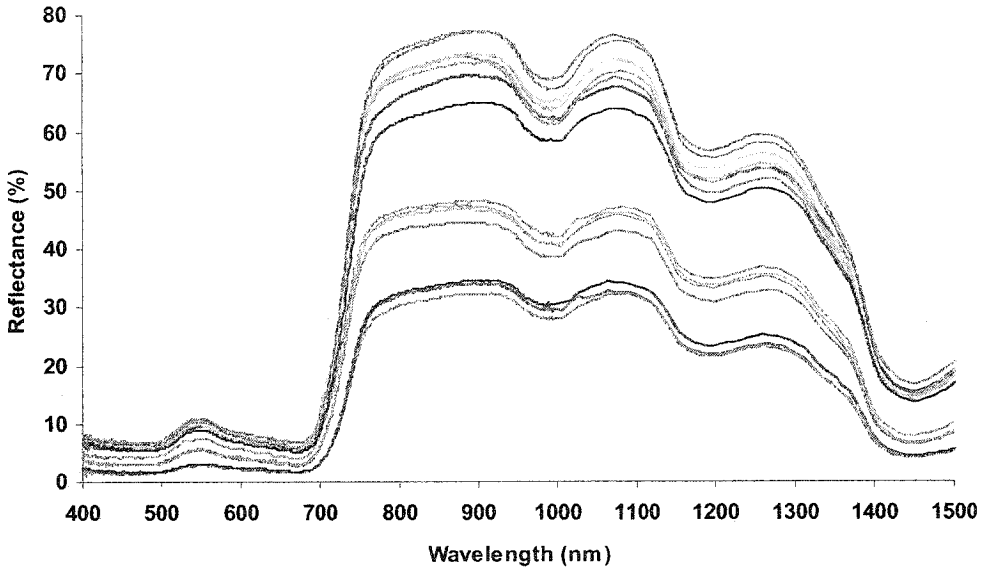

Figure 4.4: Indoor measured spectra using the GER-3700 spectroradiometer.

Table 4.2: Chlorophyll content ($\mu g / cm^2$) statistics derived from the laboratory SPAD-502 measurements.

Pigment	Mean	Maximum	Minimum	Std. Deviation	Variance
Chl-a	12.04	21.50	0.20	8.04	64.68
Chl-ab	25.24	43.76	0.64	16.07	258.34

The results of the tested indices are summarized in Table 4.3. The scatter plots of indices with significant results, i.e., SIPI, PRI, NDPI, SRPI and NPCI, are shown in Figures 4.5, 4.6, 4.7, 4.8 and 4.9, respectively. The graphical results of the remaining indices with poor performance are shown in Appendix VI. The visual assessment of the scatter plots collaborates well with the statistics in Table 4.3. Models assumptions were checked for the results. The relationship between indices and chlorophyll content shows a linear trend except NPCI. The positive slope indicates that when the index increases,

chlorophyll content also increases. If the slope is negative, the chlorophyll content decreases with the increase in index value.

SIPI and PRI (Figures 4.5 and 4.6) showed a positive linear relationship while NDPI and SRPI (Figures 4.7 and 4.8) showed a negative linear relationship with Chl-ab content. In addition, NPCI (Figure 4.9) depicted also a negative 2nd order polynomial relationship with the ratio of Chl-ab / Chl-a.

Table 4.3: Relationships between the chlorophyll indices calculated from the GER-3700 data and chlorophyll content (least square linear regression line, RMSE is the root mean square error and R^2 is the coefficient of determination significant at $p < 0.05$).

Index	Pigment	Fit-equation	RMSE	R^2
NDPI	Chl-ab	Y = –31.528 * X + 3.2955	11.06	**0.56**
SIPI	Chl-ab	Y = 230.62 * X – 227.62	10.27	**0.62**
SRPI	Chl-ab	Y = –14.829 * X + 18.141	10.96	**0.57**
PRI	Chl-ab	Y = 130.92 * X – 2.8788	11.32	**0.54**
CARI	Chl-ab	Y = –0.81581 * X + 5.2941	12.99	0.39
MCARI	Chl-ab	Y = –0.8338 * X + 5.3594	12.73	0.41
MCARI/OSAVI	Chl-ab	Y = –0.77806 * X + 5.1995	12.89	0.40
TCARI	Chl-ab	Y = –0.27793 * X + 5.3594	12.73	0.41
TCARI/OSAVI	Chl-ab	Y = –0.25935 * X + 5.1995	12.89	0.40
$PSND_a$	Chl-a	Y = 13.417 * X – 10.311	7.59	0.17
$PSSR_a$	Chl-a	Y = 0.12972 * X – 0.55493	7.45	0.20
OSAVI	Chl-a	Y = 12.67 * X –11.433	7.54	0.18
hNDVI	Chl-a	Y = 15.494 * X – 12.189	7.39	0.21
CAI	Chl-a	Y = –4.4766 * X + 3.6485	8.23	0.02
GNDVI	Chl-a	Y = 11.121 * X – 7.2981	7.28	0.23
NPCI	Chl-ab / Chl-a	Y = 8.4929 * X^2 – 0.16808 * X + 0.20684	0.11	**0.84**

When examining the results in Table 4.3, the slopes for the regression lines were high for SIPI and PRI with values of 230.62 and 130.92, respectively. However, the intercepts were negative for SIPI and PRI with values of –227.62 and –2.8788, respectively.

Figure 4.5 shows the relationship between SIPI and Chl-ab content with a R^2 of 0.62 and RMSE of 10.27 μg / cm^2. Figure 4.6 presents the relationship between PRI and Chl-ab content with R^2 of 0.54 and RMSE of 11.32 μg / cm^2.

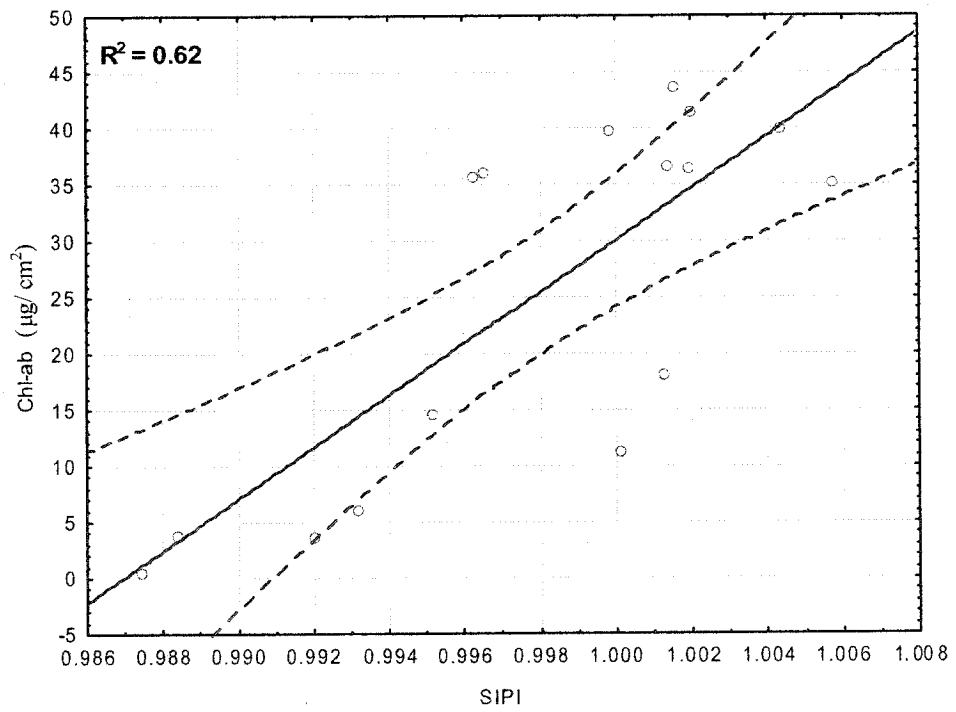

Figure 4.5: Relationship between SIPI calculated from GER-3700 data and Chl-ab content (μg / cm^2). Solid red line is the least squares regression line; dotted red line is the 95% confidence interval for the regression.

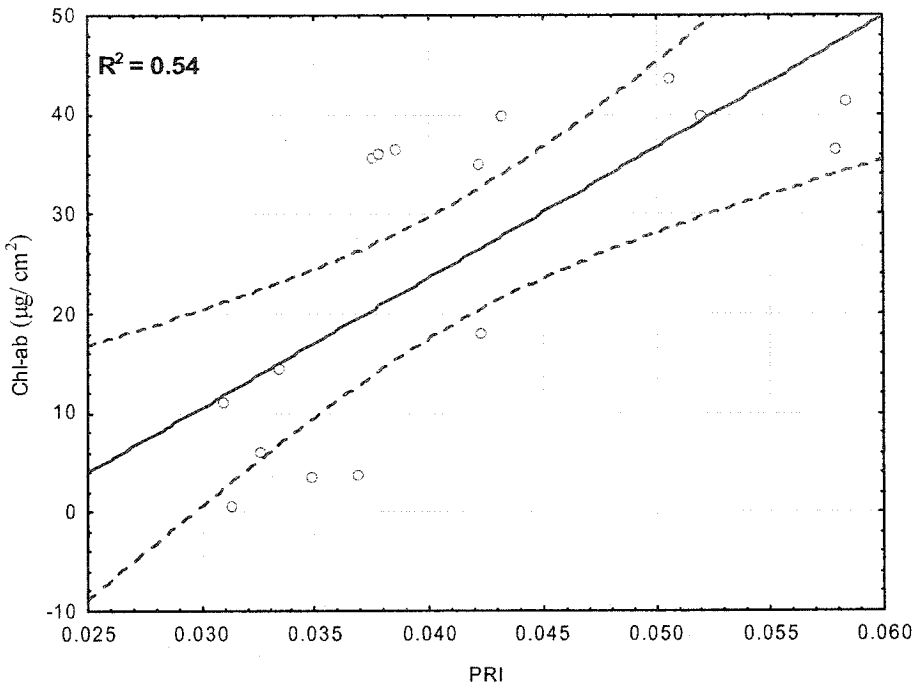

Figure 4.6: Relationship between PRI calculated from GER-3700 data and Chl-ab content (µg / cm^2). Solid red line is the least squares regression line; dotted red line is the 95% confidence interval for the regression.

In case of NDPI and SRPI, the slopes for the regression lines were negative with values of –31.528 and –14.829 and intercepts were positive with values of 3.2955 and 18.141, respectively.

Figures 4.7 and 4.8 shows a linear relationships between NDPI and SRPI indices with Chl-ab contents with a R^2 of 0.56 and 0.57 and a RMSE of 11.06 and 10.96 µg / cm^2, respectively. The majority of the data points are found within or near to the 95% confidence interval for the regression line indicating good linear relationships for these four indices with chlorophyll content.

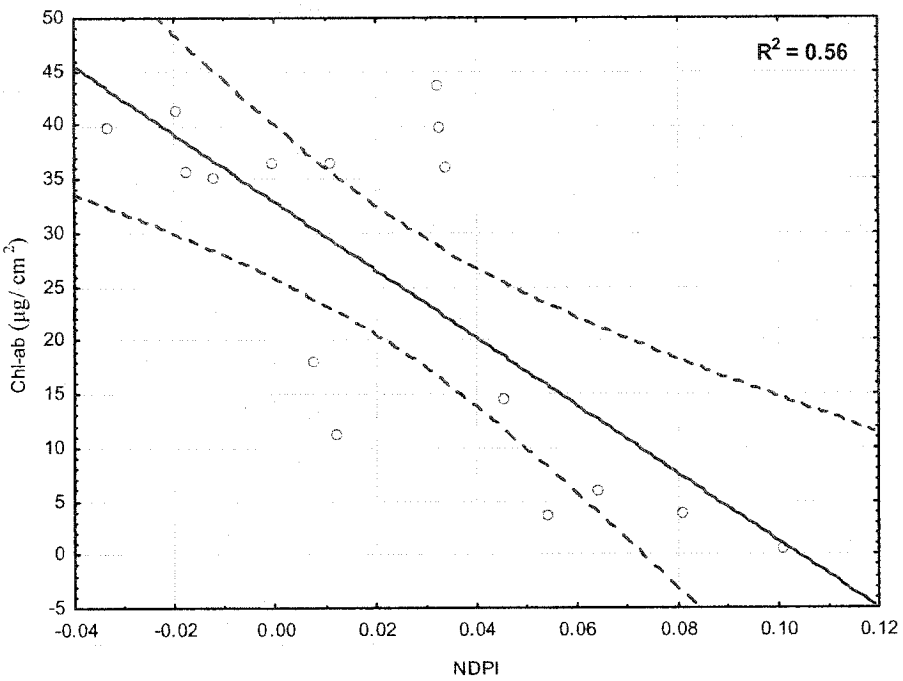

Figure 4.7: Relationship between NDPI calculated from GER-3700 data and Chl-ab content (µg / cm^2). Solid red line is the least squares regression line; dotted red line is the 95% confidence interval for the regression.

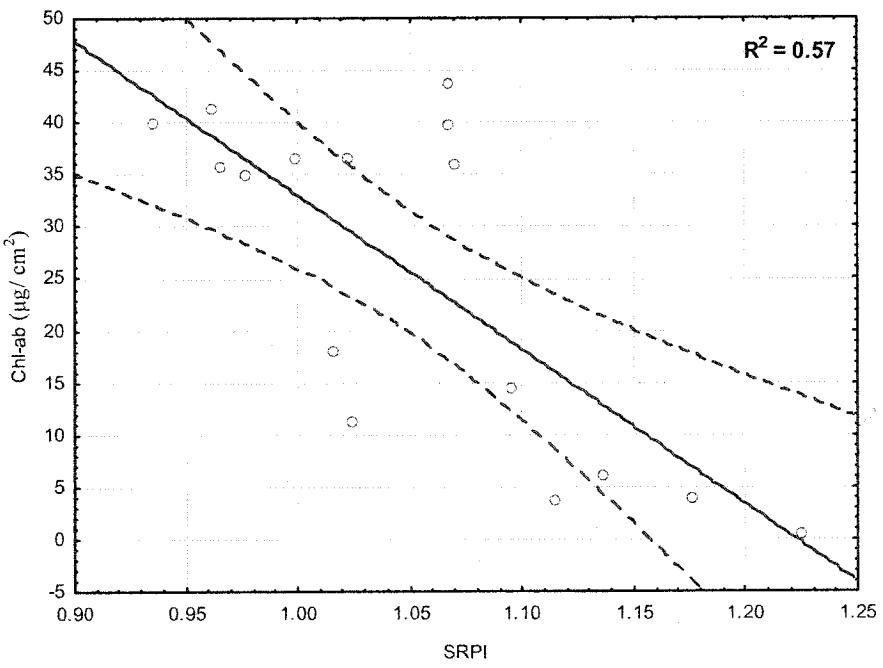

Figure 4.8: Relationship between SRPI calculated from GER-3700 data and Chl-ab content (µg / cm^2). Solid red line is the least squares regression line; dotted red line is the 95% confidence interval for the regression.

Figure 4.9 depicts the polynomial relationship between NPCI with the ratio of Chl-ab / Chl-a with a R^2 of 0.84 and RMSE of 0.11. The majority of data points are found within the 95% confidence interval for the regression line indicating a good polynomial relationship for NPCI with the Chl-ab / Chl-a ratio.

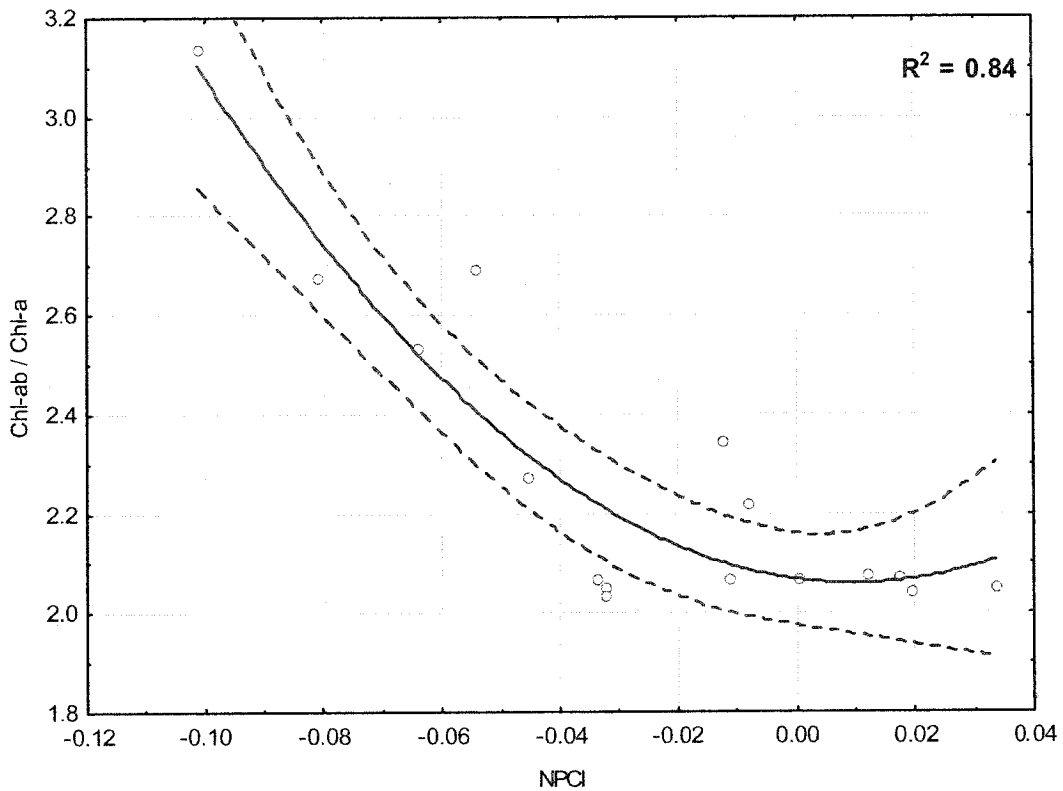

Figure 4.9: Relationship between NPCI calculated from GER-3700 data and the ratio of Chl-ab / Chl-a. Solid red line is the least squares regression line; dotted red line is the 95% confidence interval for the regression.

Overall, the SIPI, PRI, SRPI and NDPI indices showed satisfactory results for the GER-3700 spectral data for the estimation of Chl-ab contents. The SIPI depicted the best relationship for Chl-ab content than the other three indices. The NPCI showed a

significant relationship with the Chl-ab / Chl-a ratio. It was found the most sensitive index to the wheat chlorophyll content variations than the rest of the indices.

The SIPI, NDPI, NPCI and PRI indices are based on the normalized difference vegetation index and have shown good results compared to the other indices. Only one simple ratio index, SRPI, performed better than the other complex ratio indices such as the TCARI / OSAVI ratio index.

The poor results derived from the spectral chlorophyll indices may be likely due to the reason that the tested indices were developed for plants or crop species other than the wheat crop. However, published indices such as CAI, which were established specifically for wheat crop, were unable to give satisfactory results. Indices, such as SRPI, NDPI and SIPI, were originally developed for the ratio of carotenoids and Chl-a contents. However, these three indices were tested against the Chl-ab and Chl-a contents in this study. They have shown satisfactory results with Chl-ab content. The other important reason is the use of the SPAD-502 meter for chlorophyll content estimates instead of using direct chemically extracted leaf chlorophyll content for establishing the relationship against spectral chlorophyll indices. Richardson *et al.* (2002) reported in a foliar chlorophyll content study of paper birch (*Betula papyrifera*) leaves using hand-held absorbance meters such as the SPAD-502 appeared to be less accurate as the leaf chlorophyll content increased. Haboudane *et al.* (2002) preferred the use of laboratory-extracted corn leaf chlorophyll content as ground reference for hyperspectral data estimated chlorophyll to prevent the calibration problems associated with an operational use of SPAD.

4.3.2. Chlorophyll Content Estimation using the Hyperion Data

In this section result of the chlorophyll content estimation using the Hyperion hyperspectral data are presented and discussed in three main parts. Firstly, the relationship, established at leaf-level between the selected indices, which were calculated from the GER-3700 spectral data and Chl-ab or Chl-a as discussed in the previous section was used to estimate chlorophyll content from Hyperion data. Secondly, chlorophyll content prediction using a scaling-up approach from leaf to canopy-level are presented and discussed. Thirdly, the published relationships, established for wheat crop, were also used to estimate the chlorophyll content from the Hyperion image data. The resulting chlorophyll content estimates were validated against measured chlorophyll content derived from in-situ SPAD-502 measurements. The significant results are presented in scatter plots. Finally, the best index is presented that performed consistently both at leaf and canopy-levels.

4.3.2.1. Chlorophyll Content Predictions through Established Equations

Results for the image June 30th, 2002, for which ground reference measurements (twenty plots from both study sites) are available, are reported in this section. The corresponding SPAD-502 measurements for these plots were converted into Chl-a and Chl-ab contents using the calibration equations (Table 4.1). The statistics of Chl-a and Chl-ab contents are given in Table 4.4. It was found that the variability of Chl-a and Chl-ab contents were low with variance values of 0.70 and 2.65, respectively.

Table 4.4: Chlorophyll content (μg / cm^2) statistics derived from the in-situ SPAD-502 measurements.

Pigment	Mean	Maximum	Minimum	Std. Deviation	Variance
Chl-a	12.61	13.81	10.48	0.84	0.70
Chl-ab	26.87	29.18	22.71	1.62	2.65

Chlorophyll content prediction results based on established equations are summarized in Table 4.5 and scatter plots are presented in Figures 4.10, 4.11, 4.12, 4.13 and 4.14. These Figures show chlorophyll content estimation extracted from the Hyperion reflectance data using the leaf-level established equations for NDPI, SIPI, NPCI, PRI and SRPI indices. These estimates were compared against corresponding measured chlorophyll contents in the field derived from the Chl_{SPAD} values. The graphical results of the remaining established equations with poor performance are presented in Appendix VII.

NDPI showed the best result for Chl-ab estimation with a D value of 0.66 and RMSE of 2.89 μg / cm^2. Average values of estimated and measured for Chl-ab content are comparable with values of 26.50 and 27.09, respectively. The scatter plot in Figure 4.10 for NDPI illustrates a satisfactory relationship between the measured and estimated Chl-ab content where data points are close to the 1:1 line, indicating that the NDPI estimation for Chl-ab content from the Hyperion image data was in satisfactory agreement with Chl-ab content derived from the SPAD-502 measurements.

Table 4.5: Results of predicted chlorophyll content through established equations (where X_E and X_M are the average of estimated and measured Chl-ab and Chl-a, σ_E and σ_M are the standard deviations of estimated and measured Chl-ab and Chl-a, and D is the index of agreement).

Index	Pigment	(X_E)	(X_M)	(σ_E)	(σ_M)	RMSE	D
NDPI	Chl-ab	26.50	27.09	3.69	1.69	2.89	**0.66**
SIPI	Chl-ab	17.75	27.09	4.08	1.69	10.51	0.17
PRI	Chl-ab	12.93	27.09	1.19	1.69	14.24	0.16
SRPI	Chl-ab	15.81	27.09	1.14	1.69	11.35	0.19
CARI	Chl-ab	2.75	27.09	0.19	1.69	24.41	0.09
MCARI	Chl-ab	2.60	27.09	0.27	1.69	24.55	0.09
MCARI/OSAVI	Chl-ab	2.66	27.09	0.16	1.69	24.49	0.09
TCARI	Chl-ab	2.60	27.09	0.26	1.69	24.56	0.09
TCARI/OSAVI	Chl-ab	2.65	27.09	0.15	1.69	24.49	0.09
$PSND_a$	Chl-a	1.33	12.73	0.49	0.87	11.42	0.10
$PSSR_a$	Chl-a	1.43	12.73	0.57	0.87	11.32	0.11
OSAVI	Chl-a	1.37	12.73	0.52	0.87	11.39	0.10
hNDVI	Chl-a	1.35	12.73	0.54	0.87	11.40	0.10
CAI	Chl-a	1.18	12.73	0.16	0.87	11.59	0.10
GNDVI	Chl-a	0.844	12.73	0.31	0.87	11.91	0.10
NPCI	Chl-ab / Chl-a	4.79	2.12	1.48	0.01	3.03	0.003

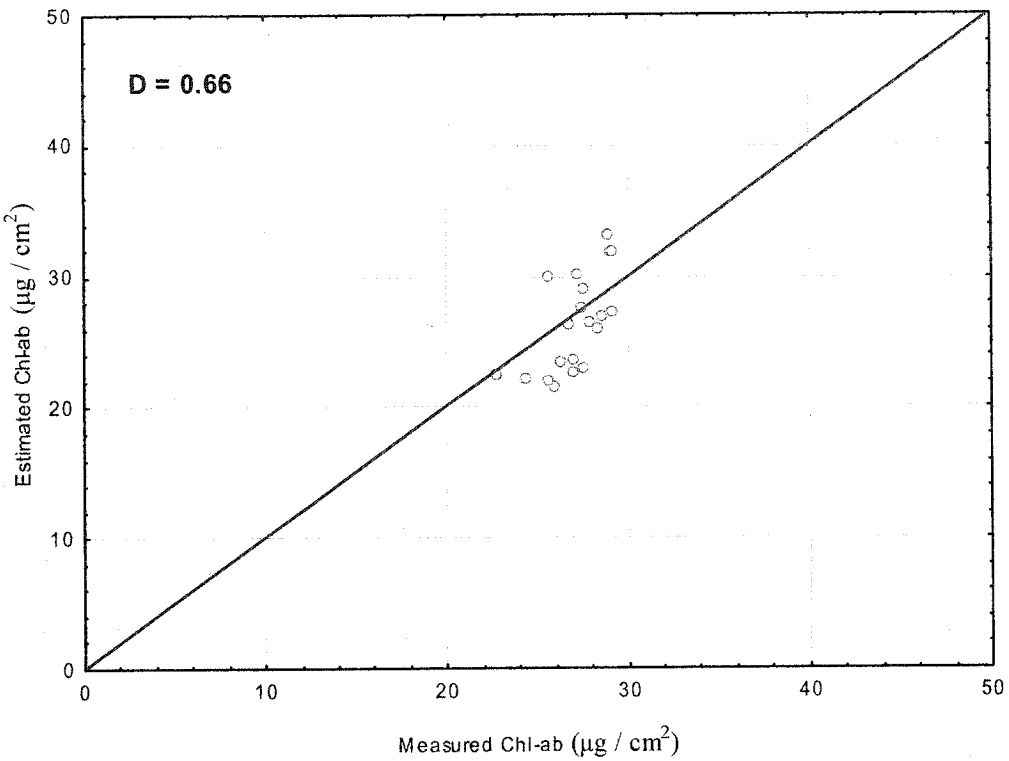

Figure 4.10: Relationship between Chl-ab (µg / cm^2) estimated from the Hyperion image data using the leaf-level NDPI calibration equation and that derived from SPAD-502 measurements.

NPCI failed to perform at the canopy-level using the Hyperion reflectance data (Figure 4.11) with a D 0f 0.003 and RMSE of 3.03 (Table 4.5). This is in context in comparing to the best performance at the leaf-level using the GER-3700 data. The average of the estimated and measured ratio of the Chl-ab / Chl-a for NPCI differed with values of 4.79 and 2.12, respectively. All of the data points for the estimated and measured ratio of the Chl-ab / Chl-a were located above the 1:1 line indicating that NPCI overestimating for this ratio retrieved from the Hyperion image data. The estimated ratio of the Chl-ab / Chl-a for NPCI using the Hyperion data was not sensitive to measured ratio of the Chl-ab / Chl-a .

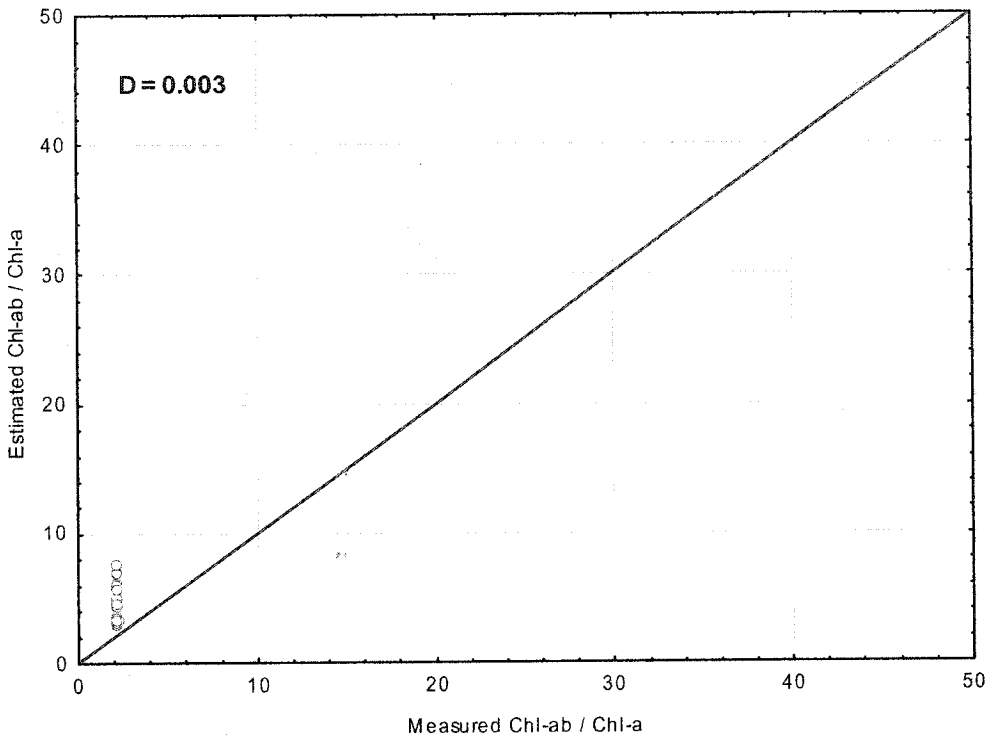

Figure 4.11: Relationship between Chl-ab / Chl-a ratio estimated from the Hyperion image data using the leaf-level NPCI calibration equation and that derived from SPAD-502 measurements.

Similarly, SIPI, PRI and SRPI performed poorly at the canopy-level using the Hyperion image data as shown in Figures 4.12, 4.13 and 4.14, respectively. Accordingly, the average values for estimated and measured Chl-ab were found significantly different as shown in Table 4.5. The scatter plots in these Figures demonstrate a very poor fit to the 1:1 line. Data points were located below the 1:1 line indicating that the three indices underestimated the Chl-ab content using the Hyperion image data. The data points for the PRI and SRPI indices as displayed in Figures 4.13 and 4.14 shows an offset from the 1:1 line.

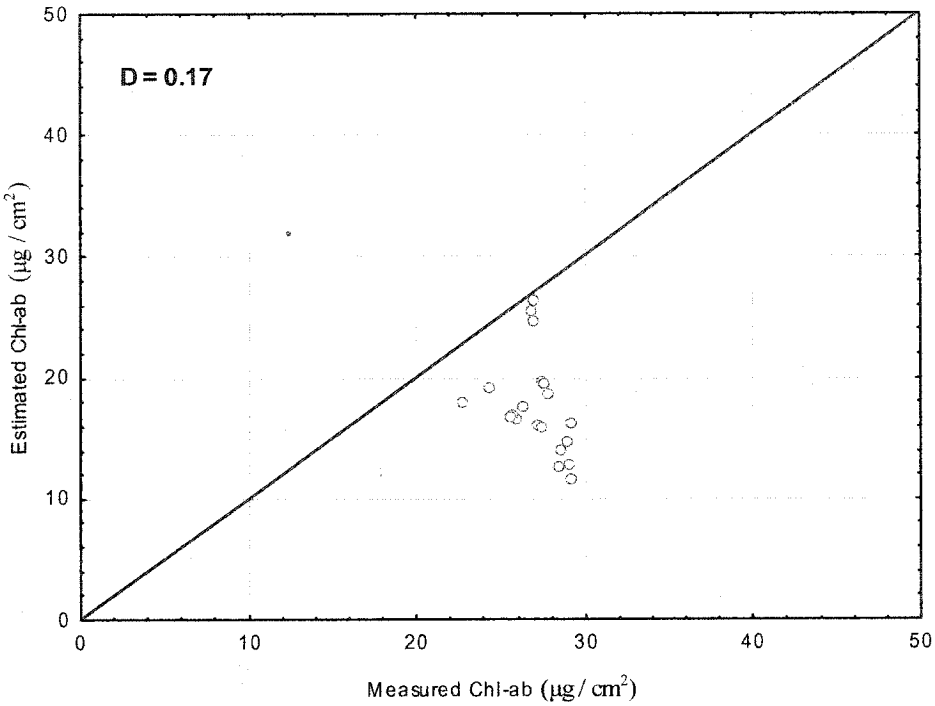

Figure 4.12: Relationship between Chl-ab (µg / cm²) estimated from the Hyperion image data using the leaf-level SIPI calibration equation and that derived from SPAD-502 measurements.

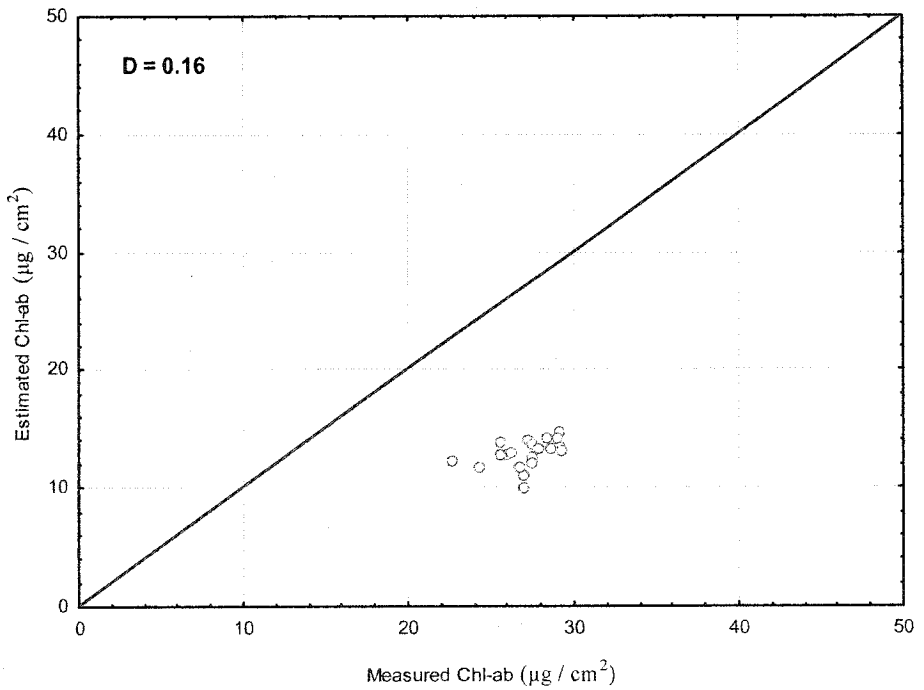

Figure 4.13: Relationship between Chl-ab (µg / cm²) estimated from the Hyperion image data using the leaf-level PRI calibration equation and that derived from SPAD-502 measurements.

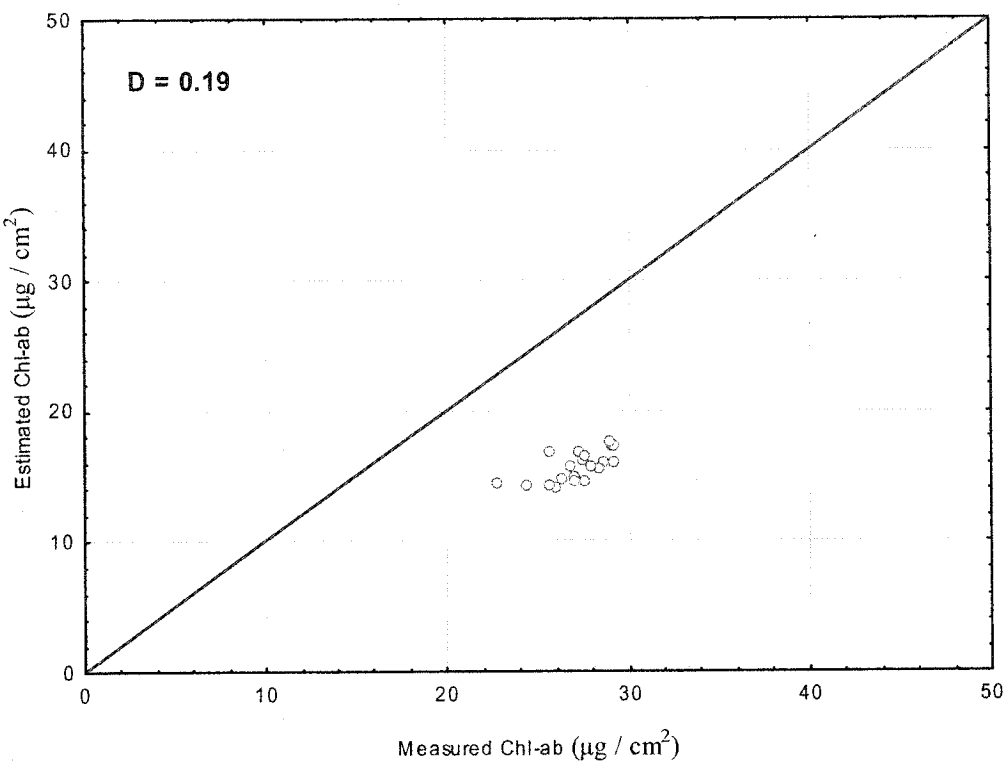

Figure 4.14: Relationship between Chl-ab (µg / cm^2) estimated from the Hyperion image data using the leaf-level SRPI calibration equation and that derived from SPAD-502 measurements.

The NDPI showed overall consistently satisfactory results for estimating chlorophyll content from the Hyperion image data. However, SIPI, NPCI, PRI and SRPI performed poorly for estimating chlorophyll content at the canopy-level for the Hyperion image data.

These results may be likely due to several reasons; the most important one is the transition from the leaf to the canopy-level, i.e., applying the leaf-level relationships derived between spectral indices and the measured chlorophyll content directly to canopy reflectance data. Therefore, the relationships derived at the leaf-level need to be calibrated in order to be useful for estimation at the canopy-level, due to the differences

between the two media (Zarco-Tejada *et al.,* 2001). In fact, the majority of an agricultural plant canopy is composed of plant leaves, stalks, stems, flowers, residue and soil. When solar radiation penetrates through a vegetation canopy, the radiation is scattered, transmitted and reflected, and its direction and spectral composition are transformed in a complex manner by the vegetation (Goel, 1988). Accordingly, the hyperspectral sensor essentially measures spectral reflectance from the total volume of the vegetation canopy. Therefore, these indices derived from the Hyperion image data include the combined response to variations of the aforementioned components of plant and environmental properties. For this purpose, some indices, which were developed to be sensitive to chlorophyll content variations and very resistant to the variations of LAI and solar zenith angle such as the combined ratio indices (MCARI / OSAVI and TCARI / OSAVI) were included in the selected list. However, these two indices performed poorly both at the leaf and canopy-level.

The second important reason is the selection of the appropriate wavelengths for each index calculated from Hyperion image data. The majority of narrow-band indices were developed using high spectral resolution data. For this purpose, wavelengths were selected to most closely match the wavelengths position proposed for the indices (Table 3.7). A better way is to use the PROSPECT (Jacquemoud and Baret, 1990; Jacquemoud *et al.,* 1996) simulated database to find the best wavelength position for each index, which give rise to the question of calibration of all published indices for the Hyperion data.

The other reasons can be the effect of leaf structure, growth stage (i.e., vegetative and generative growth stage) of the wheat plant and nitrogen fertilizer application to the

field. Some indices were found sensitive to chlorophyll content for a particular plant with particular leaf structure. In some studies, indices were found well correlated with the different growth stages of the plant (Oppelt, 2002). Despite all the above-mentioned reasons, the Hyperion image data can be used to estimate wheat crop chlorophyll content.

4.3.2.2. Chlorophyll Content Prediction using a Scaling-up Approach

The scaling-up approach did not improve the results of predictive relationships that were established through laboratory GER-3700 measurements, which were then applied to the Hyperion-derived reflectance. Poor D index values (i.e., D less than 0.48) were found for the predicted chlorophyll content derived from the Hyperion data.

The canopy chlorophyll content retrieved from the scaling-up approach had a wide range (i.e., for Chl-a 8.48 to 31.73 and Chl-ab 18.03 to 67.76 $\mu g / cm^2$) and were therefore correlated against the selected spectral chlorophyll indices (Table 2.1) calculated from the Hyperion image data. Slightly poor correlations were even obtained (R^2 less than 0.20). These results are due the fact that the reflectance of vegetation covers are not only due to the optical properties and quantity of the individual elements that make up this cover, but also to their spatial distribution and orientation, etc. (Gastellu-Etchegorry *et al.,* 1995).

4.3.2.3. Chlorophyll Content Predictions through Published Equations

For this study, the three published indices CAI, OSAVI and hNDVI for wheat crop (Oppelt and Mauser, 2004) shown in Table 4.6 were also evaluated for the estimation of Chl-a content using the Hyperion image data. Oppelt and Mauser (2004)

correlated OSAVI against Chl-a whereas; the main objective in the development of OSAVI was to estimate plant biomass using the remote sensing data.

Table 4.6: Fit statistics of the published chlorophyll indices (Oppelt and Mauser, 2004) calculated from hyperspectral data (R^2 is the coefficient of determination).

Index	Pigment	Fit-equation	R^2
CAI	Chl-a	Y=4.19046494*X-1.23467621	0.7993
OSAVI	Chl-a	Y=3.68638647*X-1.79990135	0.7569
hNDVI	Chl-a	Y=4.3473*X-1.8922	0.7377

For these published equations, leaf Chl-a content derived from the SPAD-502 measurements was calibrated to crop canopy chl-a content using the scaling-up technique described in chapter 3. The statistics of Chl-a content are summarized in Table 4.7. It was found that the variability of Chl-a content was high with a variance value of 35.89. Results of the chlorophyll content predictions through these published relationships are summarized in Table 4.8.

Table 4.7: Canopy chlorophyll content (μg / cm^2) statistics derived from the in-situ SPAD-502 measurements.

Pigment	Mean	Maximum	Minimum	Std. Deviation	Variance
Chl-a	14.77	31.70	8.48	5.99	35.89

Table 4.8: Results of predicted chlorophyll Content through published indices (where X_E and X_M are the average of estimated and measured Chl-a, σ_E and σ_M are the standard deviation of estimated and measured Chl-a, RMSE is the root mean square error and D is the index of agreement).

Index	Pigment	(X_E)	(X_M)	(σ_E)	(σ_M)	RMSE	D
CAI	Chl-a	10.81	14.77	1.54	5.99	6.92	0.47
OSAVI	Chl-a	19.08	14.77	1.52	5.99	7.22	0.42
hNDVI	Chl-a	19.25	14.77	1.50	5.99	7.13	0.42

Figures 4.15, 4.16 and 4.17 compare Chl-a content estimation from the Hyperion reflectance data via the published equations for CAI, hNDVI and OSAVI indices with the measured Chl-a content derived from the Chl_{SPAD} values. The scatter plots for CAI, hNDVI and OSAVI indices illustrate a poor relationship between the estimated and measured Chl-a content with D of 0.47, 0.42 and 0.42 and RMSE of 6.92, 7.13 and 7.22 $\mu g / cm^2$, respectively. The majority of the data points for CAI were located below the 1:1 line indicating that this index underestimated the Chl-a content retrieved from the Hyperion image data. Almost similar results were obtained for hNDVI and OSAVI indices. This similarity is may be due the wavelength positions used in their formulations. For hNDVI and OSAVI, most data points were above the 1:1 line, demonstrating that both indices were overestimating the Chl-a content from the Hyperion image data. These results contradict those found by Oppelt and Mauser, (2004).

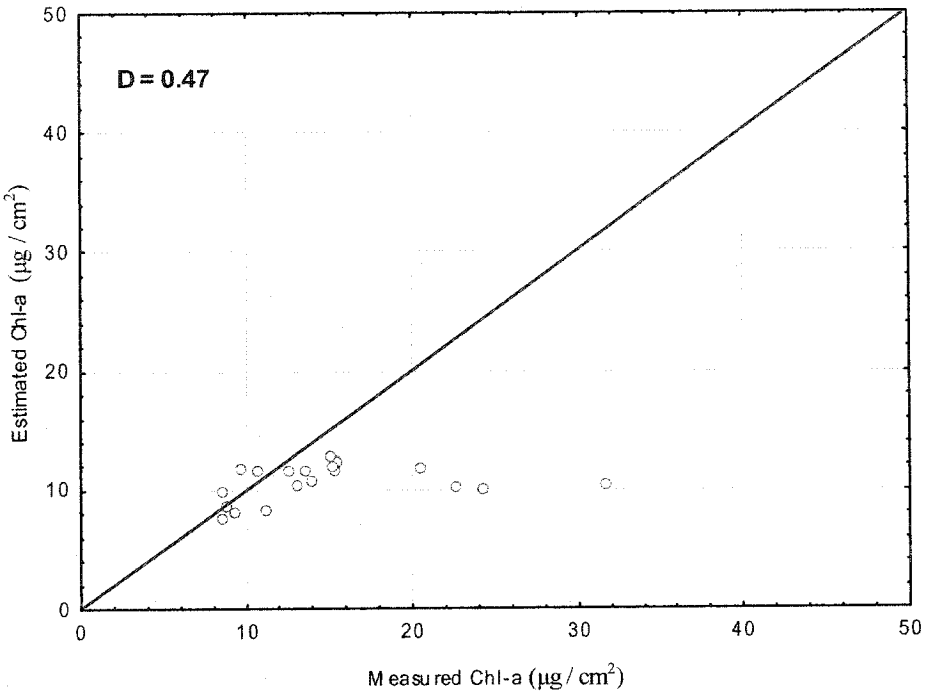

Figure 4.15: Relationship between Chl-a (µg / cm²) estimated from the Hyperion image data using the CAI calibration equation from the literature and that derived from SPAD-502 measurements.

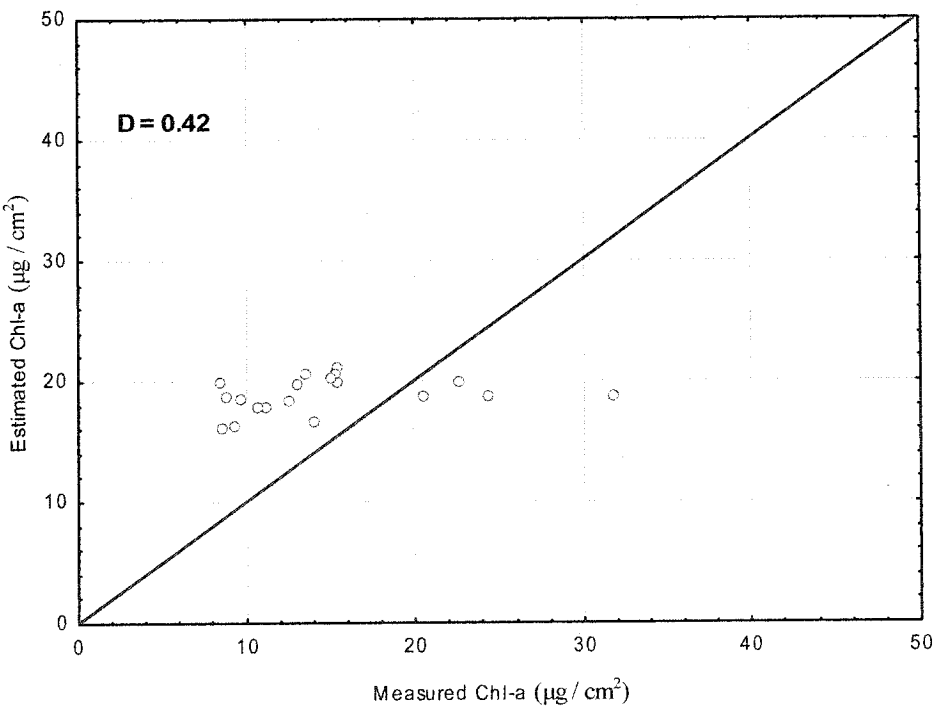

Figure 4.16: Relationship between Chl-a (µg / cm²) estimated from the Hyperion image data using the hNDVI calibration equation from the literature and that derived from SPAD-502 measurements.

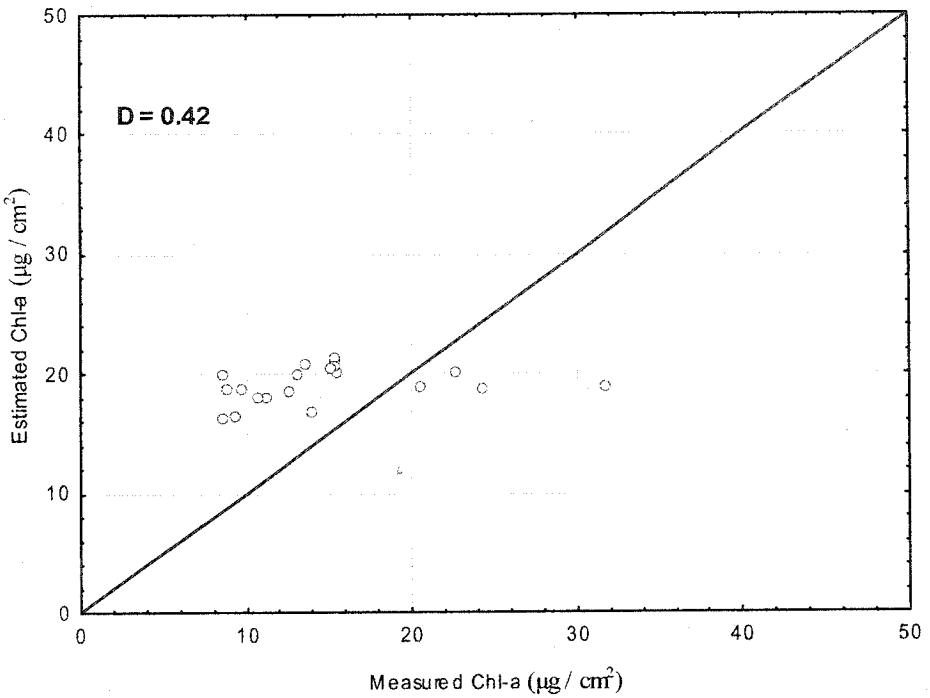

Figure 4.17: Relationship between Chl-a (µg / cm^2) estimated from the Hyperion image data using the OSAVI calibration equation from the literature and that derived from SPAD-502 measurements.

4.3.3. Best Chlorophyll Indices for Hyperion Data

NDPI showed consistent results both for leaf as well as canopy-level for chlorophyll content estimation. This index has the potential to estimate wheat crop canopy chlorophyll content on a satisfactory level using the Hyperion data. However, this consistency of the NDPI has to be thoroughly evaluated for the entire growing period of the wheat crop. Figure 4.18 shows the spatial distribution of the Chl-ab content for the Pedde and Delage fields. Pixels with blue and red color represent the low and high Chl-ab content values, respectively. A simple visual inspection of Figure 4.18 shows that the Delage field covers an area with low Chl-ab content values as compared to the Pedde field.

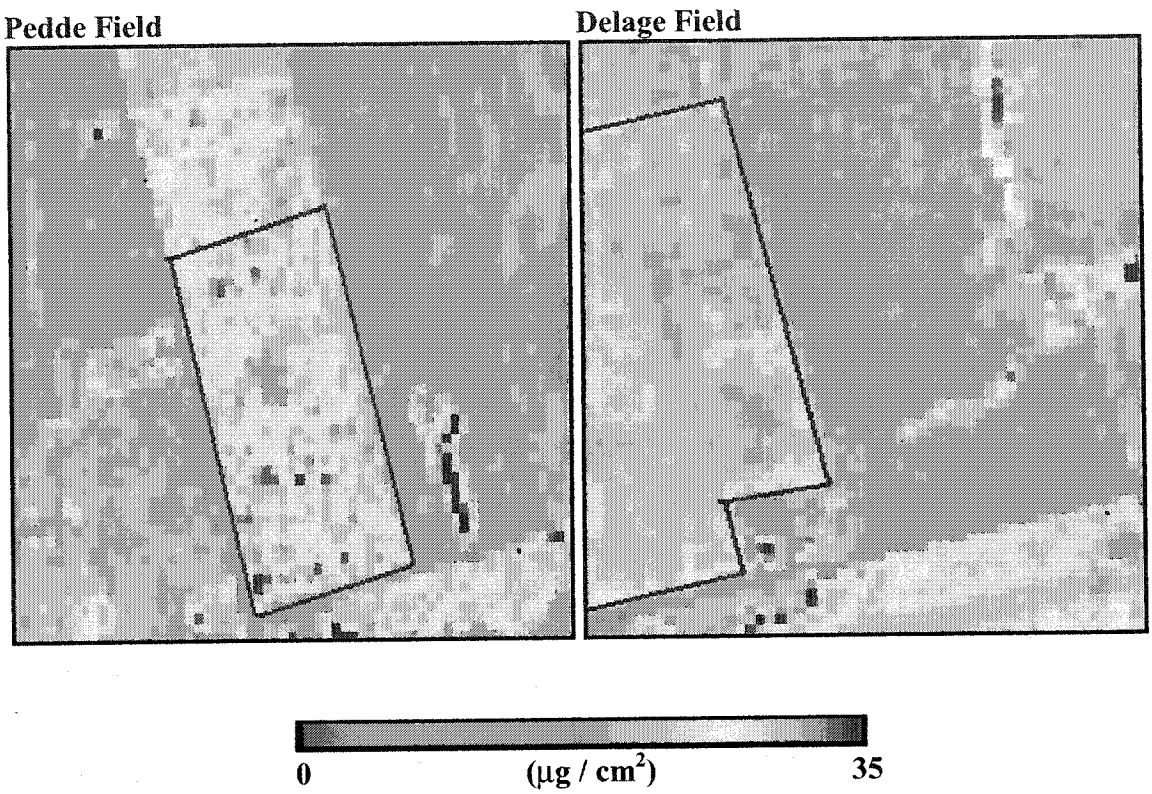

Figure 4.18: Chlorophyll-ab maps derived with NDPI for the Pedde and Delage fields (area within the red solid line).

4.3.4. Sources of Errors in Chlorophyll Content Estimation and Validation

Several sources of errors in the chlorophyll content estimation have been discussed in the sections of this chapter. These error sources are summarized in this section to provide a better understanding of the different assumptions that are made for the estimation of the chlorophyll content and the validation procedure employed. Errors can be introduced at different stages of the analysis of the data, such as field data acquisition, in the data preprocessing, chlorophyll content extraction and validation.

Preprocessing of the hyperspectral data is essential and will affect the integrity of the surface reflectance retrieval from radiance data. The sources of errors in the data preprocessing were reduced significantly by applying new techniques for the removal of

sensor artifacts. Especially the estimation of input parameters used in the MODTRAN 4.2 RT code for atmospheric correction is a critical source of error. The location of the ground sample sites in the Hyperion image data are another important source of errors. No resampling was performed on the Hyperion image data in order to preserve their radiometric integrity. Especially the GCPs selection in the image-to-image registration process for the Hyperion image influences the registration error.

The degree of crop canopy cover also plays an important role for estimation of plant biochemical constituents using remote sensing data. The image data used for this study was acquired at an early growth stage of wheat crop development and, therefore, the canopy was not entirely closed. It was found that about 70 % (results of unmixing of the Hyperion image) of both the Pedde and Delage fields were covered by wheat crop and the rest was soil and residue as shown in Figure 4.19. This means that each image pixel of the study site was a mixture of plant, soil and residue. This gives rise to the question how sensitive spectral chlorophyll indices are to environmental factors (e.g., background). For this purpose, spectral chlorophyll indices were selected, which were proposed to be sensitive to chlorophyll content variations and resistant to background soil and LAI, such as MCARI / OSAVI and TCARI / OSAVI. The results of these indices for this study proved that they are not resistant to a large background soil content and LAI values as claimed in the literature.

Figure 4.19: Photograph of a sample site.

Due to the low variability of the in-situ chlorophyll content estimates using the SPAD-502 measurements, a relationship between the spectral chlorophyll indices and measured chlorophyll content were not established directly for the Hyperion image data. For this purpose, leaf-level calibration equations were established between the spectral chlorophyll indices calculated from the laboratory GER-3700 data and chlorophyll content derived from the SPAD-502 laboratory measurements. These equations were then used to estimate chlorophyll content from the Hyperion data. The use of these calibration equations to estimate chlorophyll content at the canopy-level is a source of critical errors. For this purpose, an approach was used in this study to scale-up the leaf to the canopy chlorophyll content. Its variability was increased using this technique but no satisfactory results were achieved. However, the approach used was affected by several sources of uncertainty. One limiting factor lies in the biomass sampling method used to estimate LAI. The other most important source of error in this approach is the conversion of measured plant chlorophyll content values to stem and leaf constituents.

Validation of estimated chlorophyll content from the Hyperion data were also affected by several sources of errors. The most obvious limiting factor lies in the sampling design and technique of ground leaf chlorophyll content measurements. Especially, the acquisition of the Hyperion image and ground measurements at the same time is important to avoid errors. Therefore, chlorophyll content derived from the SPAD-502 measurements three days before and two days after the Hyperion image acquisition was used for validation purposes. Biochemical constituents such as chlorophyll content are highly variable depending on the crop growth conditions; therefore, errors in the use of these measurements would affect the results of the validation.

For validation purpose, the use of the SPAD-502 meter to estimate leaf chlorophyll content is also source of error. The SPAD-502 measurements were converted to Chl-ab and Chl-a using the calibration equations established in this study with RMSE of 0.72 and 0.69 $\mu g / cm^2$. These leaf chlorophyll content estimates at five sampling sites are then used as representative of a pixel area of 30 m^2. These representative of a pixel are also source of errors.

4.4. Conclusions

The conversion of measured Chl_{SPAD} arbitrary values into Chl-ab and Chl-a contents was successful using calibration equations established in this study. Chlorophyll content estimation using spectral chlorophyll indices from the indoor GER-3700 data was also successful. The indices NPCI, SIPI, NDPI, PRI and SRPI performed better at the

leaf-level than the rest of the indices, including CARI, MCARI, TCARI, CAI, GNDVI, $PSSR_a$, $PSND_a$, OSAVI, MCARI / OSAVI, TCARI /OSAVI, hNDVI and OSAVI. The relationships established at leaf-level were then evaluated at canopy-level using the Hyperion image data to estimate chlorophyll content. These estimations using NDPI showed satisfactory results. Accordingly, the NDPI has potential to estimate chlorophyll content from wheat canopies. The next chapter (Chapter 5) will present the conclusions of this study and will list recommendations for future research.

Chapter 5
Conclusions and Recommendations

This chapter presents the conclusions drawn from the research on chlorophyll estimation of wheat carried out in this thesis using hyperspectral remote sensing data. Recommendations for future research are also stated at the end of this chapter.

5.1. Summary and Contributions

The chlorophyll content measurements using the SPAD-502 meter were successfully converted to both Chl-ab and Chl-a contents. The two calibration equations were reported in this study for Chl-ab and Chl-a using a 2nd degree polynomial function with a coefficient of determination (R^2) of 0.72 and 0.69 and a RMSE of 3.53 and 1.94, respectively.

Selected spectral indices listed in Table 2.1 were first calculated from the laboratory GER-3700 spectroradiometric data to establish relationships at leaf-level against the chlorophyll content derived from the SPAD-502 measurements made at the same time as the GER-3700 measurements. The results indicate that the indices used have several strengths and weaknesses. The indices NDPI, SIPI, NPCI, PRI and SRPI showed satisfactory result for the GER-3700 laboratory data for wheat leaf with a R^2 of 0.56, 0.62, 0.84, 0.54 and 0.57 and a RMSE of 11.06, 10.27, 0.11, 11.32 and 10.96, respectively.

All prediction equations established at leaf-level using the laboratory GER-3700 data were then evaluated for the Hyperion reflectance data. The NDPI provided the best result of estimating wheat canopy chlorophyll content with an index of agreement (D) of

0.66 and a RMSE of 2.89 μg / cm^2. The remaining indices failed to predict chlorophyll content from the Hyperion image data. The approach to scale-up the leaf chlorophyll content to the canopy-level (weighted with LAI) failed to improve the results. Furthermore, three published equations for CAI, hNDVI and OSAVI indices established for wheat crop canopy-level were also used to estimate chlorophyll content from the Hyperion reflectance data. Poor results were obtained from these equations.

The use of new techniques for preprocessing the Hyperion image data using ISDAS at CCRS improved substantially the data quality. These new techniques include destriping, noise reduction, smile / frown and keystone detection and correction, and gain / offset detection and correction. The procedure to locate ground sample points in the Hyperion image data was successful, the RMSE for image-to-image registration process was 0.33 and 0.61 in x and y directions, respectively. These pre-processing results benefited the purpose of estimating wheat crop canopy chlorophyll content from the Hyperion satellite data.

5.2. Recommendations for Future Research

Various issues must be considered for the NDPI to be successfully implemented for operational purpose in precision agriculture. The methodology proposed in this study strongly suggests the need for future research, which is required for the use of the NDPI over the whole growing season to fully understand its potential. For this purpose, a multi-temporal dataset for wheat crop covering different growth stages needs to be investigated.

A most common problem for these empirically or semi-empirically derived spectral indices is that they are found to be species and site dependent. For this purpose,

hyperspectral data for a variety of structurally different crops covering different growth conditions would be valuable to validate the robustness of NDPI. Other issues in terms of the NDPI's sensitivity should also be addressed. For example, the implications of using the NDPI during reproductive stages of growth needs to be examined and the development of fruit on the plants might influence the chlorophyll content measured by the sensor. Further work should be focused on the development of a simple index that will have predictive capabilities in different growth stages of plants. Particularly, the determination of the appropriate set of spectral bands for such an index and their combination will enhance sensitivity to chlorophyll content variations and at the same time reduce responsivity to environmental factors. Research on the application of radiative transfer models for leaf and canopy has shown promising results and has potential to replace the empirically based approaches for estimation of plant bi-oindicators. One of the important advantages of these radiative transfer models for chlorophyll content estimation is that they can link leaf-level relationships established between spectral indices and chlorophyll content to the canopy-level.

The successful application of spectral chlorophyll indices to earth observing instruments at spaceborne platforms requires the development of links between the leaf and canopy media in order to predict canopy conditions. Therefore, future work should be focused on developing a method that relates leaf-level derived relationships to a canopy-level regardless of sites and species.

The collection of ground measurements and sampling design also requires a great deal of consideration to ensure that the measurements collected are representable of the data extracted from the remote sensing imagery.

Finally, improved agronomic models are required to implement the extracted information from the remote sensing data such as derived crop canopy chlorophyll content. Remote sensing is a very promising tool to provide spatial information in a timely and cost-effective fashion and inputs for agricultural models. In order to integrate the extracted information from remote sensing data into these models, the accuracy of approaches for the retrieval of biophysical and biochemical parameters from remote sensing data must be addressed

6. References

Adams, J.B., Smith, M.O., and Johnson, P.E. (1986). Spectral mixture modeling: A new analysis of rock and soil types at Viking Lander 1. *Journal of Geophysical research*, 91:8113-8125.

Arnon, D.I. (1949). Copper enzymes in isolated chloroplasts. Polyphenoloxidase in *Beta vulgaris*. *Plant Physiology*, 24: 1–15.

Bannari, A., Morin, D., Bonn, F. and Huete, A.R. (1995). A review of vegetation indices. *Remote Sensing Reviews*, 13:95-120.

Berk, A., L. S. Bernstein and D.C. Robertson (1989). MODTRAN: A moderate resolution model for LOWTRAN 7. *Final report*, GL-TR-0122. AFGL, Hanscom AFB, Maryland, 42 pages.

Blackmer, T.M., Schepers, J. S., and Varel, G. E. (1994). Light reflectance compared with other nitrogen stress measurements in corn leaves. *Agronomy Journal*, 86:934-938.

Blackburn, G. A. (1998a). Spectral indices for estimating photosynthetic pigment concentrations: a test using senescent tree leaves. *International Journal of Remote Sensing*, 19: 657-675.

Blackburn, G. A. (1998b). Quantifying chlorophylls and carotenoids from leaf to canopy scales: an evaluation of some hyperspectral approaches. *Remote Sensing of Environment*, 66: 273-285.

Blackburn, G. A. (1999). Relationships between spectral reflectance and pigment concentrations in stacks of deciduous broadleaves. *Remote Sensing of Environment*, 70: 224-237.

Blackburn, G. A. and C. M. Steele, (1999). Towards the remote sensing of Matorral vegetation physiology: Relationships between spectral reflectance, piment, and biophysical characteristics of semiarid bush land canopies. *Remote Sensing of Environment*, 70: 278-292.

Boardman, J.W. (1992). Automating spectral unmixing of AVRIS data using convex geometry, *Summaries of the 4th Airborne Geoscience Conference, JPL Publications* 93-26, Jet Propulsion Laboratory, Pasadena, California, USA. Volume 1, pp.11-14.

Boardman, J.W. (1995). Analysis, understanding and visualization of hyperspectral data convex sets in N-Space. *Proceedings of SPIE's International Conference on Imaging Spectrometry*, Orlando, Florida. 2480: 14-20.

Chappelle, E. W., Kim, M. S. and McMurtrey III, J. E. (1992). Ratio analysis of reflectance spectra (RARS): an algorithm for the remote estimation of the concentrations of Chlorophyll A, chlorophyll B. and the carotenoids in soybean leaves. *Remote Sensing of Environment*, 39: 239-247.

Champagne, C. (2002). Remote sensing of plant water content for precision agriculture: the potential for hyperspectral modeling. *MSc. Thesis.* Department of Geography, University of Ottawa, Ottawa, 114 pages.

Curran, P.J. 1989. Remote sensing of foliar chemistry. *Remote Sensing of Environment.*,30:271-78.

Curran, P. J., Dungan, J. L. and Gholz, H.L. (1990). Exploring the relationship between reflectance, red edge and chlorophyll content in slash pine. *Tree Physiology,* 7:33–48.

Curran, P.J., Dungan, J.L., Macler, B.A., Plummer S.E. (1991). The effect of a red pigment on the relationship between red edge and chlorophyll concentration, *Remote Sensing of Environment*, 35:69-76.

Curran, P. J. (1994). Imaging spectrometry. *Prog. Physical Geography,* 18:247–266.

Daughtry, C. S. T., Walthall, C. L., Kim, M.S., Brown de Colstoun, E. and McMurtrey III, J. E. (2000). Estimating corn leaf chlorophyll concentration from leaf and canopy reflectance. *Remote Sensing of Environment*, 74: 229-239.

Deblonde, G. and Cihlar, J. (1993). A multiyear analysis of the relationship between surface environmental variables and NDVI over the Canadian landmass. *Remote Sensing of Reviews*, 7:151-177.

Delecolle, R., Maas, S. J., Gueriff, M. and Baret, F. (1992). Remote sensing and crop production models: Present Trends. *ISPRS Journal of Photogrammetry and Remote Sensing*, 47:145-161.

Demetriades-Shah, T.H., and Steven, M.D. (1988). High resolution spectral indices for monitoring crop growth and chlorosis. *Proceedings of the 4th International Colloquium on Spectral Signatures of Objects in Remote Sensing,* Aussois (France), pp. 299-302.

Draper, N. R., and H. Smith. (1981). Applied Regression Analysis. Second edition. Wiley, New York, 709 pages.

EO-1 / Hyperion Science Data User's Guide, Level 1_B (2001). TRW Space Defence and Information Systems. One Space Park Redonde Beach, CA 90278. USA. 60 Pages.

Feng, J., Rivard, B. and Sanchez-Azofeifa, A. (2003). The topographic normalization of hyperspectral data: Implications for the selection of spectral endmembers and lithologic mapping. *Remote Sensing of Environment*, 85: 221-231.

Filella, I. and Penuelas, J. (1994). The red-edge position and shape as indicators of plant chlorophyll content, biomass and hydric status. *International Journal of Remote Sensing*, 15:1459–1470.

Filella, I., Serrano, L., Serra, J. and Penuelas, J. (1995). Evaluating wheat nitrogen status with canopy reflectance indices and discriminant analysis. *Crop Science*, 35:1400-1405.

Filella, I., Amaro, T., Araus, J. L. and Pen~uelas, J. (1996). Relationship between photosynthetic radiation-use efficiency of barley canopies and photochemical reflectance index (PRI). *Physiologia Plantarum*, 96:211-216.

Gamon J.A., Peñuelas J. and Field C.B. (1992), A narrow-waveband spectral index that tracks diurnal changes in photosynthetic efficiency. *Remote Sensing of Environment*, 41:35-44.

Gamon, J.A. and Qiu, H. (1999). Ecological applications of remote sensing at multiple scales: in F.I. Pugnaire, and F. Valladares (eds.), *Handbook of functional plant ecology*. New York: Marcel Dekker (pp. 805-846).

Gao, B.C. and Goetz, A.F.H. (1990). Column atmospheric water vapor and vegetation liquid water retrieval from airborne imaging spectrometer data. *Journal of Geophysical Research*, 95:3549-3564.

Gastellu-Etchegorry ,J.P., Zagolski, F.E., Mougin G. M. and Giordano, G. (1995). An assessment of canopy chemistry with AVRIS a case study in the Landes Forest, Southwest France. *International Journal of Remote Sensing*, 16:487-501.

Geophysical & Environmental Research Corporation (2002). *GER-3700* Spectroradiometer User's Manual, 55 pages.

Gitelson, A. and Merzyak, M.N. (1994). Quantitative estimation of chlorophyll-a using reflectance spectra: Experiment with autumn chestnut and maple leaves. *Journal of Photochem. Photobio*, 22:247-252.

Gitelson, A., Merzyak, M. N. and Lichtenthaler, H. K. (1996). Detection of red-edge position and chlorophyll content by reflectance measurements near 700 nm. *Journal of Plant Physiology*, 148: 501-508.

Goel, N.S. (1988). Models of vegetation canopy reflectance and their use in estimation of biophysical parameters from reflectance data. *Remote Sensing Reviews*, 4(1): 16-25.

Goetz, A.F.H. (1984). High spectral resolution remote sensing of the land. *Proceedings of SPIE,* 475:56-68.

Goetz, A.F.H., Vane, G., Solomon, J.E. and Rock, B.N. (1985). Imaging spectrometery for earth remote sensing. *Science*, 228 (4704): 1147-1153.

Green, R.O., Conel, J.E., Margolis, J.S., Brugge, C.J. and Hoover, G.L. (1991). An inversion algorithm for the retrieval pf atmospheric and leaf water absorption from AVRIS radiance with compensation for atmospheric scattering. *Proceedings of the 3rd Annual Airborne Visible Infrared Imaging Spectrometer (AVRIS) Workshop.* Pasadena, California, JPL Publication 91-28, pp. 51-61.

Guyot G. (1990). Optical properties of vegetation canopies. In applications of remote sensing in agriculture, edited by M.D. Stven and J.A. Clark (London: Butterworths), pp.19-44.

Haboudane, D., Miller, J. R., Tremblay, N., Zarco-Tejada, P. J., and Dextraze, L. (2002). Integrated narrow-band vegetation indices for prediction of crop chlorophyll content for application to precision agriculture, *Remote Sensing of Environment*, 81:416-426.

Hare, E. W., Miller, J.R. and Edwards, G.R. (1984). Studies of vegetation red reflectance edge in geobotanical remote sensing. *Proceedings of the 9th Canadian Symposium on Remote Sensing*, Canadian Remote Sensing Society, Canadian Aeronautical and Space Institute, Ottawa, Ontario, Canada, pp. 433-440.

Hoffer R.M. and Johannsen C.J. (1969). Ecological potential in spectral signatures analysis, *Remote sensing in Ecology*, University of Georgia, Athens (Georgia), pages 1-16.

Horler, D.N.H., Dockray, M. and Barringer, A. R. (1980). Effects of heavy metals on the absorbance and reflectance spectra of plants. *International Journal of Remote Sensing,* 1:121-136.

Horler, D. N. H., Dockray, M. and Barber, J. (1983). The red edge of plant leaf reflectance. *International. Journal of Remote Sensing,* 4:273–288.

Huete, A.R. (1988). A Soil Adjusted Vegetation Index (SAVI). *Remote Sensing of Environment,* 25:295-309.

Jacquemoud, S. and Baret, F. (1990). PROSPECT: A model of leaf optical properties spectra. *Remote Sensing of Environment,* 34:75-91.

Jacquemoud, S., Ustin, S.L., Verdebout, J., Schmuck, G., Andreoli, G. and Hosgood, B. (1996). Estimating leaf biochemistry using PROSPECT leaf optical properties model. *Remote Sensing of Environment,* 56:194-202.

Jacquemoud, S. and Ustin, S.L., (2001). Leaf optical properties: A state of the art. *Proceedings of the 8th International Symposium on Physical Measurements and Signatures in Remote Sensing*, Aussois, France, pp.223-232.

Johnson, L.F., Hlavka, C.A. and Peterson, D.L. (1994). Multivariate analysis of AVRIS data for canopy biochemical estimation along the Oregon transect. *Remote Sensing of Environment,* 47:216-230.

Keulen, H. van (1986). Plant data, *Modeling of Agricultural Production*, H. van Keulen and J. Wolf (eds), Wageningen, the Netherlands, pp.235-247.

Kim, M. S., Daughtry, C. S. T., Chappelle, E. W., McMurtrey III, J. E., and Walthall, C. L. (1994). The use of high spectral resolution bands for estimating absorbed photosynthetically active radiation (APAR). *Proceedings of the 6th Symposium on Physical Measurements and Signatures in Remote Sensing.* January. 17-21, 1994, Val D'Isere, France, pp. 299-306.

Kneubuhler, M. (2002). Spectral assessment of crop phenology based on spring wheat and winter barley. *Ph.D. Thesis.* Remote Sensing Laboratory. Department of Geography, University of Zurich, Zurich, Switzerland, 148 pages.

Kruse, F. A., Boardman, J. W. and Huntington, J. F. (2003). Comparison of Airborne Hyperspectral Data EO-1 Hyperion for Mineral Mapping. *IEEE Transactions on Geoscience and Remote Sensing,* 41:1388-1400.

Lichtenthaler, H.K., Gitelson, A. A. and Lang, M. (1996). Non-destructive determination of chlorophyll content of leaves of a green and an aurea mutant of tobacco by reflectance measurements. *Journal of Plant Physiology*, 148:483-493.

Margalef, R. (1974). *Ecología.* Omega, Barcelona, Spain, pp. 951.

Markwell, J., Osterman, J.C. and Mitchell J. L. (1995). Calibration of the Minolta *SPAD-502* leaf chlorophyll meter. *Photosynthesis Research*, 46:467-472.

McNairn, H., Deguise, J.C., Pacheco, A., Shang, J. and Rabe, N. (2001). Estimation of crop cover and chlorophyll from hyperspectral remote sensing. *Proceedings of the 23rd Canadian Symposium on Remote Sensing.* Ste. Foy, Quebec pp.

Miller, J.R., Hare, E.W. and Wu, J. (1990). Quantitative characterization of the vegetation red edge reflectance, I: An inverted-Gaussian reflectance model. *International. Journal of Remote Sensing,* 11:121-127.

Moran, M. S., A. Vidal, D. Troufleau, Y. Inoue and T. Mitchell. 1997. Combining multi-frequency microwave and optical data for farm management. *Remote Sensing of Environment,* 61: 96-109.

Moulin, S., Bondeau, A. and Delecolle, R. (1998). Combining agricultural crop models and satellite observations: from field to regional scales. *International Journal of Remote Sensing,* 19(6):1021-1036.

Neville, R.A., Staenz, K., Szeredi, T., Lefebvre, J. and Hauff, P. (1999). Automatic endmember extraction from hyperspectral data for mineral exploration. *Proceedings of the 4th International Airborne Remote Sensing Conference and Exhibition / 21st Canadian Symposium on Remote Sensing.* Ottawa, Ontario, Canada, pp. 891-897.

Neville R. A., Sun L. and Staenz K. (2003). Detection of Spectral Line Curvature in Imaging Spectrometer Data. *Proceedings of SPIE on Algorithms and Technologies for Multispectral, Hyperspectral, and Ultraspectral Imagery IX*, Vol. 5093, Orlando, Florida, U.S.A., pp 144-154.

Neville R. A., Sun L. and Staenz K. (2004). Detection of Keystone in Imaging Spectrometer Data. *Proceedings of SPIE on Algorithms and Technologies for Multispectral, Hyperspectral, and Ultraspectral Imagery IX*, Vol. 5425.

Neville R. A. (2004). Personal communication, Canada Center for Remote Sensing / Natural Resource Canada, Ottawa, Ontario, Canada.

Oppelt, N. and Mauser, W. (2001). The chlorophyll content of maize (*Zea mays*) derived with the airborne imaging spectrometer AVIS. *Proceedings of the 8th International Symposium on Physical Measurements & Signatures in Remote Sensing*, Aussois, France, pp.407-412.

Oppelt, N. and Mauser, W. (2004). Hyperspectral monitoring of physiological parameters of wheat during a vegetation period using AVIS data. *International Journal of Remote Sensing*, 25:145-159.

Pacheco, A. (2000). Contribution of hyperspectral remote sensing to the estimation of leaf area index in the context of precision agriculture. *MSc. Thesis*. Department of Geography, University of Ottawa, Ottawa, Ontario, Canada, 132 pages.

PCI Geomatics (2003). Using PCI Software. PCI, Richmond Hill, Ontario, 551 pages.

Pearson, R. L. and Miller, L. D. (1972). Remote mapping of standing crop biomass for estimation of the productivity of the shortgrass prairie, Pawnee National Grasslands, Colorado. *Proceedings of the 8th International Symposium on Remote Sensing of Environment II,* pp. 1355-1379.

Penuelas, J., Filella, I., Biel, C., Serrano, L. and Save, R., (1993). The reflectance at the 950-970 nm region as an indicator of plant water status. *International Journal of Remote Sensing*, 14: 1887-1905.

Penuelas, J., Gamon, J., Freeden, A., Merino, J. and Field, C. (1994). Reflectance indices associated with physiological changes in nitrogen and water limited sunflower leaves. *Remote Sensing of Environment*, 48:135-146.

Penuelas, J., Baret, F. and Filella, I., (1995). Semi-empirical indices to assess carotenoids/chlorophyll a ratio from leaf spectral reflectance. *Photosynthetica,* 31: 221-230.

Penuelas, J., Pinol, Ogaya, R. and Fiella, I. (1997). Estimation of plant water concentration by the reflectance water index WI (R900/R970). *International Journal of Remote Sensing*, 18:2869-2875.

Peterson D. L., Aber, J.D., Matson, P.A., Card, D.H. Swanberg, N., Wessman, C. and Spanner, M. (1988). Remote sensing of forest canopy and leaf biochemical contents. *Remote Sensing of Environment*, 24:85-108.

Richardson, A.D., Duigan, S.P. and Berlyn, G.P. (2002). An evaluation of noninvasive methods to estimate foliar chlorophyll content. *New Phytologist* 153:185-194.

Richter, N. (2004). Delineation of the Kam Kotia Mine Tailings areas (Ontario, Canada) using hyperspectral TRWIS III data. M.Sc. Thesis, Faculty of Mathematics and Natural Sciences, Institute for Geoecology, University of Potsdam, Potsdam, Germany, 98 pages.

Rondeaux, G., Steven, M. and Baret, F. (1996). Optimization of soil-adjusted vegetation indices. *Remote Sensing of Environment*, 55: 95-107.

Rouse, J.W., Hass, R.W., Schell, J.A., Deering, D.W. and Harlan, J.C. (1974). Monitoring the vernal advancement and retrogradation (greenwave effect) of natural vegetation. *NASA / GSFCT Type III Final report*. Greenbelt, Maryland, USA.

Schlapfer, D., Christoph, C.B, Keller, J. and Itten, K.I. (1998). Atmospheric precorrected differential absorption technique to retrieve columnar water vapor. *Remote Sensing of the Environment,* 65: 353-366.

Schulze, E.D. (1982). Plant life forms and their carbon, water and nutrient relations. *Physiological Plant Ecology II*, O.L. Lange, P.S. Nobel, C.B. Osmond and H. Ziegler (eds), Berlin, Germany, pp. 615-667.

Schwarz, J. (1998). Classification of hyperspectral data. *MSc. Thesis.* School of Computer Science, Carelton University, Ottawa, Ontario, Canada, 180 pages.

Spectrum Technologies (2001): Minolta *SPAD-502* meter, http://www.specmeters.com/Plant_Chlorophyll_meters/Minolta_SPAD_502_Meter.html.

Staenz, K. and Williams, D.J. (1997). Retrieval of surface reflectance from hyperspectral data using look-up-table approach. *Canadian Journal of Remote Sensing*, 23:354-368.

Staenz, K., T. Szeredi, and J. Schawaz, (1998). ISDAS - A system for processing / analyzing hyperspectral data. *Canadian Journal of Remote of Sensing*, 24: 99-113.

Staenz, K., Neville, R.A., Levesque, J., Szeredi, T., Singhroy, V., Borstad, G.A. and Hauff, P. (1999). Evaluation of CASI and SFSI hyperspectral data for environmental and geological applications - two case studies. *Canadian Journal of Remote Sensing*, 25: 311-322.

Staenz, K., Neville, R.A., Clavette, S., Landry, R., White, H.P.and Hitchcock, R. (2002). Retrieval of surface reflectance for Hyperion Radiance data. *IGARSS*, Toronto, Canada, June 24-28.

StatSoft, Inc., (1994). STATISTICA for WINDOWS, release 5.0, User manual. Tulsa, Oklahoma, USA. 1098 pages.

Sun L. (2004). Destriping Module-Help File, ISDAS, Canada Center for Remote Sensing / Natural Resource Canada, Ottawa, Ontario, Canada.

Sun L. and Neville R. A. (2004). Average Smoothing Module-Help File, ISDAS, Canada Center for Remote Sensing / Natural Resource Canada, Ottawa, Ontario, Canada.

Sun L. and Neville R. A. (2004). Gain and Offset Correction Module-Help File, ISDAS, Canada Center for Remote Sensing / Natural Resource Canada, Ottawa, Ontario, Canada.

Szeredi, T., staenz, K. and Neville, R.A. (2003). Automatic endmember selection: Part 1 Theory. (*to be published*).

Thomas J.R. and Gausman, H.W. (1977). Leaf reflectance vs. leaf chlorophyll and carotenoid concentrations of eight crops. *Agronomy Journal*, 69:799-802.

Tompkins, S., Mustard, J.F., pieters, C.M. and Forsyth, D.W. (1997). Optimization of endmembers for spectral mixture analysis. *Remote Sensing of Environment*, 59:472-489.

Tucker, C.J. (1979) Red and photographic infrared linear combinations of monitoring vegetation. *Remote Sensing of Environment*, 8:127-150.

Verdebout J., Jacquemoud S. and Schmuck G. (1994). Optical properties of leaves: modelling and experimental studies, in *Imaging Spectrometry. A tool for environmental observations* (J. Hill & J. Mégier, Eds), ECSC, EEC, EAEC, Brussels and Luxembourg, pages 169-191.

Verhoef, W. (1984). Light scattering by leaf layers with application to canopy reflectance modeling: The SAIL model. *Remote Sensing of Environment*, 16:125-141.

Verstraete, M.M. Retrieving canopy properties from remote sensing measurements, (1994). *In imaging spectrometry - tool for environmental measurements,* eds. J. Hill and Merier, Kluwar Academic Publishers, pp. 109-123.

Vogelmann, J.E., Rock, B.N. and Moss, D.M. (1993). Red edge spectral measurements from sugar maple leaves. *International Journal of Remote Sensing,* 14:1563-1575.

Willmott, C.J. (1982). Some comments on the evaluation of model performance. *Bulletin American Meteorological Society,* 63 :1309-1313.

Young, A., and Britton, G. (1990). Carotenoids and stress. In *stress responses in plants: adaptation and acclimation mechanisms* (R. G. Alscher and J. R. Cumming, Eds.), Wiley-Liss, New York, pp.87–112.

Zarco-Tejada, P.J. and Miller, J.R. (1999). Land cover mapping at BOREAS using red-edge spectral parameters from casi imagery. *Journal of Geophysical Research,* 104:27,921-27,933.

Zarco-Tejada, P.J. (2000). Hyperspectral remote sensing of closed forest canopies: Estimation of chlorophyll fluroscenece and pigment content. *Ph.D. Thesis*, York University, Toronto, Ontario, Canada, 233 pages.

Zarco-Tejada, P. J., Miller, J. R., Noland, T. L., Mohammed, G. H. and Sampson, P. H. (2001). Scaling-up and model inversion methods with narrow-band optical indices for chlorophyll content estimation in closed forest canopies with hyperspectral data. *IEEE Transactions on Geosciences and Remote Sensing*, 39: 1491-1507.

APPENDICES

APPENDIX I: PLANT PHOTOSYNTHETIC PIGMENTS AND OPTICAL PROPERTIES OF PLANTS.

1. Plant Photosynthetic Pigments

The main photosynthetic pigments of plant leaves are chlorophyll-a, chlorophyll-b, carotenoids, and xanthophylls. These different pigments are of various colors and are present in the chloroplast (i.e., green tissues) of plants. Chlorophyll is the primary photosynthetic green pigment in plant leaves. The two basic types of chlorophyll in plants, i.e., chlorophyll-a and chlorophyll-b, are slightly different in chemical structure. At the leaf scale, chlorophyll molecules absorb more of the sunlight than other pigments and convert light into chemical energy for photosynthesis process. The chemical structure of the chlorophyll has strong absorption bands, which make these molecules ideal for absorbing solar energy. Therefore, concentrations of the chlorophyll molecules relate strongly to the photosynthetic potential of plants. The absorption of electromagnetic radiation by chlorophyll molecules in a healthy leaf changes with the wavelength. The chlorophyll molecules have strong absorption in the blue (400-500 nm) and red (600-700 nm) regions of the visible spectrum and relatively less absorption in the green region (500-600 nm). The latter portion is called the green peak area. The other photosynthetic pigments absorption of sunlight, present in the leaf, are usually masked by the chlorophyll molecule absorption. Carotenoids (commonly yellow to red in color) also absorb the sunlight, but transfer their absorbed energy to chlorophyll. When plants are under stress or during leaf senescence, total chlorophyll content tends to decline more rapidly than the other photosynthetic pigments. This decline in total chlorophyll content allows other photosynthetic pigments, such as carotenoids and xanthophylls to become dominant. This variation in total chlorophyll content in plant leaves results in changes of leaf optical properties, which increase the leaf transmittance at visible wavelengths and, therefore, leads to less overall absorption. Differences in reflectance between healthy and stressed plant leaves due to changes in total

chlorophyll content levels have been detected by remote sensing methods in the green peak area and along the red edge (690-750 nm) (Gitelson *et al.,* 1994; Gitelson and Merzlyak, 1996).

Chlorophyll content in green vegetation is positively related to nitrogen content at the plant scale. It means that nitrogen content is indirectly related to one of the basic plant physiological processes, the photosynthesis. Therefore, the nitrogen content or concentration is an indicator of a canopy's ability to photosynthesize because the chlorophyll molecule is a key constituent of photosynthetic enzymes. Various crop types have different requirements for the amount of nitrogen during their critical growth stages. When nitrogen supply exceeds the nutritional needs of vegetation, the excess is eliminated by runoff and water infiltration leading to environmental pollution (Daughtry *et al.,* 2000). This loss of nutrients to the environment is a loss for farmers as well as a threat to ecosystems. On the other hand, inappropriate reduction of the nitrogen fertilizer application could result in low yields and, subsequently, will cause economic losses. This problem can be overcome by finding the optimal and rational solution for adequate assessment of nitrogen status in agricultural fields. Crop yield is determined by the condition of a specific crop at the early stages of its growth cycle. Accordingly, it is important to provide farm managers and farmers with nitrogen status at those critical stages in order to apply appropriate nitrogen fertilizer rates based upon an accurate assessment of crop growth requirements and deficiencies. For this purpose, remote sensing can play a critical role in detecting spatial variation in the field for nitrogen status for specific soil and crop conditions.

The availability of water content also affects the variations in the greenness of plants at the plant scale. Water plays a critical role in a plant's life; it is used for photosynthesis, transportation of nutrients from soil to the roots and within plants, for the distribution of assimilates within organs, ensuring a sufficient turgescence or freshness to maintain canopy structure for optimal interception / protection of light, and for the thermo-regulation of the plant tissues. The exchanges of water between the leaf and the atmosphere are controlled by stomates,

which are the small holes in the leaf surface. For the photosynthesis process, the atmospheric carbon transfers to chloroplasts through the stomates. This is the case when insufficient water is available to meet the transpirational and physiological demands of the plants. Besides other effects, unavailability of water also causes variations in the photosynthesis process and stress may develop in plants. Therefore, the primary plant pigments chlorophyll-a and chlorophyll-b are named as the engine of plant biomass production and the resulting crop yield. The reflected radiation from crop leaves and canopies has been used to estimate chlorophyll content of crop canopies (Daughtry *et al.*, 2000).

2.Optical Properties of Plants

The optical properties of plants will be divided in to the two parts, optical properties of plant leaves and canopy.

2.1. Optical Properties of Plant Leaves

Leaf optical properties are a function of concentration of leaf biochemical constituents, and water content, and are also dependent on the morphology and anatomy of leaves, such as size, form and arrangement of cells and aerial interspaces (Gitelson and Merzlyak, 1996). Incident sunlight radiation on a leaf surface can be reflected, transmitted or absorbed. The basic optical laws of reflection, absorption and refraction can be applied to plant leaves.

Firstly, leaf surface reflection is a combination of diffuse and specular reflection. It is not a Lambertian surface and depends on the physiological state of the leaf surface. The spongy mesophyll with intercellular air spaces of a leaf are responsible for the diffuse reflection of light. Different plants such as monocotylednous and dicotylednous plants have different leaf morphology and a mesophyll structure with different intercellular spaces. These differences

between leaves cause changes in reflectance, with a higher reflectance for the dicotylednous leaves.

Secondly, the photosynthetic pigments, present in the chloroplasts of plant leaves, mainly cause the absorption of electromagnetic radiation (Verdebout, 1994). The visible and near infrared (VNIR) and shortwave infrared (SWIR) wavelengths can be divided into three spectral regions for the evaluation of spectral properties of plant leaves as shown in Figure AI-1. The first one is the visible wavelength region (400 to 750 nm according to Hoffer and Johnnsen, 1969) where absorption is mainly due to the plant photosynthetic pigments (chlorophyll-a, chlorophyll-b, carotenoids, and xanthophylls). This spectral region is also important for the visual appearance of a plant leaf and is related to the concentration of the photosynthetic pigments. A plant appears green due to the presence of chlorophyll content. During early growth and senescence stages of a plant, the non-chlorophyll pigments concentrations, such as carotenoids are higher, which result in the yellow to brown appearance of plant leaves. The second spectral region covers the near-infrared wavelengths (750 to 1350 nm according to Hoffer and Johnnsen, 1969) where absorption is mainly caused by the internal leaf cell structure. Higher reflectance occurs in this spectral region as compared to the visible spectral region. The third spectral region is the shortwave infrared wavelengths (1350 to 2500 nm according to Hoffer and Johnnsen, 1969) where absorption is mainly due to the water concentration in plant tissues. All plants contain water, but this is vaculate water that affects the reflectance in this spectral region. These three spectral regions make it possible to study the physiological and morphological properties of plant leaves in detail using remotely sensed data.

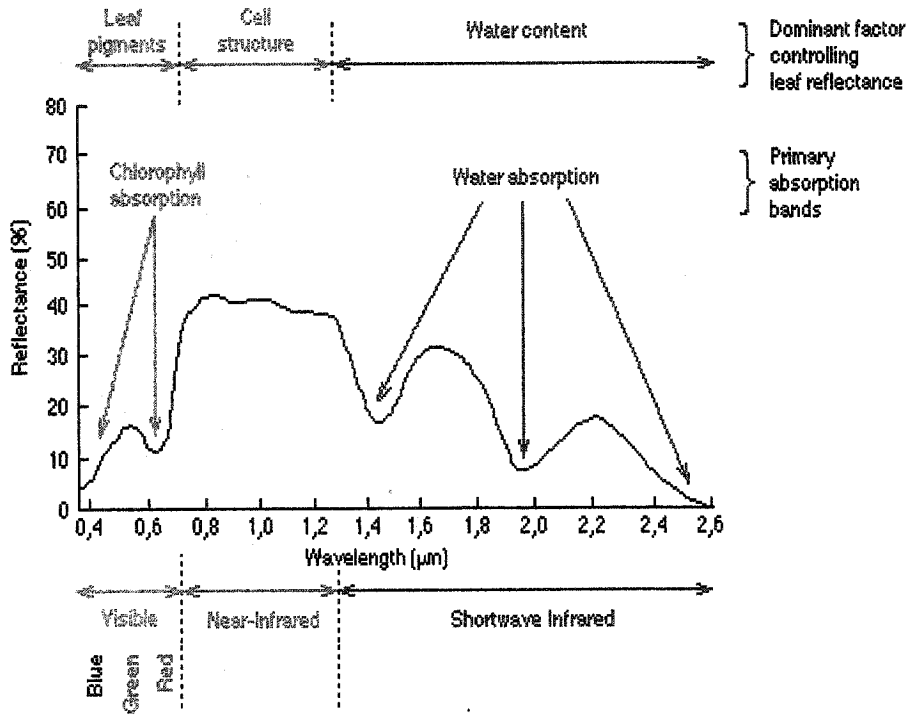

Figure AI-1: Typical response characteristics of green vegetation (Hoffer and Johnnsen, 1969).

Thirdly, a plant leaf transmits the sunlight. The transmittance of a leaf is mostly determined by the leaf morphology, leaf thickness and concentration of leaf pigments.

2.2. Optical Properties of Crop Canopies

The spectral characteristics of plant leaves is insufficient to describe the remotely sensed data acquired over a canopy where the response is often a contribution of plant leaf, stem, residue, background soil and shadow. The canopy structural properties and arrangement of leaves control the proportions of these elements. The optical properties of the background soil and shadow also influence the spectral response of a crop canopy. Besides these elements, the solar and sensor viewing geometry must be taken into account, since they largely affect the

spectral response of a canopy (Blackburn, 1998). Therefore, several canopy reflectance models have been developed for understanding the photon-vegetation interactions for different plant species under different structural and illumination conditions (Zarco-Tejada, 2000). Modeling canopy spectral properties is often based on optical properties of single leaves that are combined with structural characteristics. Jacquemoud *et al.,* (2001) reported different approaches for modeling leaf and canopy optical properties to retrieve biophysical and biochemical parameters from remotely sensed data.

APPENDIX II: PEDDE AND DELAGE FIELD GRID, SAMPLING SITES WITH DISTRIBUTION OF NITROGEN APPLICATIONS.

Pedde N Treatments

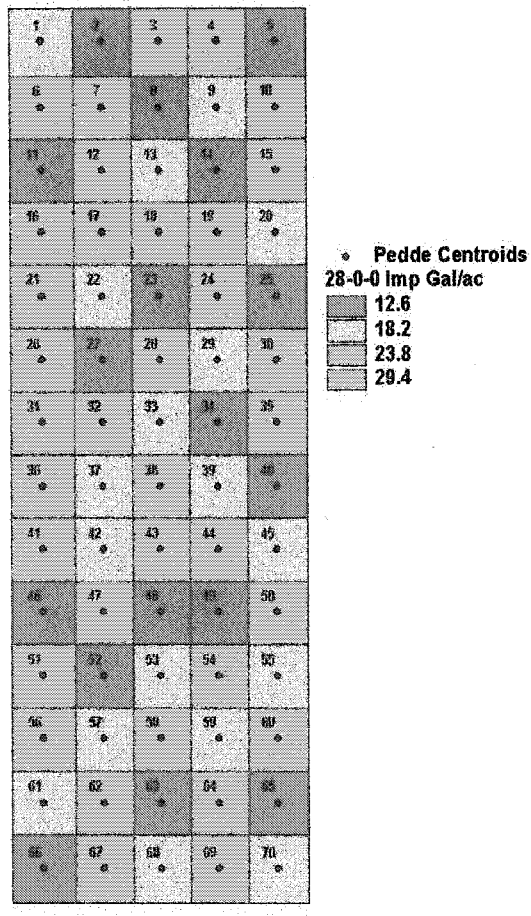

Figure AII-1

Delage N Treatments

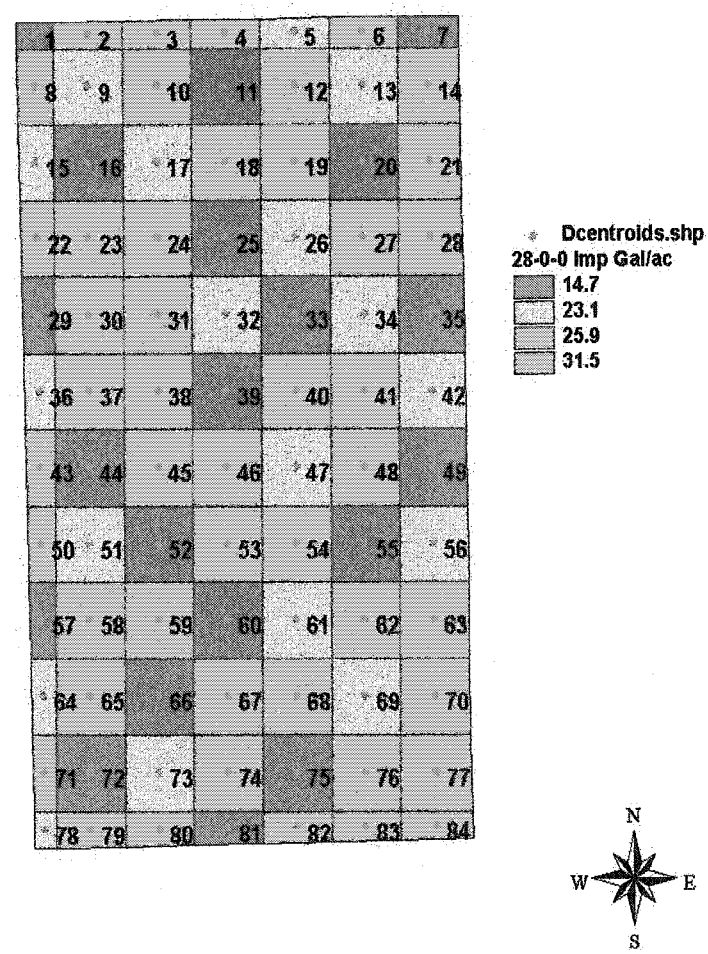

Figure AII-2

Both fields received a starter fertilization of 28-0-0 gallons/acre (i.e., Nitrogen-Phosphorous-Potassium or N-P-K). The range 12.6-29.4 and 14.7-31.5 represents the minimum and maximum nitrogen fertilizer application for the Pedde and Delage fields, respectively. Small circles represent the plot centroids.

APPENDIX III: FLIGHT LINE AND PASS LAYOUT FOR HYPERION IMAGES FOR INDIAN HEAD, SASKATCHEWAN.

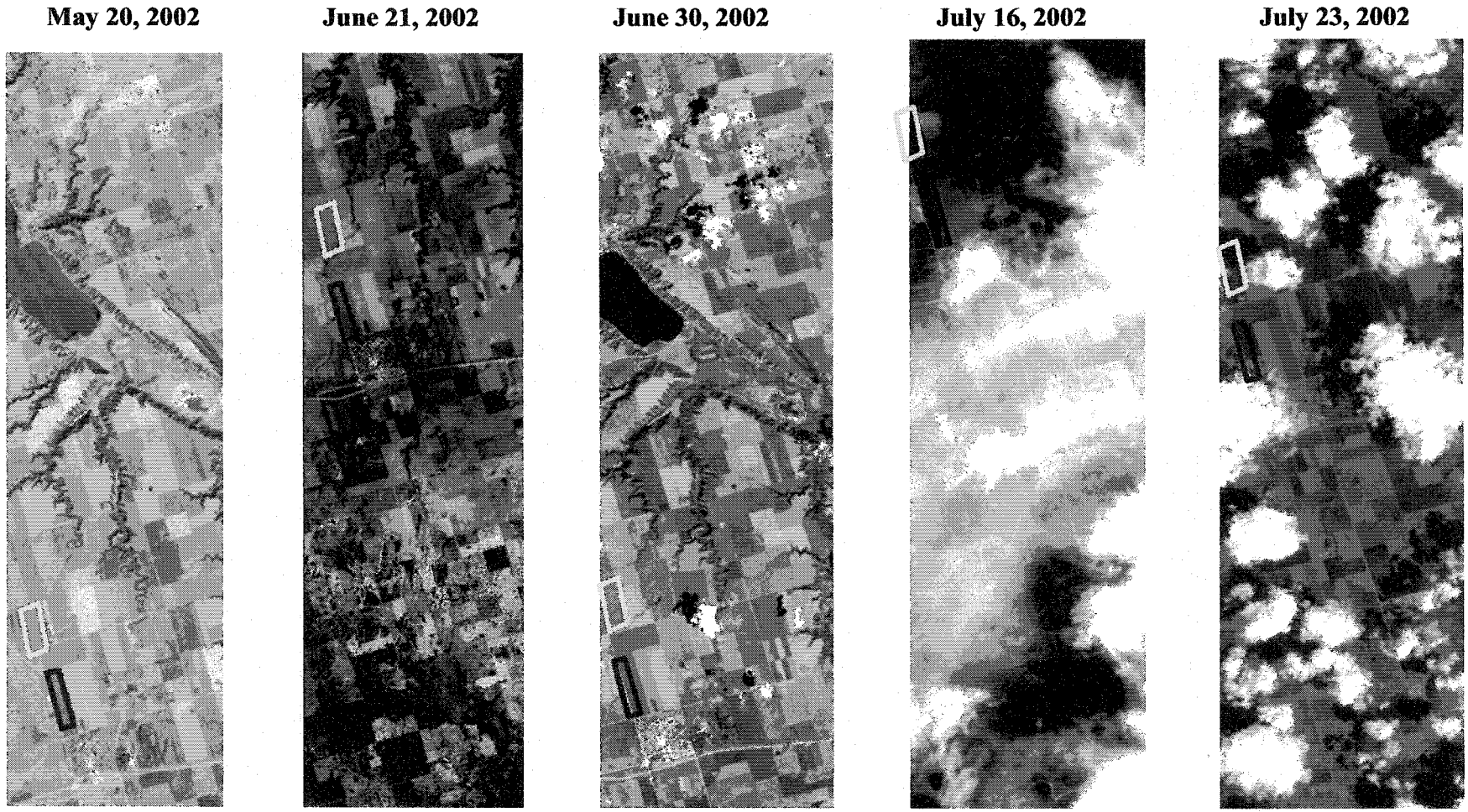

Figure AIII-1: Study fields: Yellow- Delage; Blue – Pedde

APPENDIX IV: COMPARISON OF THE PRINCIPAL COMPONENT (PC) IMAGES BEFORE AND AFTER THE NOISE REDUCTION.

Original (VNIR)

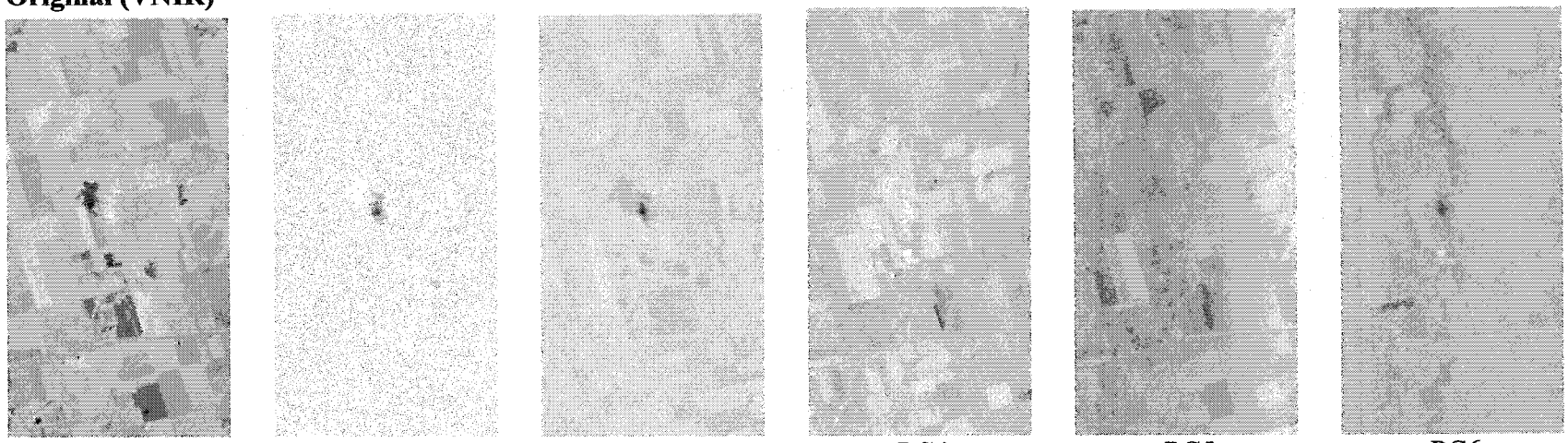

PC1 PC2 PC3 PC4 PC5 PC6

Noise reduced (VNIR)

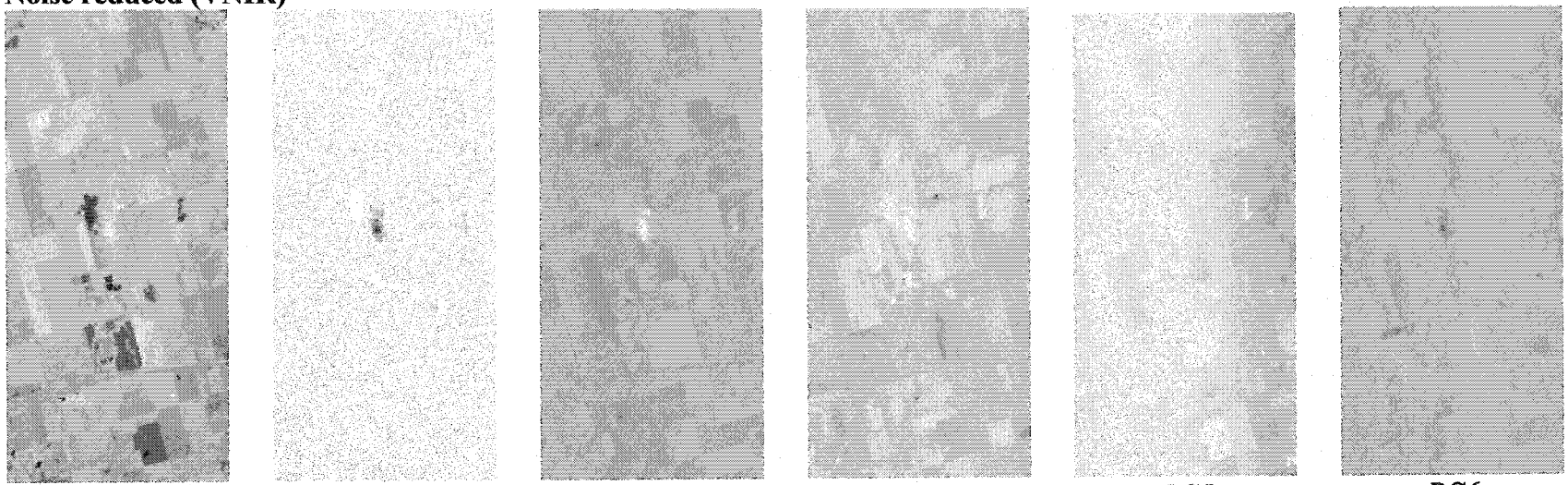

PC1 PC2 PC3 PC4 PC5 PC6

Figure AIV-1: Principal components of original and noise reduced VNIR data.

Original (SWIR)

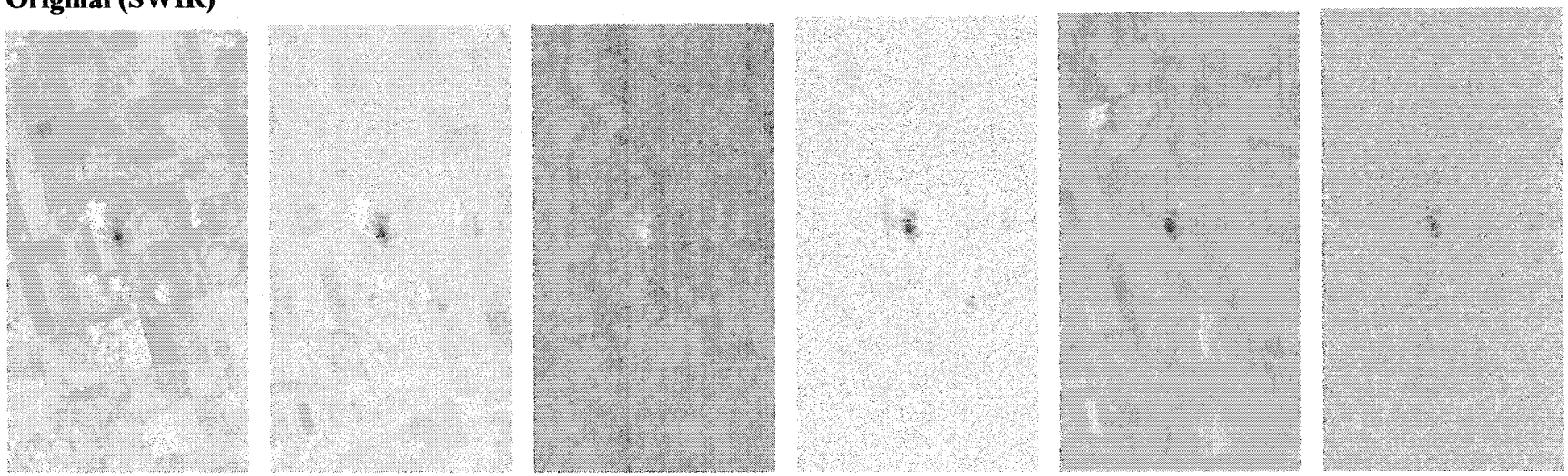

Noise reduced (SWIR)

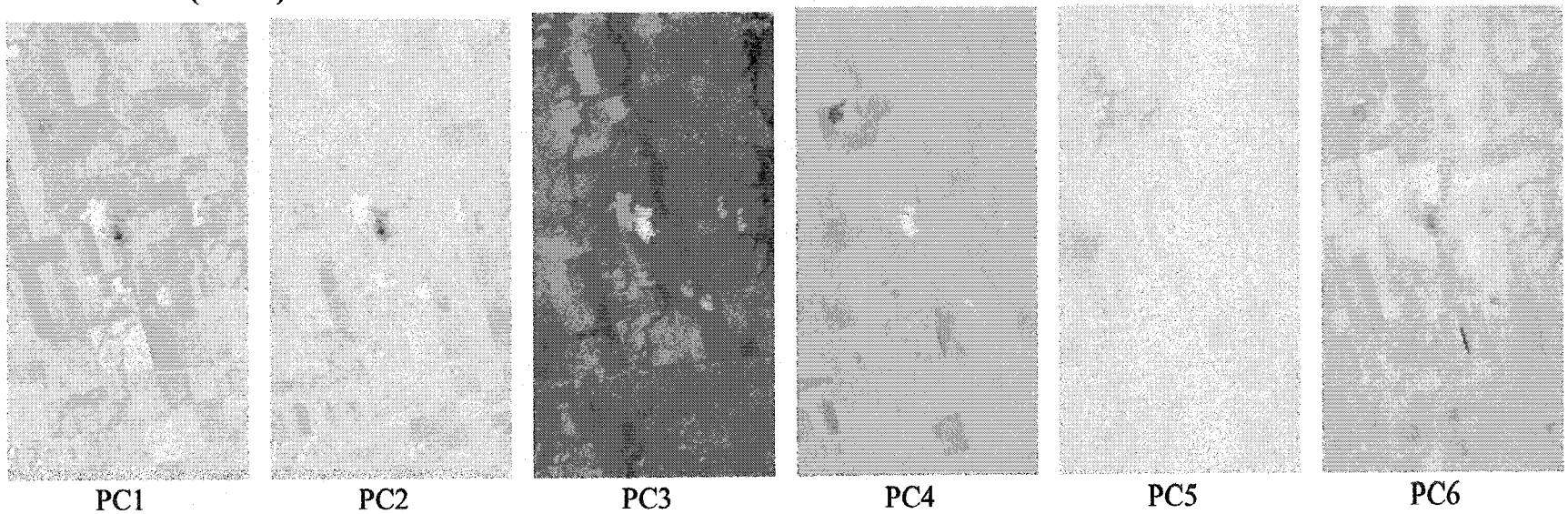

Figure AI-2V: Principal components of original and noise reduced SWIR data.

APPENDIX V: SPECTRAL MIXTURE ANALYSIS (SMA).

Spectral Mixture Analysis (SMA)

Hyperspectral spectra from spacecrafts or aircrafts are close to the one found in laboratories and field measurements, thus enhancing its ability to identify materials on the earth's surface. Many surface materials have specific absorption features in their spectra, which can be related to their composition. For example, a vegetation spectrum shows specific chlorophyll and liquid water absorption features in the VNIR region. Reflectance spectra of hyperspectral data can be used to discriminate a large variety of surface cover materials, which is not possible with broadband sensors (Goetz *et al.,* 1985). Linear spectral mixture analysis (SMA) is a technique to unmix the spectrum of each pixel into its components (Adams *et al.,* 1986; Boardman, 1992; Tompkins *et al.,* 1997; Neville *et al.,* 1999; Feng *et al.,* 2003; Szeredi *et al.,* 2003).

The following sections discuss the processing steps performed on the retrieved hyperspectral surface reflectance data. The processing, which includes endmember selection and SMA was done to retrieve fractions of wheat which are required for the calculation of the CAI from Hyperion data. For this purpose, only the VNIR dataset ranging from 428 to 1004 nm was used.

Spectral Endmember Selection

Spectral endmember or component selection is the most important step to successfully unmix reflectance data and produce fractional abundances of the different materials of the study site. Various techniques are used to select and extract endmembers from hyperspectral datasets (Boardman, 1995; Tompkins *et al.,* 1997; Neville *et al.,* 1999; Feng *et al.,* 2003; Szeredi *et al.,* 2003). Among these, there are two main groups; manual and automatic endmember selection, as reviewed by Pacheco (2004).

For this study, the manual method of selecting endmembers for the SMA was used. For this purpose, in-situ and indoor measured spectra acquired with the GER-3700 spectroradiometer were tested for endmember selection. Ten vegetation (wheat) endmembers and one soil endmember were selected, which acquired in the laboratory (Figure AV-1). The soil endmember was acquired before seeding of the wheat crop. The individual spectra were convolved to match the Hyperion band center wavelength position using the "Spectral Simulation" tool in the ISDAS. A spectral array was then created containing the eleven endmembers for spectral unmixing analysis.

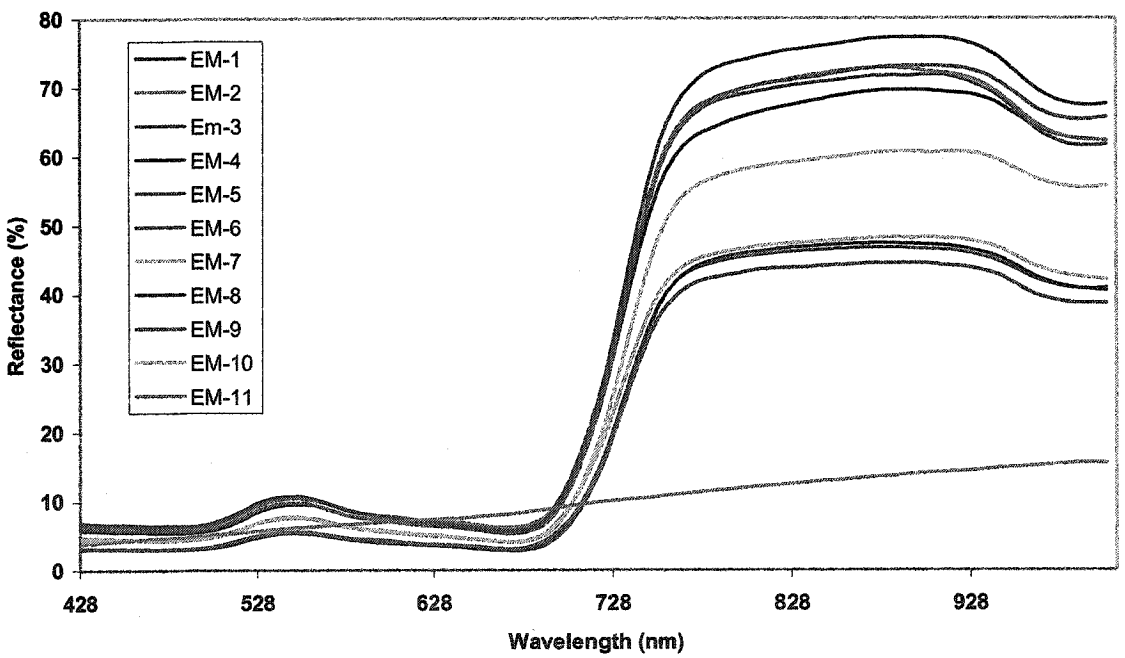

Figure AV-1: Endmember (EM) spectra used for spectral unmixing analysis for the Indian Head dataset. EM-1 to EM-10 represent the vegetation (wheat) endmembers and EM-11 is the soil endmember.

Spectral Mixture Analysis (SMA)

Linear SMA assumes that each pixel on the surface is a physical mixture of various components weighted by the surface abundance (Schwarz, 1998). Two main methods are used for linear umixing, the unconstrained and constrained version. The general equations that express constrained linear SMA are (Boardman, 1992):

$$r_b = \sum_{i=1}^{m} f_{em} . r_{b,em} + e_b , \tag{1}$$

where

$$\sum_{i=1}^{m} f_{em} = 1.0 , \tag{2}$$

R_b is the reflectance of a pixel in band b, f_{em} is the fractional abundance of endmember em, m is the total number of endmembers, $r_{b,\ em}$ is the reflectance in band b of endmember em, and e_b is the residual error in band b of the model.

For this study weakly constrained SMA was performed using an algorithm implemented in ISDAS. The advantage of the weakly constrained SMA is that it will force the fraction of some of the pixels to get assigned to an inappropriate endmember (e.g., shadow). This method relaxes the constraint that the fractions sum to one.

APPENDIX VI: RELATIONSHIPS BETWEEN REMAINING SPECTRAL CHLOROPHYLL INDICES CALCULATED FROM THE GER-3700 DATA AND Chl-ab OR Chl-a CONTENT ($\mu g / cm^2$) DERIVED FROM THE SPAD-502 MEASUREMENTS. THE SOLID LINE IS THE LEAST SQUARES REGRESSION LINE; DOTTED RED LINE IS THE 95% CONFIDENCE INTERVAL FOR THE REGRESSION.

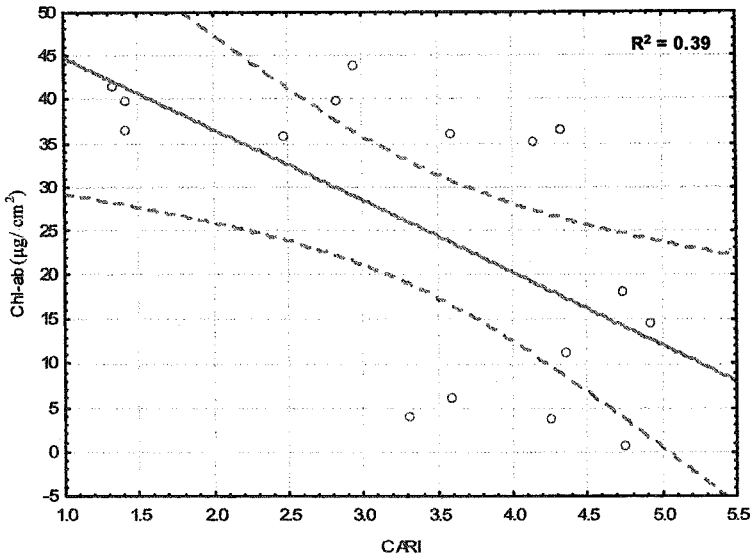
R² = 0.39
Chl-ab (µg/ cm²)
CARI

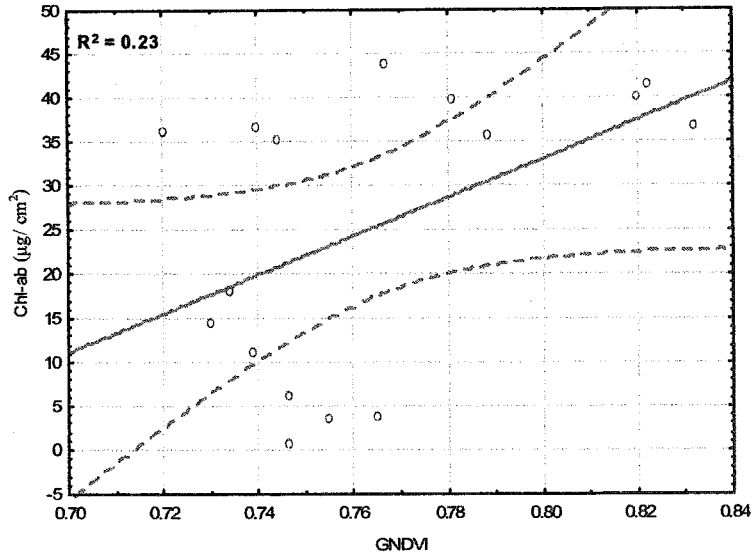
R² = 0.23
Chl-ab (µg/ cm²)
GNDVI

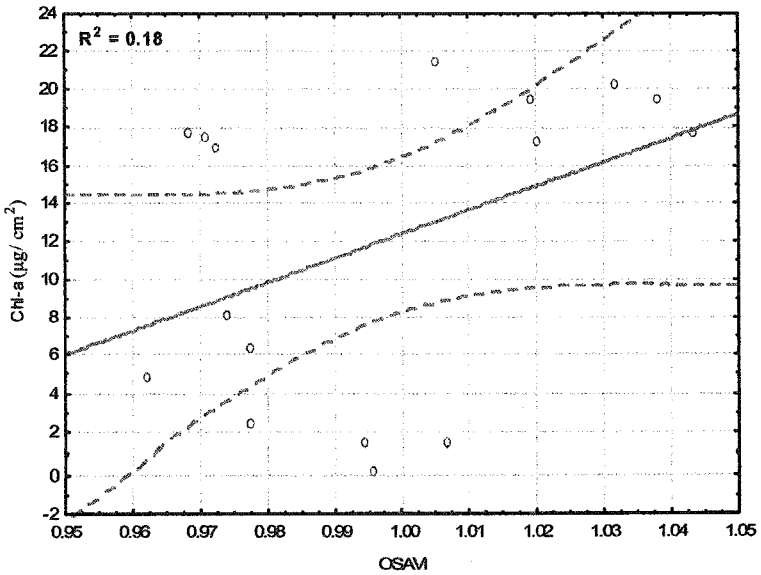
R² = 0.18
Chl-a (µg/ cm²)
OSAVI

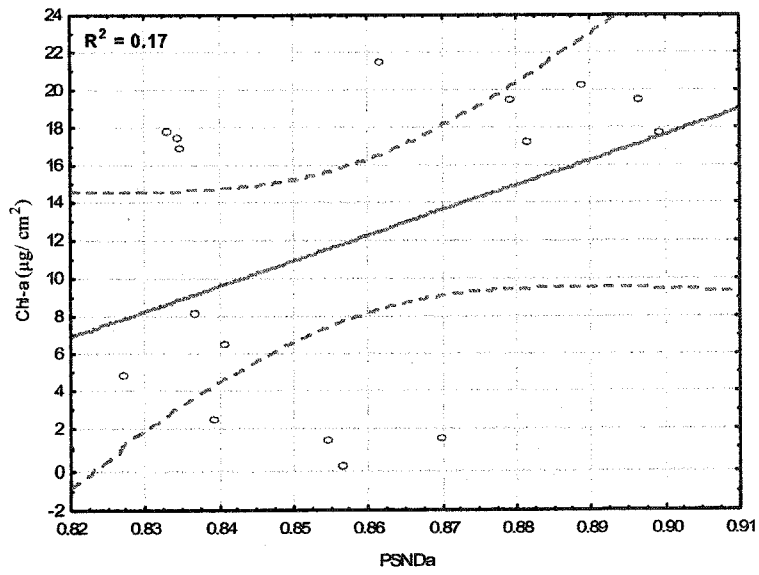
R² = 0.17
Chl-a (µg/ cm²)
PSNDa

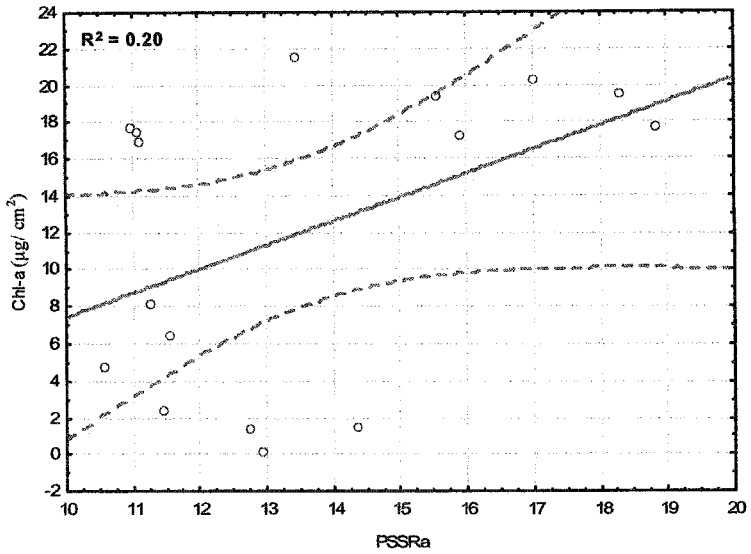
R² = 0.20
Chl-a (µg/ cm²)
PSSRa

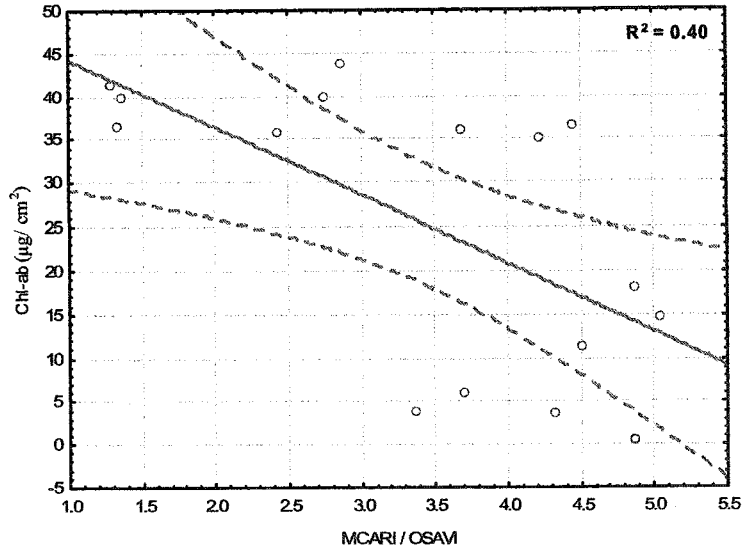
R² = 0.40
Chl-ab (µg/ cm²)
MCARI / OSAVI

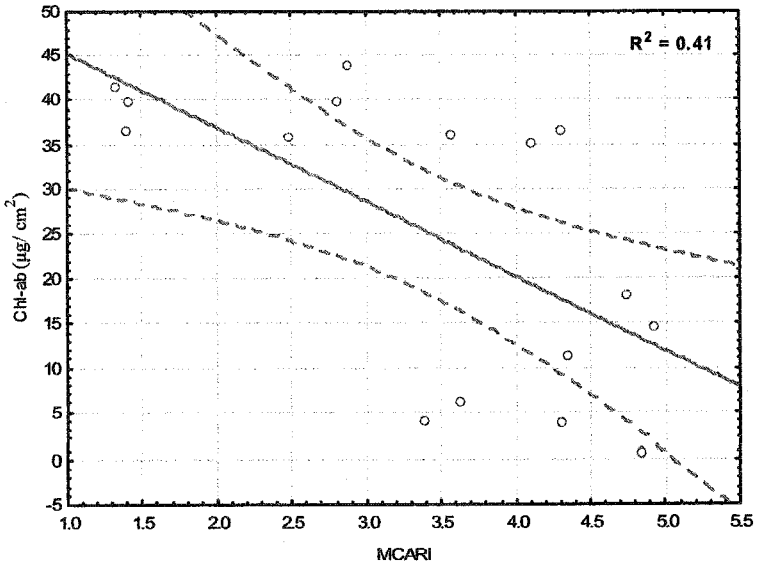
R² = 0.41
Chl-ab (µg/ cm²)
MCARI

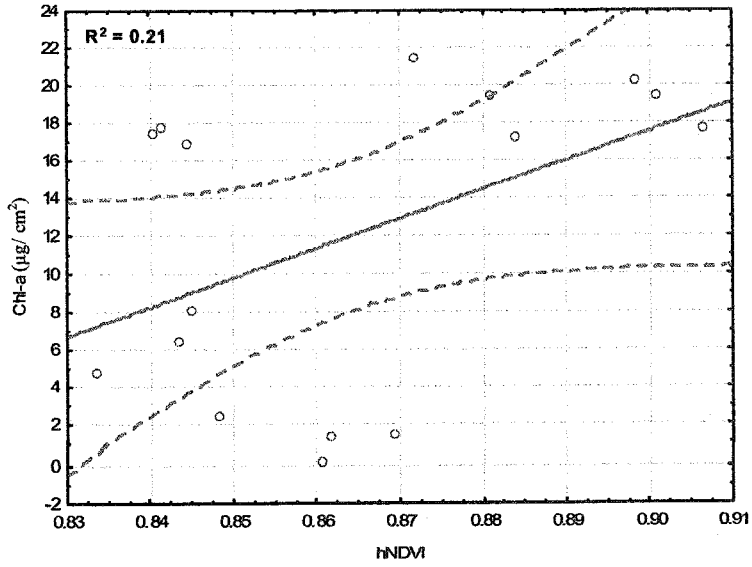
R² = 0.21
Chl-a (µg/ cm²)
hNDVI

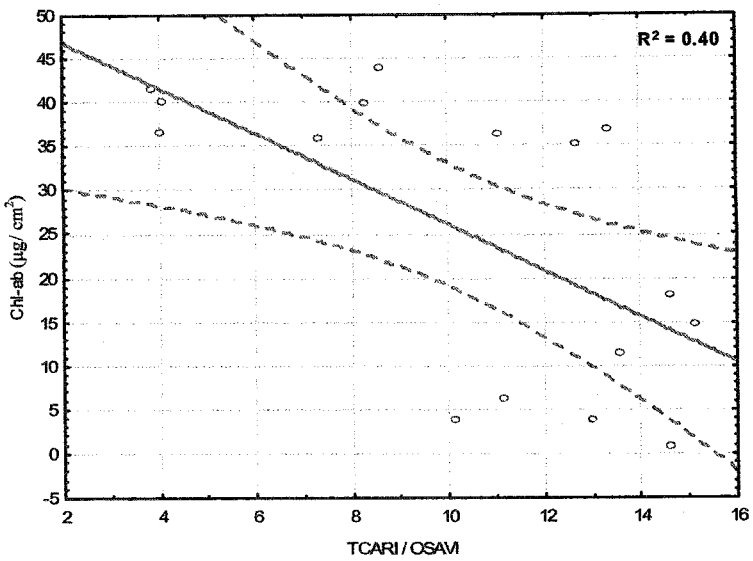
R² = 0.40
Chl-ab (µg/ cm²)
TCARI / OSAVI

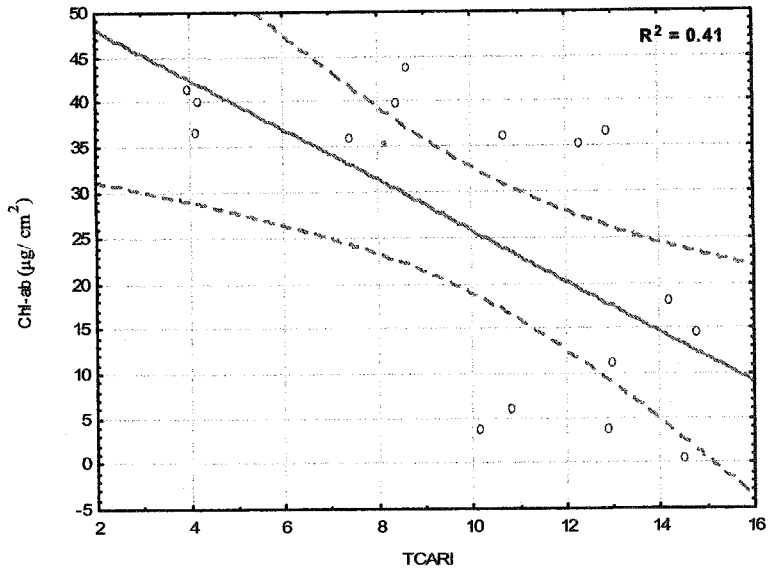
R² = 0.41
Chl-ab (µg/ cm²)
TCARI

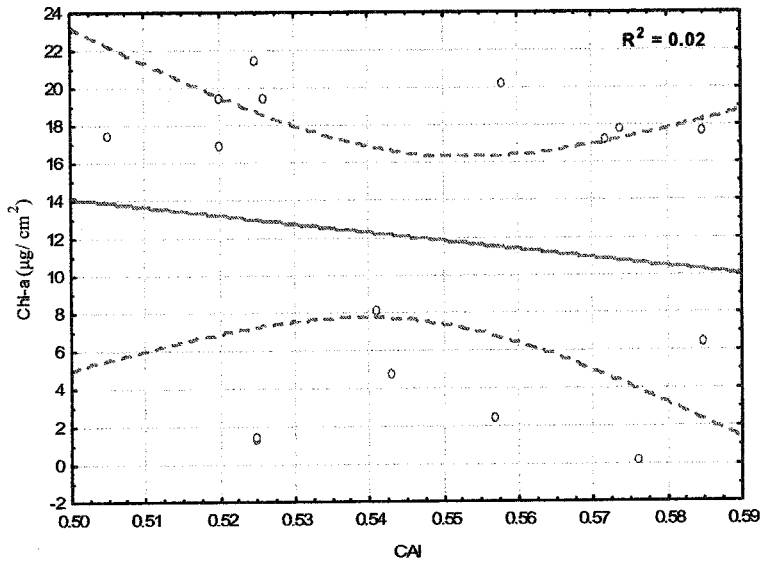
R² = 0.02
Chl-a (µg/ cm²)
CAI

APPENDIX VII: RELATIONSHIPS BETWEEN CHLOROPHYLL CONTENT(Chl-ab OR Chl-a IN μg / cm^2) ESTIMATED FROM THE HYPERION IMAGE DATA USING THE LEAF LEVEL CALIBRATION EQUATIONS AND DERIVED FROM THE SPAD-502 MEASUREMENTS.

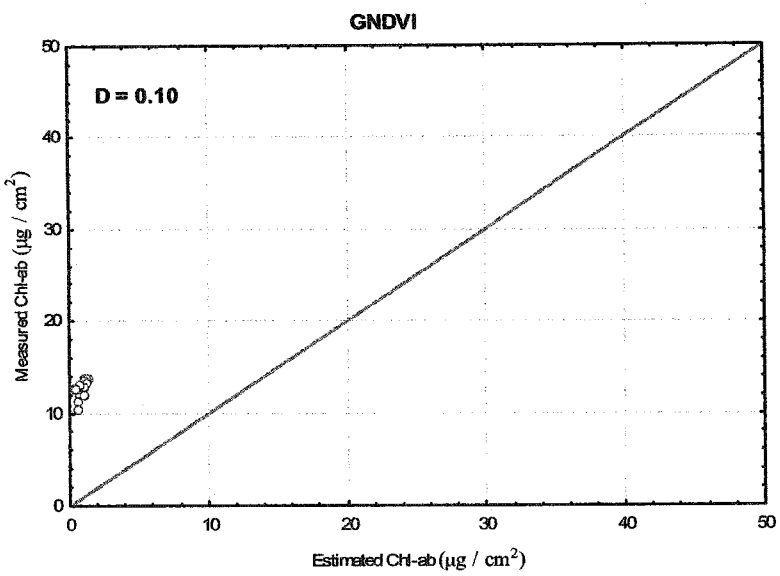
GNDVI
D = 0.10
Measured Chl-ab (µg / cm²)
Estimated Chl-ab (µg / cm²)
0
10
20
30
40
50

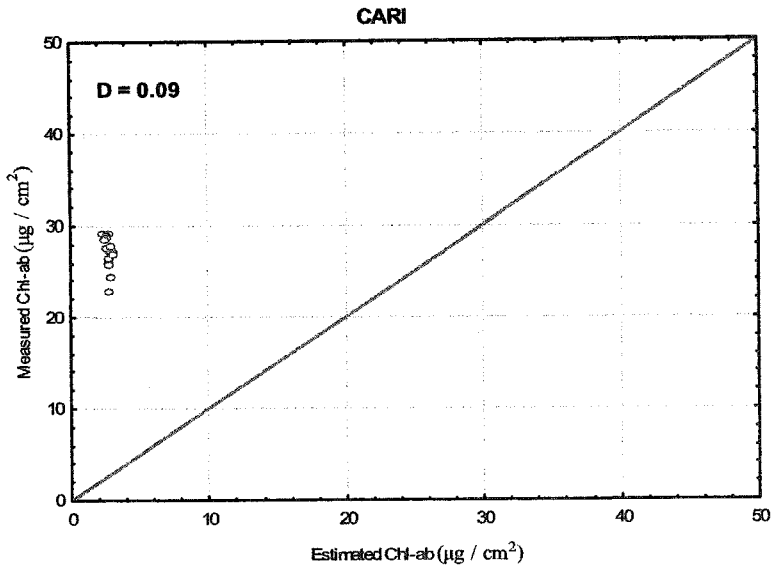
CARI
D = 0.09
Measured Chl-ab (µg / cm²)
Estimated Chl-ab (µg / cm²)
0
10
20
30
40
50

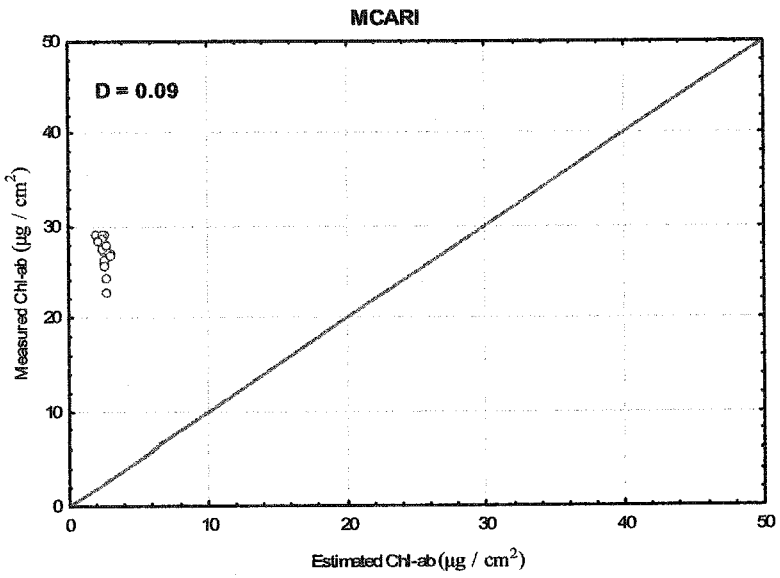
MCARI
D = 0.09
Measured Chl-ab (µg / cm²)
Estimated Chl-ab (µg / cm²)
0
10
20
30
40
50

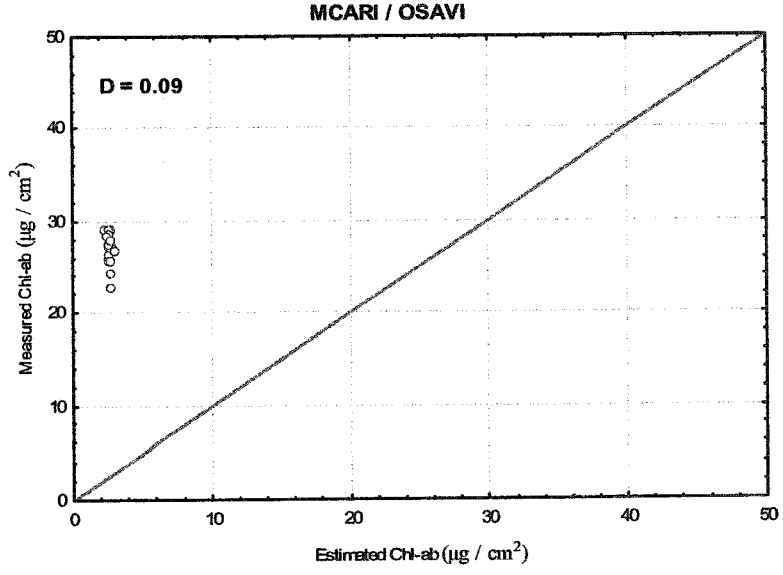
MCARI / OSAVI
D = 0.09
Measured Chl-ab (µg / cm²)
Estimated Chl-ab (µg / cm²)
0
10
20
30
40
50

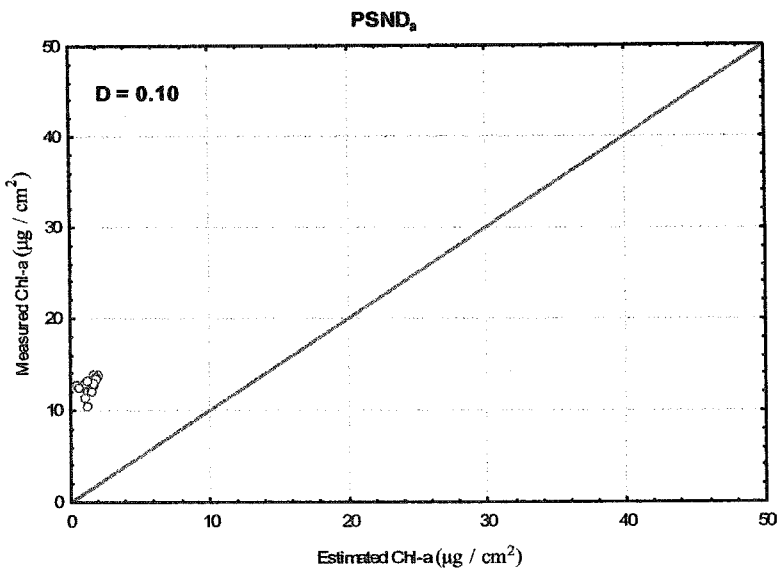
PSND$_a$
D = 0.10
Measured Chl-a (µg / cm^2)
Estimated Chl-a (µg / cm^2)
0
10
20
30
40
50

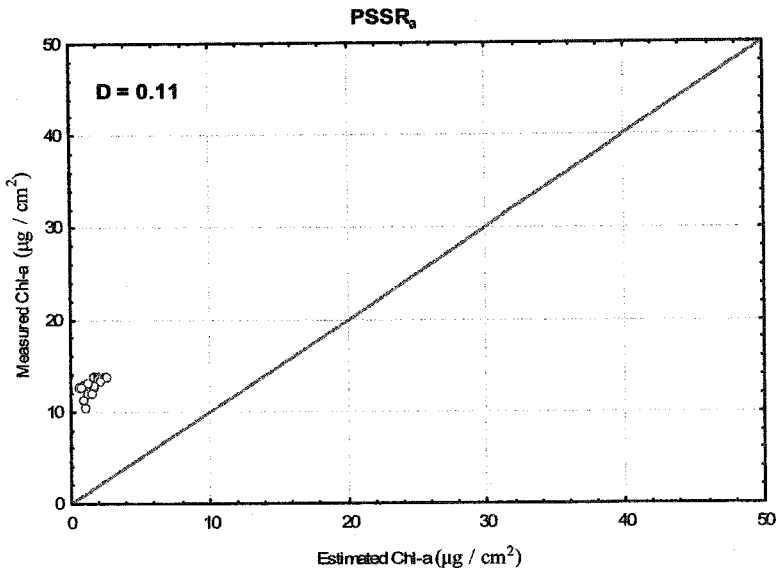
PSSR$_a$
D = 0.11
Measured Chl-a (µg / cm^2)
Estimated Chl-a (µg / cm^2)
0
10
20
30
40
50

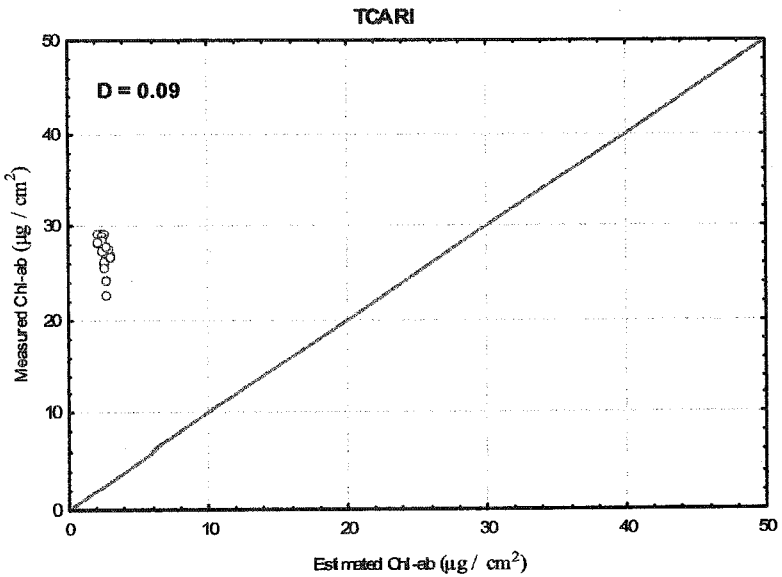
TCARI
D = 0.09
Measured Chl-ab (µg / cm^2)
Estimated Chl-ab (µg / cm^2)
0
10
20
30
40
50

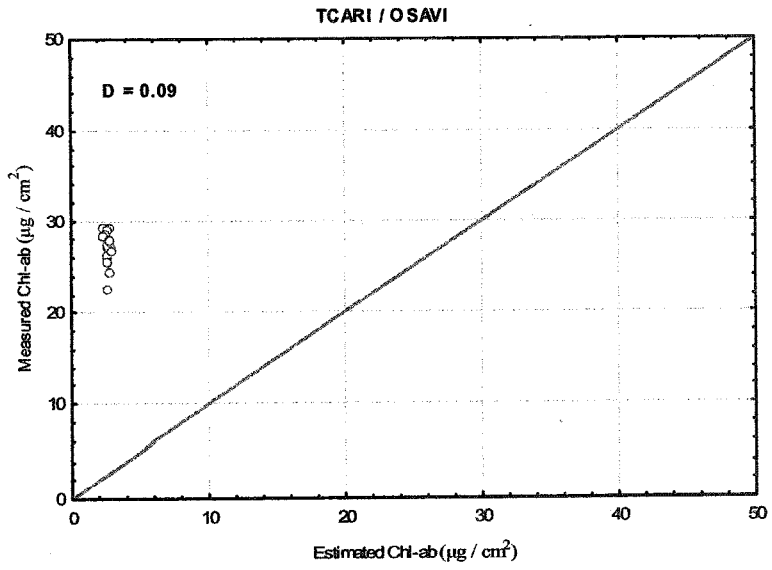
TCARI / OSAVI
D = 0.09
Measured Chl-ab (µg / cm^2)
Estimated Chl-ab (µg / cm^2)
0
10
20
30
40
50

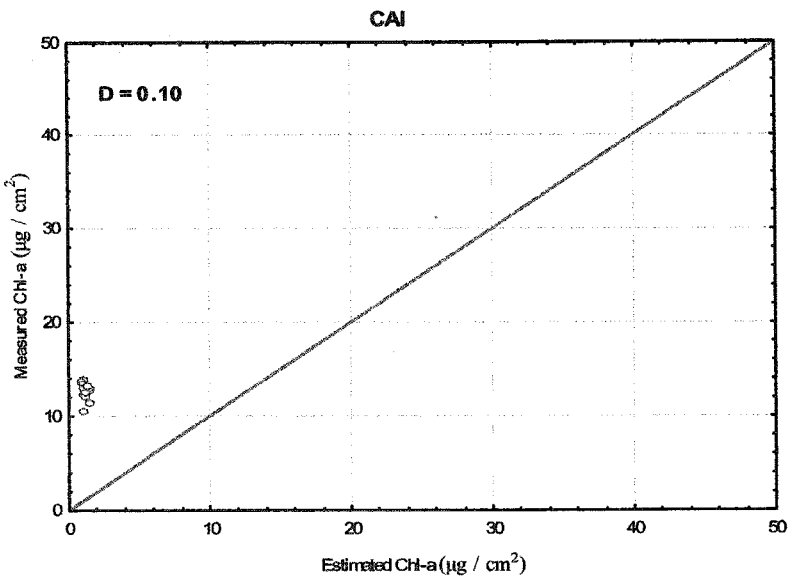
CAI
D = 0.10
Measured Chl-a (µg / cm²)
Estimated Chl-a (µg / cm²)
0
10
20
30
40
50

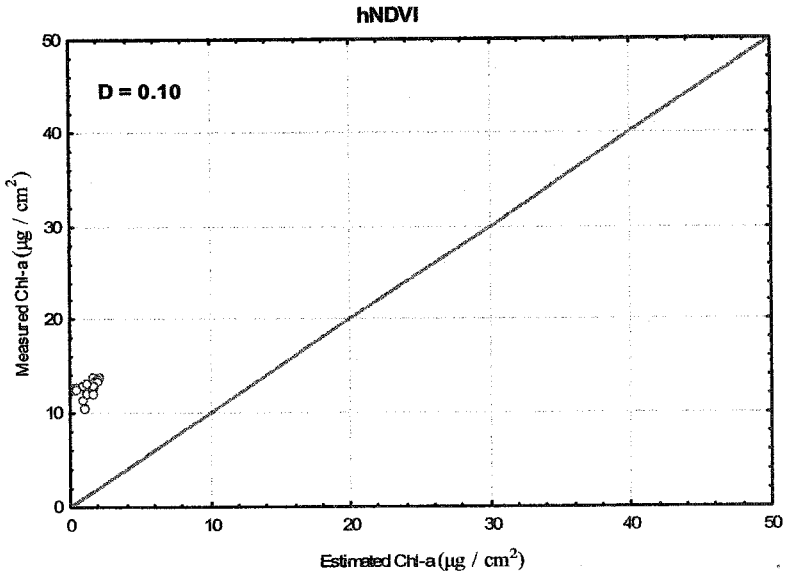
hNDVI
D = 0.10
Measured Chl-a (µg / cm²)
Estimated Chl-a (µg / cm²)
0
10
20
30
40
50

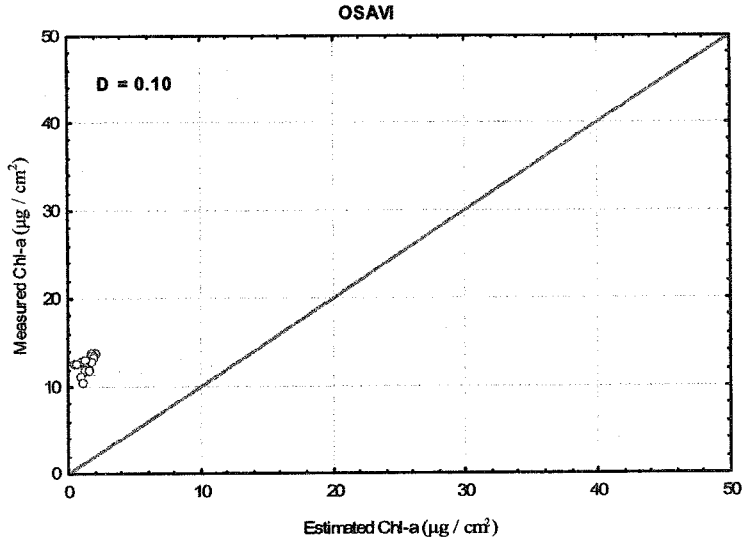
OSAVI
D = 0.10
Measured Chl-a (µg / cm²)
Estimated Chl-a (µg / cm²)
0
10
20
30
40
50